Année 2012

DOCUMENT DE THESE

présenté à

L'U.F.R. DES SCIENCES ET TECHNIQUES
DE L'UNIVERSITÉ DE FRANCHE-COMTÉ

pour obtenir le

GRADE DE DOCTEUR DE L'UNIVERSITÉ DE FRANCHE-COMTÉ
spécialité : Sciences pour l'Ingénieur

Etude expérimentale et analyse du comportement de mousses syntactiques pour grande profondeur d'immersion

Experimental study and analysis of the mechanical behaviour of syntactic foams used in deep sea

par

Dominique CHOQUEUSE

Soutenue le 15 novembre 2012 au centre IFREMER de Brest devant la Commission d'Examen :

Rapporteurs	F.	JACQUEMIN	Professeur – Université de Nantes
	Y.	REMOND	Professeur – Université de Strasbourg
Examinateurs	J.Y.	COGNARD	Professeur – ENSTA Bretagne, Brest
	D	HALDANE	Professeur, Herriot Watt University , Edimburgh (GB)
	F	PIERRON	Professeur, University of Southampton (GB)
Directeurs de thèse	D	PERREUX	Professeur – Université de Franche Comté
	P.	DAVIES	Ingénieur de recherche – IFREMER

« Il est moi grave de perdre que de se perdre »

Romain Gary

Remerciements.

J’ai longuement réfléchi avant de rédiger ce petit paragraphe avec les craintes suivantes :

celle, en l’écrivant, d’oublier quelqu’un et d’être maladroit dans la rédaction

celle, en l’occultant, de m’attribuer un travail que je n’aurais pu réaliser seul.

Je prends donc le risque d’en oublier et d’être maladroit.

Mes remerciements vont tout d’abord vers Dominique et Peter. Sans eux, et c’est certain, ce document n’aurait pas vu le jour. L’un a su faciliter la mise en place de ce parcours, essayer entre autre de m’initier à l’art de la modélisation mécanique et m’apporter le soutien amical qui dépasse, et de loin, celui d’un directeur de thèse. L’autre, et c’est simplement le pendant de l’un, fut là pour me donner l’idée de m’attaquer à ce travail et, disons-le, de m’y pousser et, derrière des monticules de papiers, de souvent me rappeler « Alors, et la thèse … ». Pour compléter son apport, outre les conseils avisés, il me serait difficile d’oublier que l’anglais est loin d’être ma langue maternelle et là son soutien fut une fois de plus indéfectible.

A Yves Remond et Frédérique, je voudrais rappeler l’honneur et la sympathie qu’ils m’ont faits d’avoir accepté de « rapporter » ce document. Ma facilité rédactionnelle n’a sûrement pas rendu aisé ce travail. Donc un grand merci à eux. La menthe sera pour moi la référence à mes rapporteurs, en me rappelant pour Yves les thés partagés du côté de Béchar et, pour Frédérique, une longue soirée nazairienne où les échanges furent animés.

Fabrice et David m’ont fait l’amitié de traverser le Channel pour participer à mon jury. Je les en remercie vivement by a Thank you so much …et je n’oublierai pas les rencontres stéphanoises ni le long périple de la normalisation organisé par Denis que nous avons pu partager.

Jean Yves s’est vu attribué le titre de président du jury et j’en suis sincèrement ravi et honoré. Ses conseils et son amitié me furent toujours de grande d’utilité.

Les soutiens d’ordre technique ou moral provenant d’horizons divers me furent nombreux et, à ce que je me souvienne toujours accompagnés d’une saine cordialité. Collègues de travail, partenaires universitaires ou industriels, sans oublier les stagiaires, en voici une liste ordonnée alphabétiquement (ça m’évite plein de tracas …) : Albert (là ça tombe sincèrement bien qu’il soit en tête), Amandine, André, Bernard, Bertrand, Christophe, Denis, Denise, Eric, Florence, François, Jean, Jérôme, Joël, Laurent, Lionel, Luc, Marie-Michèle, Matthias, Mickael, Nicolas, Pascal, Philippe, Pierre, Pierre-Yves, Romain, Trung, Yves, Yvon (là il n’y pas de raison qu’il soit en dernier), ….A vous tous un grand Merci.

Je ne saurai terminer ce paragraphe sans rappeler le soutien indéfectible et si important des amis et de la famille avec, bien sûr, une mention particulière à Nicole, qui va pouvoir retrouver un compagnon de marche pour le dimanche après midi, Vincent, qui ce coup là n'est plus tout seul, Gaëlle, qui trouveras quand même quelque chose à me raconter au téléphone et Julie, qui sait si bien nous faire profiter du sourire de Lily.

TABLE OF CONTENTS

LIST OF FIGURES

LIST OF TABLES

INTRODUCTION

This report describes a study of syntactic foam materials for underwater applications. It is based on the experience gained at Ifremer on the use of syntactic foam for deep sea application, and on the information collected during the evaluation programmes and research studies conducted for the offshore industry.

The aim of this study is not to draw up a list of data for a specific material, but rather to provide elements useful for the evaluation and the modelling of the mechanical behaviour of syntactic foam for deep sea applications. The document is organized in four chapters.

In the first part a presentation of the material and its application is given, together with a review of recent scientific work on this type of material. This addresses both long term behaviour and mechanical modelling and testing. Information on the use of syntactic foam in the offshore oil industry is given, deeper exploitation is generating a significant increase in demand for syntactic foam.

The second and third chapters present the experimental part of this study.

Two types of syntactic foam, widely used in the oil and gas deep sea domain, have been retained for this evaluation; GSEP (Glass syntactic epoxy foam) and GSPU (Glass syntactic polyurethane foam). These materials have been chosen because they exhibit quite different behaviour, corresponding to those of a wide range of syntactic foams, and can thus be considered as model materials.

In order to characterize the material behaviour correctly a series of original tests has been developed, and these are presented in the second chapter. They include determination of elastic constants from ultrasonic wave speed measurements, uniaxial compression loading, hydrostatic compression tests and shear testing. These methods have been developed and evaluated. In particular a new hydrostatic compression test based on buoyancy measurement has been set up and has clearly revealed the behaviour of these materials under such loading. An evaluation of shear tests on syntactic foam has also been conducted. Modified Arcan fixture testing has been developed to investigate shear behaviour and allow investigation over a wide range of shear deformation. This development has been carried out in collaboration with the LBMS (Brest Laboratory for structural mechanics).

Damageable behaviour of the materials has been identified which is, a priori, related to microsphere collapse and will be investigated in the third chapter

Original methods have been developed to quantity the damage occurrence and identification. Unique in situ Xray microtomography analysis under hydrostatic loading has been developed at the ESRF in Grenoble with the support of the Mateis INSA laboratory. Kinetics of damage

development can be estimated from such experiments. In complement to this method an ex situ evaluation of microsphere collapse has been set up, based on the determination of glass microsphere specific gravity by means of pycnometer measurement. This is an alternative approach to quantify damage in GSPU material. Acoustic emission under hydrostatic compression has also been evaluated in this study.

These two chapters are the core of the study, and are the result of many years of experience in evaluating syntactic foam behaviour.

The fourth chapter addresses modelling of the mechanical material behaviour based on the observations in the two previous chapters. Prior to establishing the basis of a mechanical model of syntactic foam behaviour, a mechanical analysis of glass microsphere collapse and its consequences for the specific properties of syntactic foam is presented.

In the final chapter, the conclusions from the study are presented, and future developments aiming to improve the models and to extend them to other materials are discussed.

Chapter 1. PRESENTATION

This work addresses the behaviour of materials in a deep sea environment. It has been performed within the framework of the activities of the Ifremer Materials and Structures laboratory. One of the aims of this laboratory is to focus on the knowledge of the behaviour of materials dedicated to deep sea applications, where specific properties are required.

Deep sea exploration (at depths > 500 meters) concerns different activity sectors (oil and gas, navy, oceanography, mineral resources …) and requires materials offering specific properties: light weight and the ability to withstand high hydrostatic pressure over a long period of time (typically 20 - 25 years). In this field syntactic foams can be considered as a typical deep sea material, even if with time other land-based applications of this material have been developed.

Syntactic foams were initially developed in the 1960's in response to a need for buoyancy material for deep sea applications [1].

From the Greek term "suntaktikos" (taktidos = disposal and sun = with), syntactic means a global arrangement of cavities in a material.

For syntactic foams this arrangement is generally obtained by incorporation of mineral or polymeric fillers in a polymeric matrix.

The nature of the component (fillers and polymer) confers to the material its functional properties including:

- light weight
- high hydrostatic strength
- long term integrity in a deep sea environment.

Over the last twenty years, in addition to the need for buoyancy for the design of deep sea offshore oil exploitation structures, new applications of syntactic foam have been developed providing thermal insulation.

Large volumes of this type of material are now used in deep sea oil exploitation, and this has generated renewed interest in the understanding of the behaviour of syntactic foams in the deep sea environment.

The materials used for these applications (buoyancy and thermal insulation) are essentially made of glass microspheres included in a polymeric matrix and are the object of this study.

Various recent conferences have been organized on the topics of syntactic and composite foams. International conferences on Syntactic and Composite Foams (SCF), were held in Banff (SCF-I 2004) , in Davos (SCF-II 2007) and recently in Cetraro (SCF-III, 2011).

1.1 Glass microspheres

Hollow glass microspheres are the basis of syntactic foam materials. The manufacturing technology was developed by 3M in the 1960s, and today this material is used in aerospace and military systems, paints and coatings, marine structures, oil and gas exploration and production and other industrial uses (Figure 1).

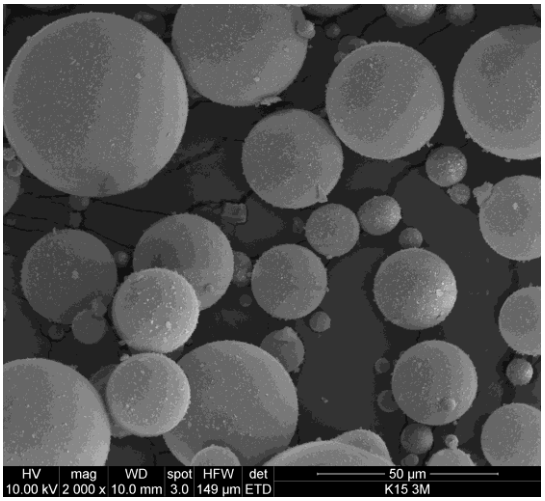

Figure 1: Glass Microspheres

Ruckebush [2] has described the glass microspheres in detail. They originated in the USA, in the 1960s; hollow glass microspheres were industrially manufactured for the first time following the observation, during a quality control of auto-reflecting panels made of glass micro balls, that in some places the incident light instead of being reflected was diffused in all directions. The analysis of the defect revealed that during the manufacturing process of the micro balls, impurities in the glass formulation played the role of expanding agent, resulting in glass microspheres which diffused the light.

Different manufacturing processes are explained in [1]. A classical technique consists of melting a paste of sodium borosilicate and lime in a furnace (around 1000°C) and introducing an expanding agent before rapid cooling. The glass balls obtained are ground in order to obtain the required particle size. The glass powder is then placed in a flame. The glass particles soften and the expanding agent included in them breaks down to produce gas inside the glass paste. Glass particles expand to form hollow glass spheres which are air-cooled and

collected in a downstream cyclone before sifting to obtain the required particle sizes. The physico-chemical properties of the glass microspheres are also described in [3]. The compaction of a sample of microspheres is a function of the particle size distribution. Due to the manufacturing process the particle size is not unique (Figure 2).

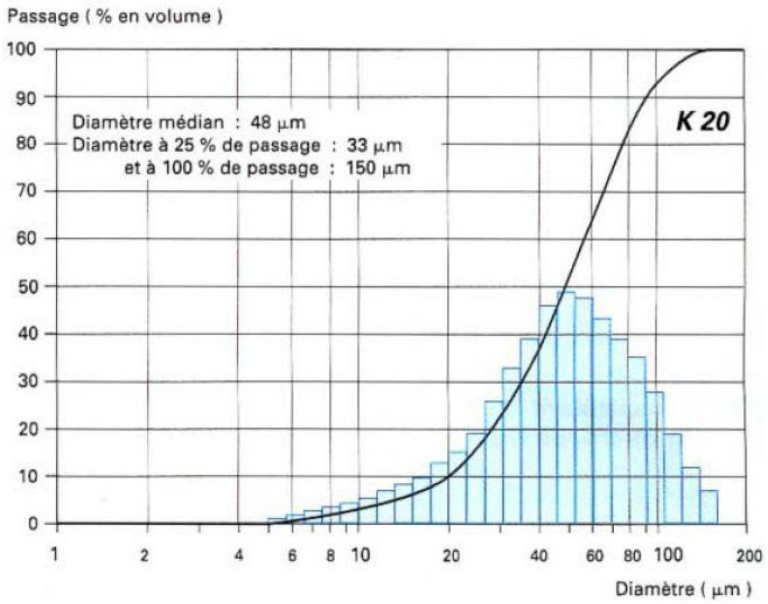

Figure 2 : K20 3M™ grade micro spheres glass sizing

Taking into account that small diameter microspheres will occupy the place left between the particles of larger diameter, an optimization of the particle size distribution can result in packing factors up to 0.8 - 0.85.

The packing factor is a dimensionless ratio that describes the amount of volume that a substance takes up in a particular volume.

For a one-dimensional system (all spheres of the same diameter) the maximum packing factor is obtained with a face-centred cubic structure.

Different grades of glass microspheres are available. The grades used in the oil exploitation industry are reported on Figure 3.

3M™ Glass Bubbles General Purpose Series

	Target Crush Strength (90% survival, psi)	True Density (g/cc)	Particle Size (microns, by volume) Distribution 10th%	50th%	90th%	Color (unaided eye)
K1	250	0.125	30	65	115	white
K15	300	0.15	30	60	105	white
S15	300	0.15	25	55	90	white
S22	400	0.22	20	35	65	white
K20	500	0.20	25	55	95	white
K25	750	0.25	25	55	90	white
S32	2000	0.32	20	40	70	white
S35	3000	0.35	10	40	75	white
K37	3000	0.37	20	45	80	white
XLD3000	3000	0.23	15	30	40	white
S38	4000	0.38	15	40	75	white
S38HS	5500	0.38	15	40	75	white
S38XHS	5500	0.38	15	40	70	white
K46	6000	0.46	15	40	70	white
XLD6000	6000	0.30	10	18	30	white
K42HS	8,000	0.42	11	22	37	white
S60	10,000	0.60	15	30	55	white
S60HS	18,000	0.60	11	30	50	white
iM30K	28,000	0.60	9	16	25	white

Figure 3 : 3M™ microspheres grade

It can be noted that globally there is a direct relationship between the true density of the microspheres and their crush strength. However, depending on the particle size distribution, for the same density the crush strength can be improved.

1.2 Behaviour of syntactic foam

By incorporation of microspheres in a polymeric matrix syntactic foam is manufactured.

Concerning the choice of material for a particular application, the properties of syntactic foam, which can be considered as a composite material, will depend on:

- the type of resin used,
- the grade and nature of microspheres,
- the volume content of the microspheres in the material.

Published references to syntactic foams date from the 1980's.

Shutov [4] provided a good overview of the early knowledge of syntactic polymer foams. The main application at the time was buoyancy for deep sea exploration (6000 meters), and a review of the materials available (fillers and binder or matrix) was given. The influence of the nature and proportion of the components on the physical properties was explained, and the

strengthening effect was highlighted. It was noted that depending on the stiffness of the binder the specific strength values of the syntactic foam are higher than those of the plastic in all cases, but the change is more substantial in the case of lower stiffness binders. Some results on water absorption and resistance to hydrostatic pressure were given, together with a first approach to the calculation of elastic parameters and strength.

Watkins [5] has described buoyancy materials for offshore riser pipes and gave details on the development of such materials for this application The improvements needed to guarantee long term performance in a deep sea environment were given : chemical nature of the glass and the resin, interface quality, …

Lamy [6] provided the results from a characterization of buoyancy material for use in deep sea with information on the test methods used to evaluate hydrostatic compression behaviour.

Improvements in the understanding of the knowledge of the behaviour of syntactic foams were made at the same period in France, described in various PhD theses.

For example, Fontblanc [1] described the design of a material for deep sea application with a description of the choice of resin and microsphere grade sizing distribution. Mechanical characterization of the material (uniaxial loading: tension, compression, shear) was described, including multiaxial tests (tension under hydrostatic pressure, internal pressure + compression) and a first investigation with acoustic emission during hydrostatic pressure tests. That study concluded with ageing tests, revealing the difficulty in using time-temperature equivalence for this type of material to predict life time.

Avena [7] carried out a study on the long term behaviour of immersed syntactic foam. The study was performed on epoxy syntactic foam and revealed the effect of hydrostatic pressure on the kinetics of water absorption. In her conclusion on the hydrostatic compression strength of the microspheres, the influence of the quality of the interface between filler and binder, and of the chemical nature of the binder was highlighted (Figure 4).

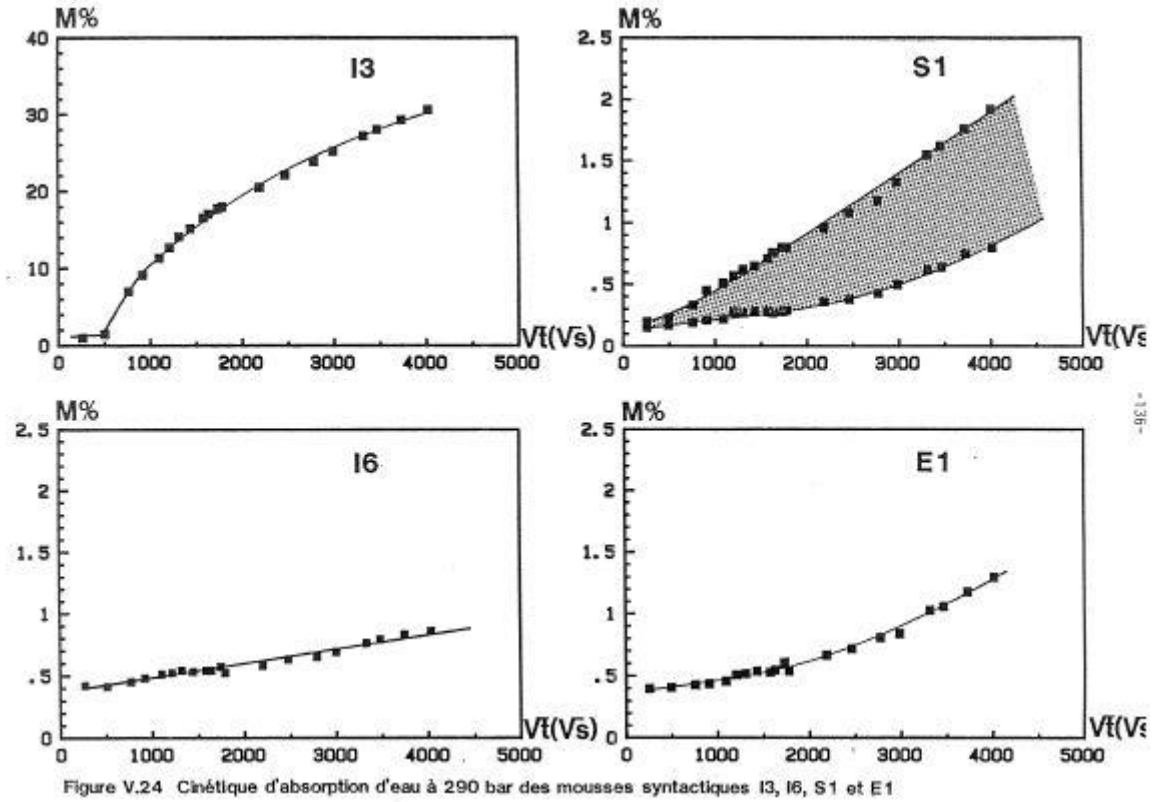

Figure V.24 Cinétique d'absorption d'eau à 290 bar des mousses syntactiques I3, I6, S1 et E1

Figure 4 : Water absorption curves of different syntactic foams from [7]

Dan [8] and Baptiste [9] performed studies on the damageable behaviour of syntactic foam using a micro-mechanics approach. Elastic moduli were determined by a homogenization method, and the damage mechanisms were studied in tension. A three-phase method developed by different authors, and in particular Hashin [10] and Christensen [11], was used. Crack propagation was also studied.

Ben Hamida [12] implemented a model aiming to describe the macroscopic behaviour of an elementary cell. This elastic model allowed the local stresses in the filler and the binder to be estimated from finite element analysis (Figure 5).

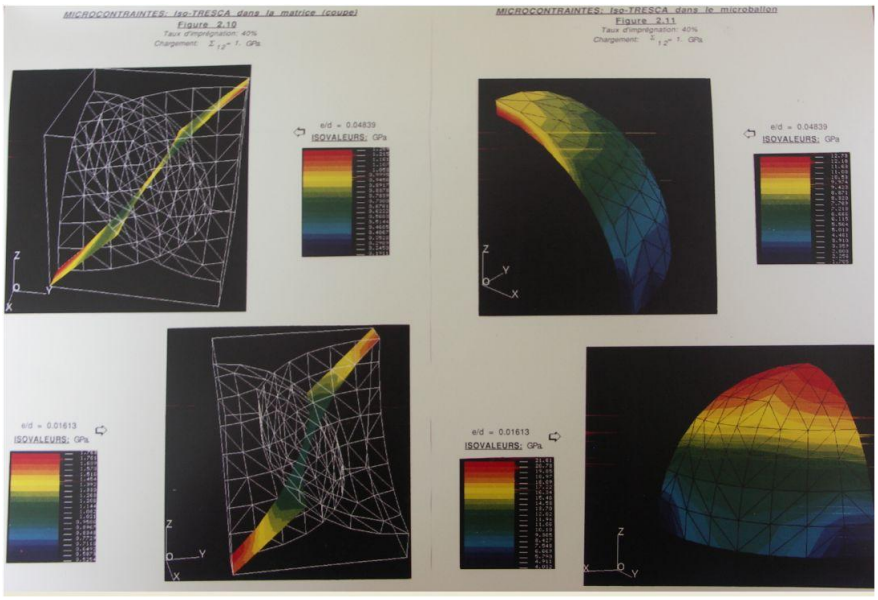

Figure 5 : Stress repartition in syntactic foam from [12]

Microscopic failure criteria were proposed including collapse of microspheres in tension and in compression. However, there was a lack of experimental results for validation of this model.

In addition to these studies, the work of Krzkechlowskii on the fracture mechanics of syntactic foam composites can be mentioned [13] [14]. A theoretical diagram of limiting states for syntactic foam composite was proposed (Figure 6).

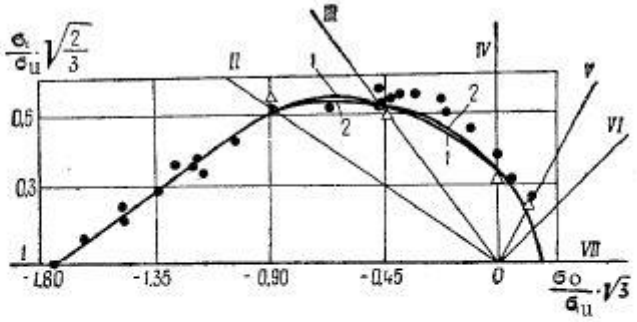

Fig. 3. Theoretical diagram of limiting states for the syntactic foam composite: I) hydrostatic compression; II) biaxial compression; III) uniaxial compression; IV) shearing; V) uniaxial tension; VI) biaxial tension; VII) hydrostatic tension 1) $\mu_\sigma = -1$; 2) $\mu_\sigma = +1$; • and Δ, experimental data from [11] and [12]).

Figure 6 : Diagram of limit state from Krzkechlowskii

In contrast to the proposal of Ben Hamida [12], where collapse of glass microspheres occurs in tension by exceeding the tensile strength of the glass, fracture is supposed here to occur mainly by disruption of the bond between the matrix and the filler.

More recently, most studies on syntactic foams have focused on three points which concern:

- the development of models in order to predict the thermo mechanical behaviour,
- the long term behaviour in a wet environment
- the characterization of the mechanical behaviour.

Concerning the predictive models most of these are limited to the elastic behavior, and are globally based on the same approach using homogenization techniques including RVE (representative volume elements) (Figure 7). Bardella [15, 16] ,Yuan [17], Rizzi [18] , Marur [19], and Brini [20] can be cited. These will be discussed in more detail in Chapter 4.

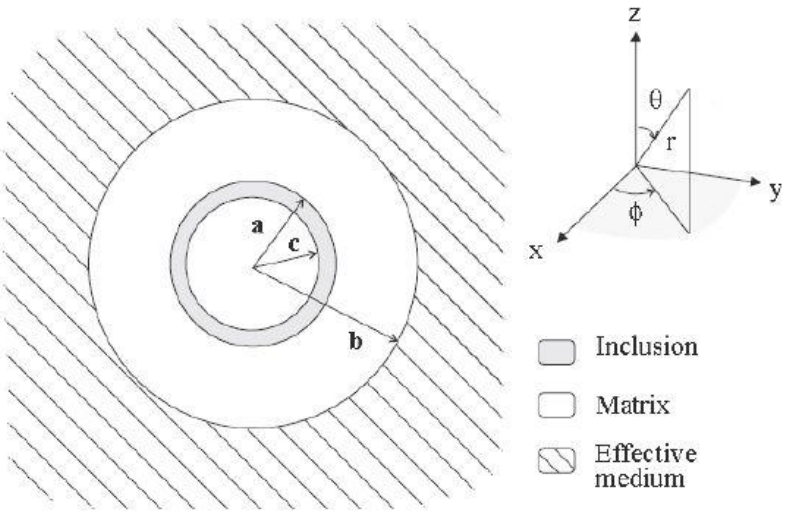

Figure 7 : Three phase model

Zouari [21, 22] has recently introduced the variability of the size of particles in a model, and identified a neutral size of particle for which the elastic properties of the material are independent of the volume fraction of particles. The model has been applied to introduce a damage parameter induced by hydrostatic pressure or glass degradation. This work has recently been completed by Antunes [23]

It should be underlined that all the models developed are based on a linear elastic behaviour of the matrix.

Due to novel applications in deep offshore oil exploitation, the long term behaviour in wet environment has recently been the subject of renewed interest. Following the initial general study of Avena[7] and additional work performed by Gupta [24], Kochetov [25], and Tagliavia [26]. Gimenez [27] has focused on the understanding of the hot wet aging of glass

epoxy syntactic foam. After a detailed review of the hydrothermal aging of amide cured epoxy and of glass aging, a phenomenological model of water absorption was proposed including: diffusion through the matrix, hydration of the glass surface and filling of the microspheres. The study examined syntactic foams with different types of glass microspheres in terms of chemical composition. 3D X-ray tomography and laser particle size measurements were used to characterize the geometry of the microspheres. Aging was performed in de-ionized water and artificial sea water at different temperatures and pressures, and different techniques (TGA, Impedance spectroscopy, …) were used to evaluate water absorption kinetics and degradation processes, Sauvant [28, 29]. These revealed damage to the microspheres in the syntactic foam induced by hot wet aging, and indicated the influence of the nature of water on the water absorption kinetics (de-ionized water diffuses more quickly and at higher levels than sea water).

Most of the studies performed on long term behaviour of syntactic foam concern epoxy syntactic foams. For this type of material, the basis of water absorption kinetic models has been developed.

The last point which is currently receiving considerable attention is the characterization of the mechanical behaviour of syntactic foams. This is of considerable importance in the qualification of materials for critical offshore components. It is one of the main subjects of this thesis and will be discussed briefly in the next section and then in detail in Chapter 2.

1.3 Mechanical characterization of syntactic foam

The characterization of the mechanical behavior of syntactic foams has been extensively studied during the last decade. For example, Carlisle et al. [30, 31] have used nano identation compression tests to identify micro balloon behavior. Thermo-mechanical analysis has been performed on foams using dynamic mechanical analysis (DMA) by Sankaran [32] and Lin [33]. The latter noted that the matrix glass transition temperature is affected by the filler content percentage. An original shear property characterization has been developed by Chavez [34] using a triaxial compression cell, but most published studies refer to compressive behavior, e.g. Kim [35], Gupta [36, 37], Karthikeyan [38], Song [39], Tagliavia [40], Aureli [41], Poveda [42], Porfiri [43]. Many of these studies are concerned with sandwich applications for marine or aeronautical applications. Adrien [44] has used an in-situ compression test under 3D X-ray tomography to identify the damage processes in epoxy, polypropylene and polyurethane glass syntactic foams, Figure 8.

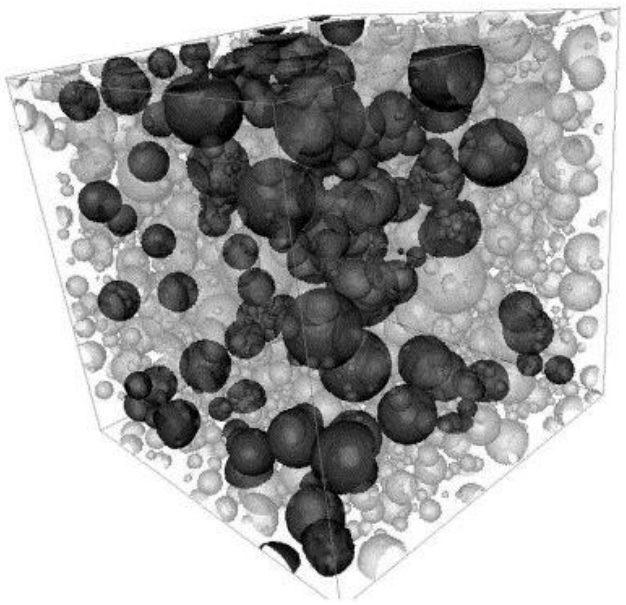

Figure 8 : Xray Microtomography 3D view of syntactic foam from [44]

It should be mentioned that this last paper is the only one presenting results on materials with a matrix other than epoxy or similar thermoset resins.

1.4 Applications of syntactic foams

The application areas of syntactic foams are very wide:

As noted above syntactic foams are used in the marine and oil industry for their buoyancy and thermal insulation properties. In addition to oil and gas applications, which will be detailed later, these materials are also used for buoyancy for submersibles and ROVs. As an example, the *Nautile* 6000 m manned submersible uses about 10 m^3 of high strength syntactic foam to guarantee the buoyancy of the structure. In order to limit the weight of submarine structures the French Navy uses these materials as cores of sandwich structures (in particular deck panels) and also in the design of large rudder panels, e.g. Lemiere [45].

These materials are also used in the aeronautical domain as densification resins and in the manufacture of moulds for structural composites.

When compared with classical core materials (PVC and PS foam, balsa, …) improvement in shear properties, impact resistance, and higher temperature of manufacturing and in use can be achieved.

In the automotive domain weight reduction can be obtained by incorporating glass microspheres in compounds in order to produce thermoplastic or thermoset syntactic materials.

Microwave applications are another domain where these materials are used. The structure of the foam confers interesting properties in term of low loss and low dielectric constant.

All these applications are detailed by Bibin [46] who recently provided an exhaustive review of applications and uses of syntactic foams. His book is divided into four chapters. The first chapter gives an introduction to syntactic foams. The basics of syntactic foams, matrix systems used in syntactic foams, different types of micro balloons, structure of syntactic foams, general methods of preparation and properties of syntactic foams are covered. Chapter 2 deals with syntactic foams based on different types of resin systems. Chapter 3 focuses on recent advances in the field of syntactic foams including fibre reinforced, nanoclay-reinforced, rubberised, functionally graded, core sandwich composites, and cement-based syntactic foams. The applications of syntactic foams in different fields are detailed in Chapter 4. The applications of some commercial grades of syntactic foams are presented in this chapter to give the readers a better understanding of the importance of these materials.

Once again it should be stressed that most of the literature addresses syntactic foams with epoxy matrix and that mechanical properties generally concentrate only on uniaxial compression behaviour.

1.5 Buoyancy application

As indicated in the introduction, syntactic foams were initially designed for submarine buoyancy applications. Figure 9 shows the Nautile submersible. This manned French deep sea submarine is described in detail below, in order to illustrate the interest and the need of high performance syntactic foam materials in terms of buoyancy.

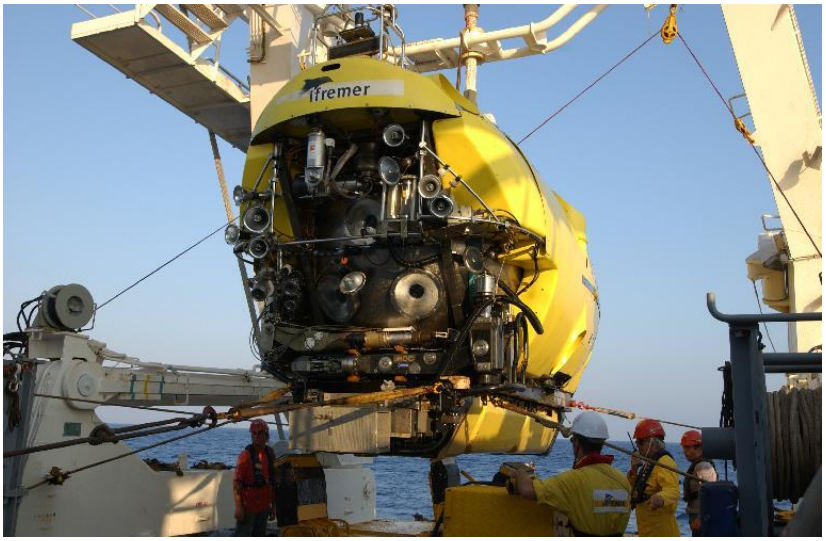

Figure 9 : Ifremer manned submersible, Nautile

In the 1970's the French Ocean Research Institute (at that time named CNEXO) decided to develop a manned oceanographic submarine. A study was given to the STCAN (Technical Service for the French Navy) to design the submarine. The main general requirements were as follows:

- Maximum operating depth : 6000 meters (this covers 97% of the deep sea ocean floor, and justified the design name of the submarine SM 97)
- 3 passengers (2 pilots and 1 scientist)
- Payload : about 500 kg of scientific equipment
- Maximum weight in air 18 Tons. This was imposed by the lifting capabilities of the naval support vessels.

Considering that in order to guarantee optimum safety the submarine must have a positive buoyancy of 3000 N (this does not include emergency safety possibilities) and taking into account all the equipment of the submarine (titanium sphere, engine …) and their payloads in air and in water, a requirement on the buoyancy can be obtained (see 6.1).

In this case a maximum specific gravity of the buoyancy material of 580 kg/m3 is requested.

Following the development of offshore oil exploitation in deep water the use of these materials has been expanded and the requirements for thermal insulation have led to new interrogations concerning the behaviour of these materials, in particular under hot wet conditions.

Although other fillers than glass microspheres can be used in the manufacturing of syntactic materials (polymer microballons, ceramic microspheres, carbon), only glass will be considered here. The characterization methods and models developed and reported in this dissertation can obviously be used or adapted for syntactic foams based on the other types of fillers.

1.6 Deep sea Oil & Gas exploitation

The present study is mainly concerned with the use of syntactic foam for deep offshore oil exploitation. Over the two last decades novel applications and properties have been extensively investigated in the domain of thermal insulation.

One of the biggest economical and technical challenges of the oil industry is deep sea exploitation in depths between 1500 and 3000 m, Bouchonneau [47]. This area is still hardly explored, and exhibits extraordinary potential. The areas concerned are the Gulf of Mexico, Atlantic margins off Brazil and West Africa (Nigeria, Angola, ….), Egypt, and Australia. (Figure 10).

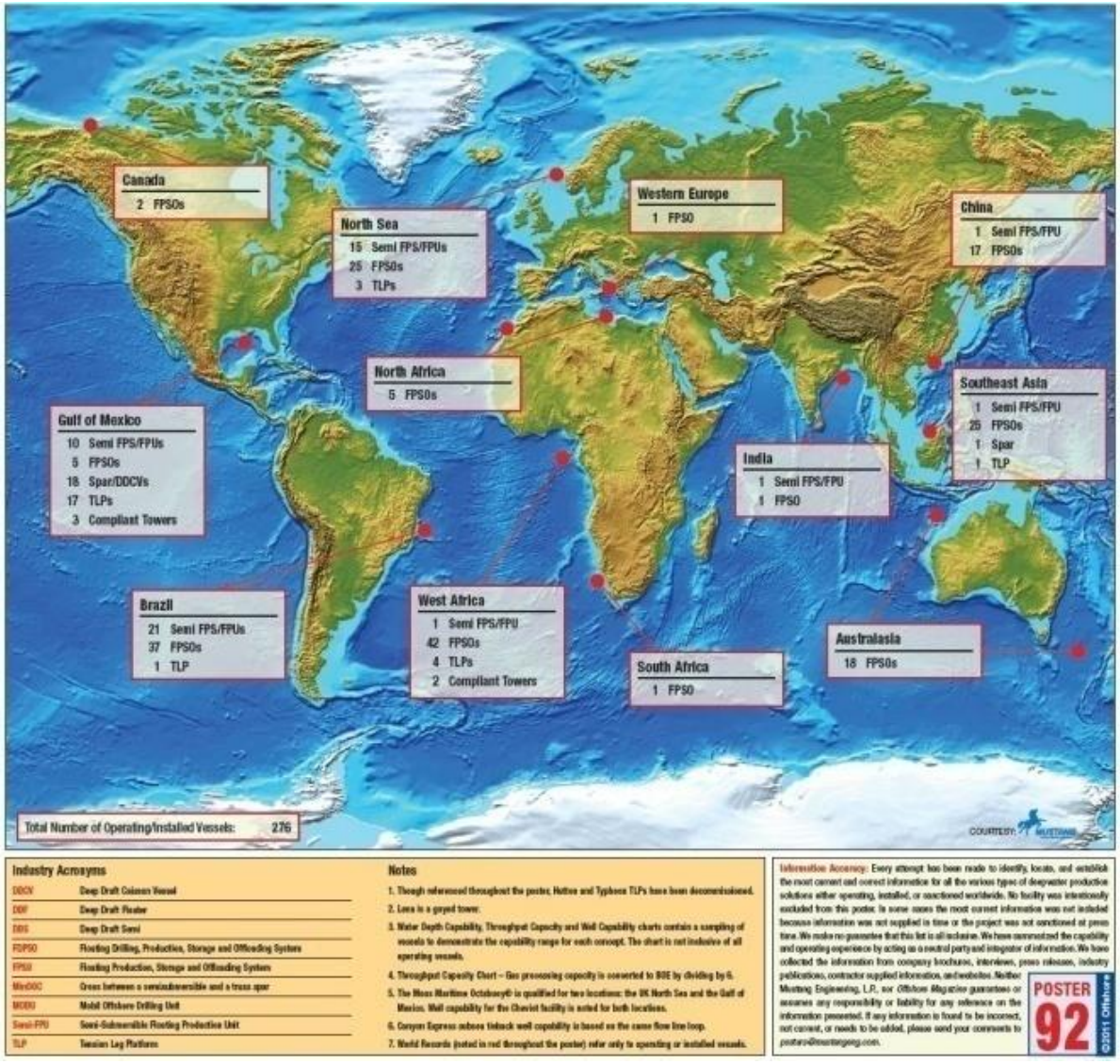

Figure 10 : Offshore oil exploitation potential

The potential reserves are estimated between 30 to 100 $*10^9$ of barrels equivalent petrol which can represent in 2015 25% of the whole offshore production. In recent years, the

offshore industry has beaten numerous records in terms of water depth to reach 3000 meters today (Figure 11).

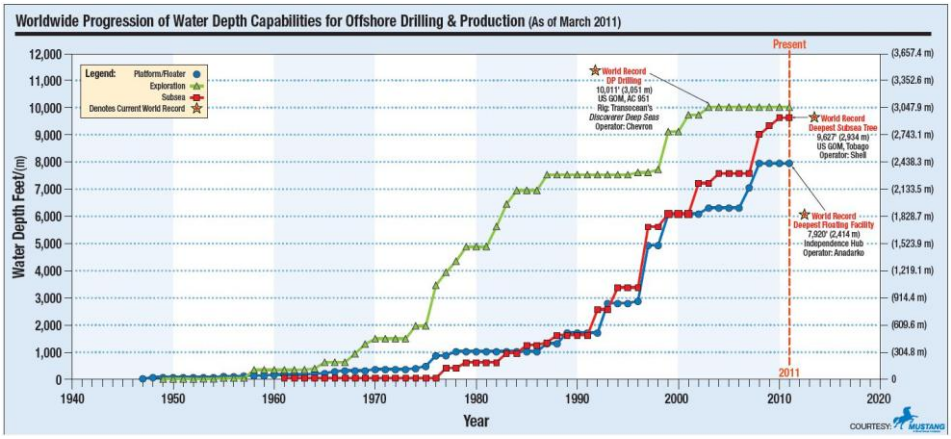

Figure 11 : Deep sea exploitation evolution

Another tendency is the development of subsea tiebacks, connecting new discoveries to existing facilities which can extend the life of production infrastructure, and minimize the development of new offshore structures. Length of tens of kilometres between the different wellheads of the same field can be involved (Figure 12).

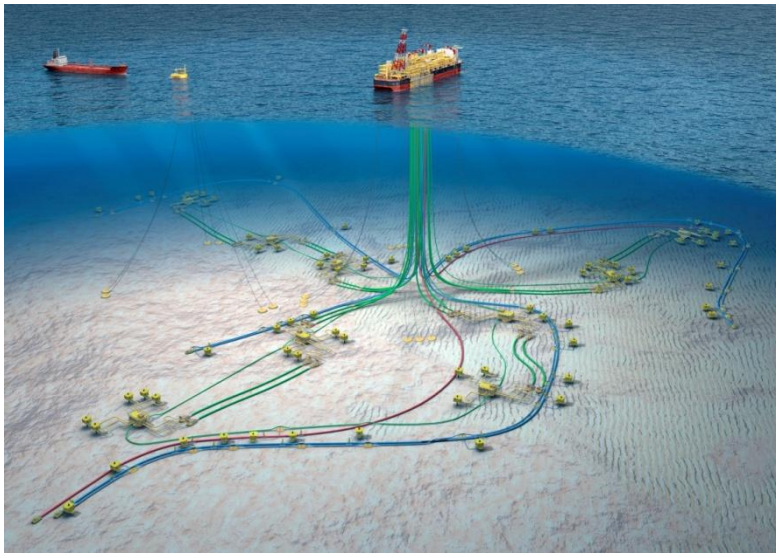

Figure 12 : Dalia West Africa Total Field

The volume of material used for this application can be considerable (>10 000 m^3). As an example [48] for a recently started field, Pazflor, a total length of 175 km of pipeline is installed in order to provide 220,000 barrels per day from subsea production systems including 49 wells. For this field new underwater separation (gas/liquid) units have been installed. The diameter of the pipe for liquid production is 10" (254mm) while for gas production flow 6" (152mm) diameter pipe is used. All require thermal insulation.

The increase in both water depth and length of tie backs in deep sea is driving flow assurance developments. At these depths the water temperature is around 4°C, while the oil effluent temperatures can reach, depending of the location, 150°C. The pipeline or subsea structures are also subjected to high pressures (about 30 MPa for 3000 metre depth) and the temperature of the effluent and of the external water result in high temperature gradients. The key point is to maintain the oil flow up to a design temperature (which depends on the field) in order to avoid wax and asphalt deposits and gas hydrate formation. Wax formation in subsea hardware occurs through the build-up of deposits as a result of decreasing temperatures. Hydrate formation within a multi phase flow can occur below a certain temperature. The formation of these hydrates within subsea structures can act as an obstacle for the flowing media causing reduced flow rates and can lead to physical damage to subsea systems. An example of a curve of hydrate stability is reported on figure 13.

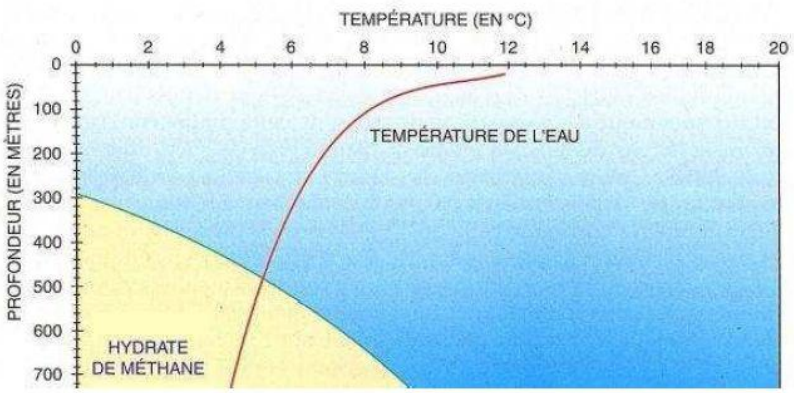

Figure 13 : hydrate stability curve

Globally the approach is to minimize the thermal leaks and to satisfy thermal property requirements for the structure: these are a maximum U value requirement together with a minimum cool down time requirement. The thermal performance requirements of a pipe are defined from flow insurance calculation (an example of such a calculation is given in [49]).

In terms of material properties the U value is then governed by the k value of the material. (see 6.2 for detail of calculation).

The cool down time (CDT) is the time taken for a fluid contained within a pipeline to reach a pre-determined temperature from a specified start temperature when fluid flow is stopped. The calculation of the cool down time is more complex than the calculation of the U value, and different methods of calculation can be used (lumped capacitance method [50], finite difference method, FEA …) but in terms of material properties the main parameters acting on the CDT value are the Cp, k and ρ of the material.

Different solutions have been proposed. Passive insulation by coating of the structure is currently the most common solution (non chemical flow assurance). For small depths foam products can be considered, but for deep sea applications other materials have to be

considered. Maximum temperature and depth of use are also parameters which must be taken into account in the choice of material.

In order to highlight the interest of using syntactic foam material in comparison with other insulation some properties of materials are reported on the Table 1 (data are informative).

Material		ρ (Kg/dm³)	Cp (J/g.K)	λ (W/m.K)	Max depth (m)
Solid polypropylene	PP	0.9	2	.23	N/A
Polypropylene foam	PP foam	0.7	2	.15	700
Glass syntactic Polypropylene	GSPP	0.66	2	.17	3000
Polyurethane	PU	1.15	1.7	.195	N/A
Glass syntactic Polyurethane	GSPU	0.72	1.7	.17	2000
Epoxy	EP	1.22	1.2	.22	N/A
Glass syntactic Epoxy	GSEP	0.7	1.2	.14	3000

Table 1 : nominal properties of insulation material

Improvements to these capacities can bring a significant economical gain.

For example, from a simple analysis based on a simple thermal model applied to a steel pipe with an insulating material layer, a gain in terms of thermal conductivity of the material will significantly affect the volume of material necessary to obtain the desired U value [51], particularly for small pipe diameters. In some cases a reduction in conductivity of the material of about 10% can reduce the volume of material by more than 30% (Figure 14).

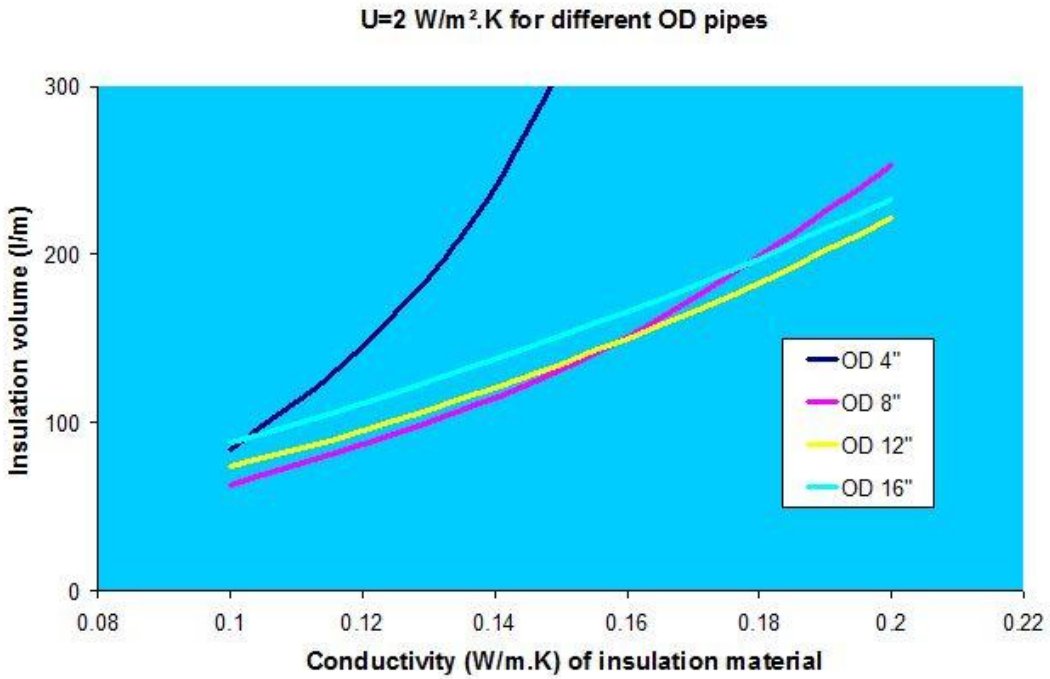

Figure 14 : Volume of insulation needed for coated insulated pipe (1 meter) to reach a U value of 2

When more stringent values, in terms of CDT and U, are required other solutions can be used such as pipe-in-pipe or pipe heating. These solutions are generally significantly more costly in terms of material and installation.

Ideally, the insulation material must have a low thermal conductivity, high resistance to hydrostatic pressure, and excellent long term behaviour in a deep sea environment. In addition to these properties, for some specific applications (i.e. riser tower) light weight is also required.

In order to illustrate the use of a syntactic foam, in this case GSPP (glass syntactic polypropylene), a typical design specification for a recent field (not specified in order to maintain the confidentiality of the data) is provided in 6.3.

Different solutions may be retained, and the choice is governed by different parameters:

- the service depth and maximum service temperature,
- the installation process of the structure, in particular for pipelines and risers.

The installation of pipes and riser is described in [52]. Different solutions can be retained (S Lay, J Lay, reeling, ...) and the loads generated during the installation process can govern the choice of insulation material. High elongations can be reached (5% for the reeling process)

during the installation, which may generate damage affecting the in service behaviour of the material.

An ISO committee has recently been set up in order to define a standard for wet thermal insulation coatings for pipelines, flow lines, equipment and subsea structures [53]. In the development of an industrial standard different points are being addressed, in particular the qualification of materials. Considering that syntactic foam is the most popular material in this domain both mechanical tests and wet ageing are being considered.

The draft standard is now in ballot, and for information the general qualification requirements are reported on Table 2

Layer property	**Test Specification**	**Room temp**	**Max temp**	**Min temp**	**Aged values**
Thermal conductivity	ISO 8301	X	X		**X**
Specific heat capacity	ISO 11357	X	X		
Hydrostatic test	Annex A	X	X		
Water absorption	ISO 62	X	X		
Density	ISO 1183	X			**X**
Tensile properties	ISO 527, ISO 37	X	X	X	**X**
Hardness	ISO 868	X			**X**
DSC (differential scanning calorimetry) +DMA (dynamic mechanical analysis) spectra	ISO 11357 (for DSC)	N/A	N/A	N/A	
Hydrostatic Creep	Manufacturer specific	X	X		

Table 2 : Test requirements for insulation material

Examples of structures using syntactic foam are shown on figures 15 to 17.

For pipelines the most common material is currently Glass Syntactic Polypropylene (GSPP). GSPP is directly coated onto pipe, by application of several layers of syntactic polypropylene

compound using side extrusion (thickness of each layer about 3-4 mm). Total thickness of the layer can reach 100 mm. Before application of the GSPP layers the pipe is coated with different layers in order to guarantee bonding of the material onto the pipe. The full system is known as Five layer Syntactic polypropylene [54] (Figure 15)

Figure 15 : GSPP insulated pipelines courtesy Socotherm

Glass Syntactic Polyurethane (GSPU) is also widely used, providing high elongation at break, and an easy and fast casting process. GSPU is directly cast onto subsea structures (Xmas tree, manifold, doghouse….) (Figure 16), and can also be used for pipe coating. It offers better thermal insulation than polyurethane elastomers. Glass microspheres are mixed with the polyol and then mixed with the isocyanate in a two component pump in order to be cast directly. However, GSPU offers a lower use limit temperature in comparison with most of the other syntactic materials. Currently, based on commercial recommendations, the use of GSPU is limited to 115°C while PU can be used up to 125°C.

Figure 16 : Subsea structure insulated with GSPU material (courtesy Trelleborg)

Syntactic epoxy foam was the first syntactic material used for this application, for the Girasol project which started producing oil in 2001 [55]. For this project epoxy syntactic foam was widely used to build a buoyancy tower, coupling with the same material the functions of buoyancy and thermal insulation. More than 10 000 m^3 of syntactic material were used. The chemical composition of the resin, in particular the type of hardener (amine or anhydride) governs the long term behaviour of the material in a hot wet condition. Amine hardener is generally retained due to the high temperature of the oil effluent. Glass syntactic epoxy is now widely used for drilling riser buoyancy modules (Figure 17).

Figure 17 : Insulation Covers (courtesy Trelleborg)

In order to increase the temperature limit, phenolic syntactic foam has also been proposed. This foam is used in a deep sea environment and is applied either fully bonded or as pre-cast multi layer components.

The volume contents of microspheres in the syntactic materials depend on the manufacturing process. Typically a volume content of 50-60% is reached for the epoxy material, while volume contents around 25% are obtained for GSPP and GSPU. Attention must be paid to the potential risk of collapse of the microspheres during the manufacturing process.

Large programmes aiming to evaluate the behaviour of syntactic foams for thermal insulation for deep sea applications started about 10 years ago. (Tideep JIP, Clarom). These programs have focused on different points:

- Providing a database of material properties
- Classical mechanical characterization (uniaxial compression and tension)
- Evaluation of the thermal and hydrostatic compression properties at different temperatures.

Aging of the material has also been considered. The aging test programs of the insulation materials have been performed at high temperatures and under hydrostatic pressures, to simulate the in service conditions

Materials were aged under hot wet conditions in seawater under pressure for 10000 hours. Water absorption kinetics were measured and properties of materials after aging were evaluated.

Aging was performed on samples of different sizes in order to provide data allowing a long term behaviour model to be established.

The results obtained show that for critical properties such as thermal conductivity or hydrostatic pressure resistance, the use of accurate testing protocols is necessary in order to obtain reliable results. Wet aging of the material is a critical aspect for the long-term behaviour. The prediction of the long term behaviour is only accessible through long duration tests coupling the temperature and the hydrostatic pressure. There is an influence of the nature of water for the aging test. Aging in de-ionized water is generally more aggressive than sea water in terms of water absorption kinetics, but this is strongly dependent on the nature of the polymer [56-58].

From these studies the damage development behaviour of the material has been identified [59].

1.7 Summary

To summarize this introduction:

- syntactic foams have a large field of application and some literature is available on their behaviour, mainly as sandwich material cores,
- the literature available on mechanical modelling is mainly limited to elastic behaviour,
- use of syntactic foam in deep water, which was initially limited to buoyancy, and to epoxy syntactic foam, is now completed by applications where thermal insulation is critical,
- use as a thermal insulation material has resulted in a new set of parameters: new materials (GSPP, GSPU, …) , consideration of temperature, coupling between water ingress, temperature and pressure,
- very few scientific studies have been performed on these topics,
- there is a need for improved, adapted, methods of characterization and modelling for deep sea applications,
- damageable behaviour of this type of material has been identified, and the kinetics must be identified.

1.8 Study overview

Considering these remarks, the scope of the present study has been established.

For the choice of material, two generic classes of material have been retained:

- Glass epoxy syntactic foam

- Glass syntactic polyurethane.

This choice was governed both by the current applications and future requirements. Materials were available from various previous studies carried out at Ifremer.

However, taking into account non disclosure agreements signed with the partners of the previous studies (sponsors and material manufacturers) no commercial material references will be given.

The nominal properties of these materials are described in Table 3.

denomination		Type of microsphere	Specific gravity	Manufacturing process
GSPU	Glass syntactic polyurethane	3M S38	0.860	Casting
GSPE	Glass syntactic epoxy	3M S38	0.720	Casting

Table 3 : Nominal Characteristics of material tested in this study

The main objective of the experimental study is to provide reliable data for the establishment of a behaviour model suitable for all types of syntactic foams.

Considering the behaviour of the syntactic foam, the study will focus on the mechanical behaviour, and in particular the identification and quantification of damage.

For each type of test in the experimental part of the study the following points are developed:

- definition and description of the experimental set-up,
- description of the associated experimental procedure,
- examples of relevant results obtained, providing data for the establishment of models.

All these tests are original, and most have been specifically developed for syntactic foams, both at Ifremer and in collaboration with different partners.

The tests which have been developed are reported in the following table

- evaluation of mechanical properties from ultrasonic wave speed measurements
- instrumented hydrostatic compression test
- uniaxial compression test
- hydrostatic compression test associated with acoustic emission
- shear test
- evaluation of the percentage of collapsed glass microspheres by means of physical techniques including a gas pycnometer

- in-situ compression test under hydrostatic pressure and evaluation of percentage of collapsed glass microspheres, by means of X-ray microtomography.

The water uptake kinetics under different conditions of temperature and pressure will not be addressed in this report. Descriptions of testing methods and results have been detailed elsewhere [60]. In that paper a water uptake model has been developed and predictions are compared to experimental results. The model allows the water profile uptake of a thermal insulated structure subjected to real service conditions to be estimated (hydrostatic pressure and through thickness temperature gradient).

Chapter 2. EXPERIMENTAL CHARACTERIZATION

In order to be able to model and predict the mechanical behaviour of syntactic foam structures it is essential to possess reliable property data. An extensive characterization campaign has been carried out, both to evaluate the limitations of existing test methods and to propose new improved test procedures.

2.1 Elastic constants from ultrasonic wave speed measurement

The use of ultrasonic wave speed measurement techniques for the determination of elastic constants has been evaluated on syntactic foam. Mylavarapu [61], has used this method to evaluate mechanical properties of syntactic foam using a pulse echo method. An immersion technique is used here, in order to investigate compression and shear waves.

This method will be investigated on syntactic foam here in order to verify its potential in particular:

- to provide information on G and ν values of the material,
- as a non destructive technique to follow the evolution of the mechanical properties during aging sequences.

2.1.1 Presentation

The method of Christoffel tensors allows, for a given material, the speed of ultrasonic waves to be related to the elastic constants of the material. This technique has been widely used in the field of composite materials for the determination of anisotropic elastic constants [62, 63] and will not be developed in detail here.

In the present study, an evaluation of the different compression and shear wave speeds has been carried out first, on samples of different thickness with different sensors, in order to determine the most suitable sensor for this measurement.

The elastic properties determined from this method will then be compared with the values obtained using the other methods developed in this study.

2.1.2 Principle

The method of determination of elastic constants from ultrasonic wave speed measurement consists of injecting in the fundamental laws of mechanics the solution for a displacement u having the shape of a sinusoidal wave.

the displacement vector u is in the form:

$$u_i = u_i^\circ . \cos(\omega . t - k . p_j . x_j)$$

With

u_i° polarization of the wave

p_j vector of direction of wave propagation

k wave number : $k = \omega / V$ with V = speed of the wave propagation.

The fundamental law of dynamics applies to the materials and can be expressed as:

$$\rho \frac{\partial^2 u_i}{\partial t^2} = \sigma_{ij,j} + f_i$$

With

ρ : specific gravity

σ : stress tensor

f : volume force field (here =0)

Resolution of the problem is not detailed here, but can be found in references [64][65, 66]

The following equation is obtained by considering the density as a constant and uniform in the material:

$$\rho . V^2 . u_i^\circ = u_l^\circ \times \Gamma_{il}$$

where:

$$\Gamma_{il} = C_{ijkl} . p_j . p_k$$

Note: The assumption of constant and uniform density of the material may obviously be discussed but must be considered at the wavelength scale.

Γ is the Christoffel tensor and is symmetrical. As a consequence the Eigen values are real and positive and the Eigen vectors are orthogonal.

The speed and the polarization of the plane wave propagating in the p direction in a body with Cijkl stiffness are obtained by solving for the Eigen values and Eigen vectors of the Christoffel tensor.

In order to obtain the Eigen values the following equation is solved:

$$\Gamma_{il} - \rho.V^2.\delta_{il} = 0$$

Eigen values depend on the stiffness, the specific gravity and the wave speed.

For each Eigen value, the u Eigen vector is then calculated and corresponds to the polarization of the wave considered.

The knowledge of Eigen values allows the relation between stiffness sensors C and the scalars ρ and S to be established. Using this method, the stiffness tensors of a material can be determined from the study of the transmission of ultrasonic waves through the material.

If the material is isotropic, the method based on Christoffel tensors gives simple results which are summarized in the two following equations:

$$S_C^2 = \frac{E(1-\nu)}{\rho(1+\nu)(1-2\nu)} \qquad S_s^2 = \frac{G}{\rho}$$

With

S_c = speed of compression wave

S_s = speed of shear wave

More complex relations can be established for orthotropic materials, and this method allows the 9 elastic constants of an orthotropic material to be obtained, making it very interesting in the study of composite materials.

2.1.3 Equipment

In order to generate ultrasonic waves and analyze their behaviour a test setup based on an ultrasonic inspection in an immersion tank (water) has been designed (Figure 18 & 19). Two wide bandwidth ultrasonic sensors are placed face to face in the water tank. One sensor is used as the emitter and the other as the receiver. One sensor is fixed and the other can be moved laterally by means of a precision step motor. The specimen is placed between the two sensors and can also be rotated by means of a second precision step motor. The distance between the sensors is optimized, in order to avoid analysis in the depth zone of the sensors.

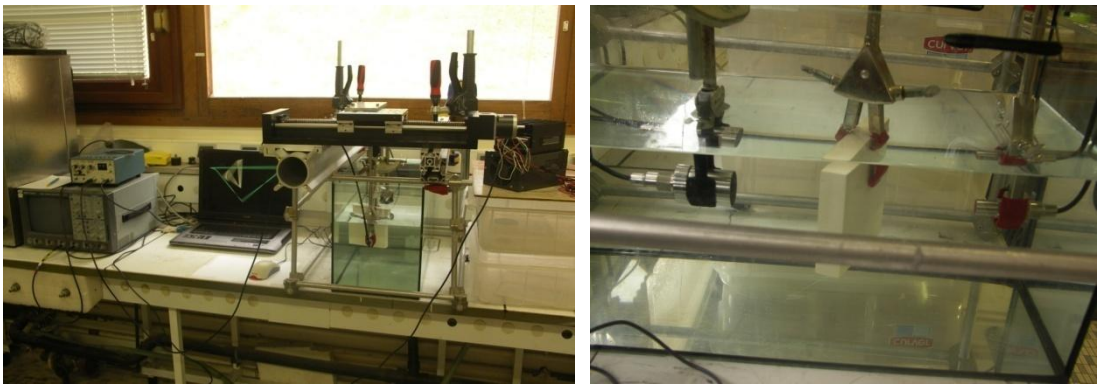

Figure 18 : Photos of ultrasonic equipment

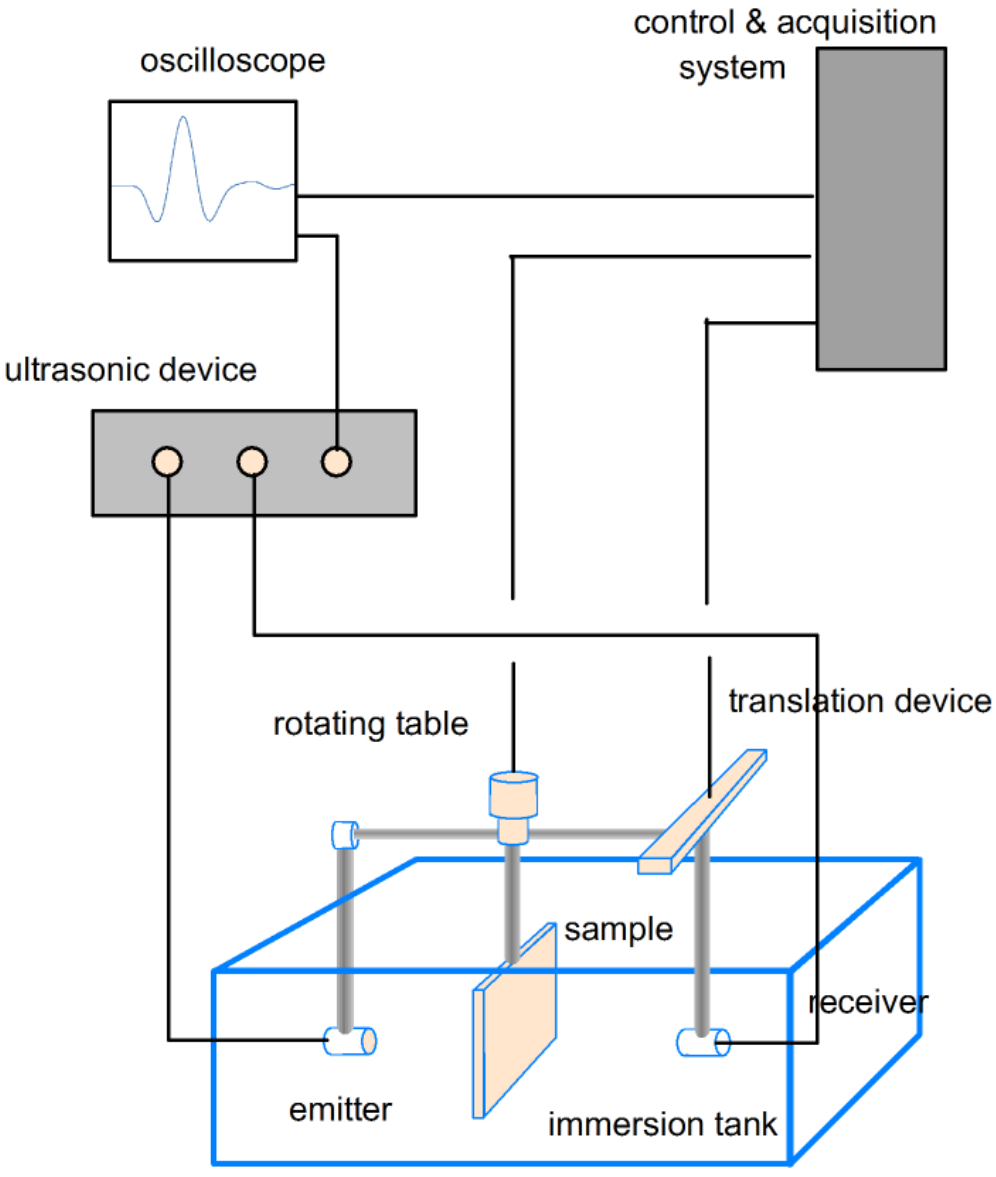

Figure 19 : Schematic diagram of ultrasonic equipment

2.1.3.1 Close range zone

In the close range of a sensor the ultrasonic signal is difficult to analyze. The close range is limited by the distance N, given by:

$$4\lambda.N = D^2$$

where

- λ is the wavelength (=C/f),
- D is the sensor diameter.

2.1.3.2 Central Frequency

Taking into account the nature of the material tested, which may induce diffraction phenomena due to heterogeneity at the wavelength size, the central frequency has to be chosen in order that the wavelength is significantly higher than the largest pattern of the material. A decrease of the central frequency of the sensor will result in loss of resolution of the signal, so a compromise has to be found between resolution of the sensor and wavelength. The central frequency of the sensors has been limited to 2 MHz here.

2.1.3.3 Sensor diameter

Another parameter affecting the choice of sensor is the diameter of the sensor. With a large diameter the power of the emitted signal is much higher, simplifying the signal detection, but this increase induces an increase of the divergence angle of the signal. This divergence angle has to be limited in order to localize the signal on the zone to be analyzed and to favour the generation of planar waves. The localization of the beam requires an accurate device for the positioning of the receptor sensors. The divergence angle is characterized by

$$D.\sin(\alpha) = 1.22\lambda$$

2.1.3.4 Damping

To conclude on the choice of sensor types and in order to increase the resolution of the signal, large bandwidth sensors (high damping) have to be chosen.

Based on all these considerations 2 sensors were retained for this study, with the characteristics reported on the Table 4.

Central frequency	2.25 MHz	0.5 MHz
Sensor references	NDT system 2.25/.500dia	QMI LRI 29/05
Diameter (mm)	12	15
Depth zone N (mm)	48.6	19.0
Angle α (°)	4.3	6.1

Table 4 : Ultrasonic sensors characteristics

2.1.3.5 Equipment used

The following table summarizes the type of equipment used for the measurements.

Acoustic amplifier	Type Pulser-receiver Sofranel 5077Pr
Oscilloscope	ACUTE type DS 1202
Rotating table	Computmotor CK57-61
Translation device	Parker M506-121S

Table 5 : Ultrasonic equipment

2.1.4 Immersion through-transmission technique

In a liquid only compression waves are generated. In a solid, both compression and shear wave are generated as shown on figure 20 following Descartes' law. At each interface, waves are reflected and transmitted. The reflected waves are not considered here. These transmitted waves (shear and compression waves) in the material will be transmitted at the material-water interface and converted in the liquid into compression waves. These waves will be analyzed to determine the compression and shear wave speeds in the material.

The path of ultrasonic waves in a through-transmission technique is shown on Figure 20.

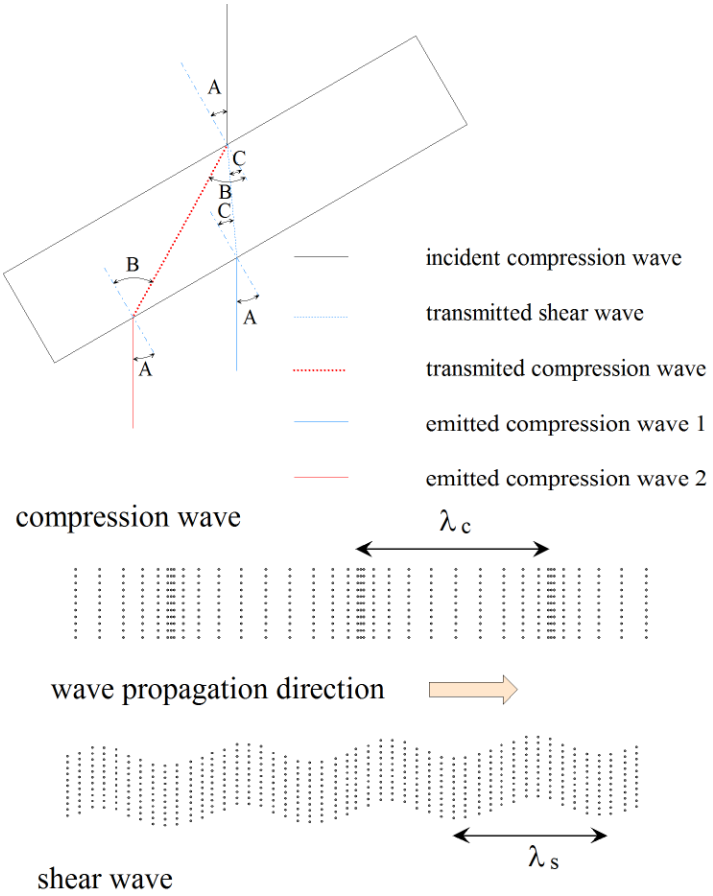

Figure 20 : Ultrasonic waves propagation

With

$$\frac{sinA}{S_w} = \frac{sinC}{S_s} = \frac{\sin B}{S_c}$$

And S_w = speed of the wave in water

The measurement principle is to study the time of flight change of the ultrasonic wave when a piece of the material to be studied is incorporated between the sensors. Knowing the change in flight time, the thickness of the sample and the wave propagation speed in water, the wave speed in the material can be deduced.

Then the sample is placed at a different angle between the two sensors and the time flight delay is again measured, in order to evaluate the speed of the two different waves.

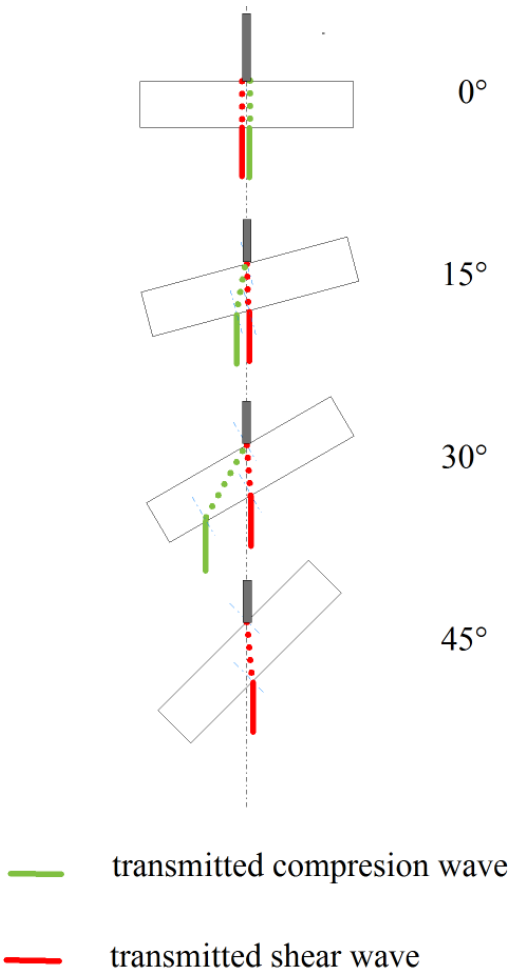

Figure 21 : Travel of ultrasonic waves for different incident angles (true angles for GSEP)

2.1.5 Time delay determination

Knowing the thickness of the material, the wave speeds are calculated from the measurement of the time delay between the signal observed in direct incidence with no material and the signal observed after incorporating the material between the emitter and the receiver.

Classically this time delay can be determined by using different methods which have been implemented as a function in Matlab™ software:

- maximum of the cross correlation function,
- Hilbert's transform.

Considering two signals f and g, the cross correlation method consists in calculating:

$$I(\Delta t)=\int f(t)g(t-\Delta t)\partial t$$

where I is called correlation function. This function is a maximum for Δt which corresponds to the delay between the two signals.

Hilbert's transform of a s(t) signal is obtained by convolution of the signal by the function $1/(\pi.t)$. Then:

$$TH(s)(\tau)=\int \frac{s(t)}{\pi(t-\tau)}\partial t$$

The method consists of calculating the Fourier transform of the two signals and identifying the abscissa where the value of the transform is zero, and then to subtract them. If there is more than one root, a mean of the different delays can be calculated.

This method is described in the document [67].

In order to improve the method, to take into account an eventual phase shift between the two signals considered (Figure 22), we have operated as follows:

- First the cross correlation method is calculated;
- The Hilbert transform of the cross correlation transform is then calculated to obtain a complex function;
- The modulus of the complex function is calculated to obtain the envelope of the cross correlation function;
- Finally the abscissa of the maximum of the function corresponds to the delay between the two signals.

It can be noted that Hilbert's transform reveals the envelope of the cross correlation function. The maximum of this envelope does not necessarily correspond to the maximum of the signal as show in the Figure 23. The cross correlation function is reported in red with the maximum

noted at 760. The maximum of the envelope reported in blue is noted at 730, which must be used as the delay time.

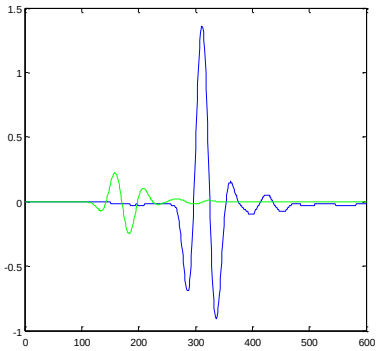

Figure 22 : Ultrasonic signal

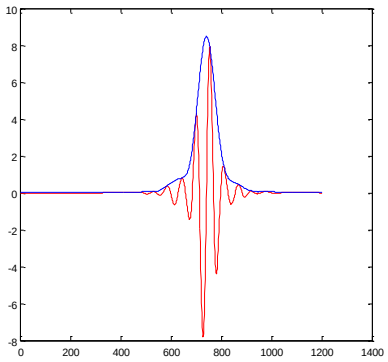

Figure 23 : in red, cross correlation function; in blue, envelope of the cross correlation function

The method coupling cross correlation with Hilbert transform has been implemented in MatLab ™ and is detailed in 6.4.

2.1.6 Wave speed evaluation

As the delay between flight times with and without the sample can be estimated using the method presented above, the geometrical calculation allowing the wave speed to be estimated is now presented. This calculation has to take into account the angle between the sample and the sensors as reported on figure 24.

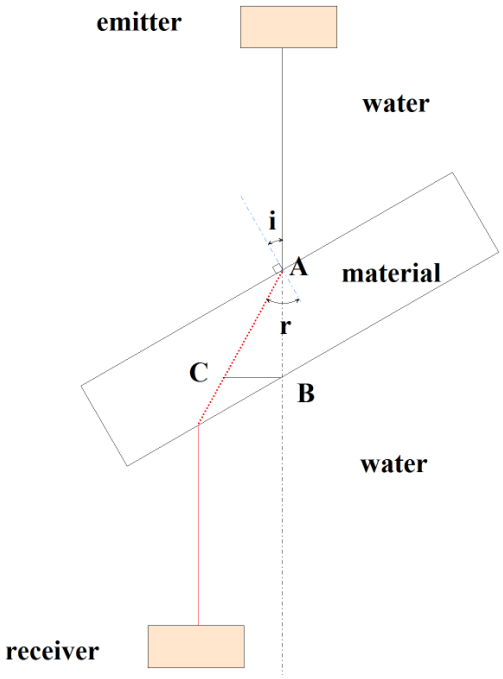

Figure 24 : Ultrasonic waves path

$$\Delta t = \frac{AC}{Sw} - \frac{AB}{Sm}$$

where :

- Sw the wave speed in water,
- Sm wave speed in material (unknown).

Trigonometrical formulae give:

$$AB = \frac{e}{\cos(r)}$$

$$AC = e * \frac{\cos(i-r)}{\cos(r)}$$

Noting n the ratio Ve/Vm, Snell-Descartes' law gives :

$$\frac{\sin(i)}{n}=\sin(r)$$

Then Δt can be expressed as a function of the thickness e, the incidence angle i, and the wave speeds Sw and Sm :

$$\Delta t = \frac{e}{Sw}\left(\cos(i) - \sqrt{\left(\frac{Sw}{Sm}\right)^2 - \sin(i)^2}\right)$$

Or:

$$Sm = \frac{Sw}{\sqrt{1+\frac{Sw.\Delta t}{e}\left(\frac{Sw.\Delta t}{e} - 2.\cos(i)\right)}}$$

2.1.7 Measurement

For a given specimen the technique consists of collecting the signal with and without the specimen. With the rotating device the incident angle is controlled from 0° to the limit refraction angle at the first interface with a 5° step. The measurement is performed for the two different waves.

Samples of different thicknesses have been machined. These samples are 100 mm square blocks of 5, 10 and 20 mm of thickness, figure 25:

The measurements have been performed at 20°C (+/-1°C) with tap water as the immersion liquid.

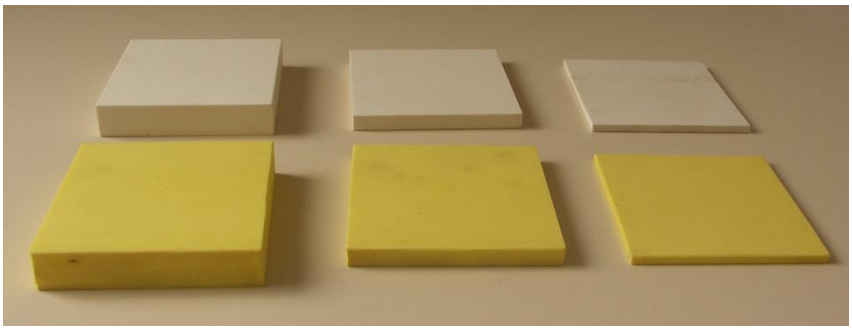

Figure 25: Specimens for ultrasonic evaluation

In Figure 26 an example of the signal obtained for the compression wave in a 20 mm thick sample of epoxy syntactic foam is given

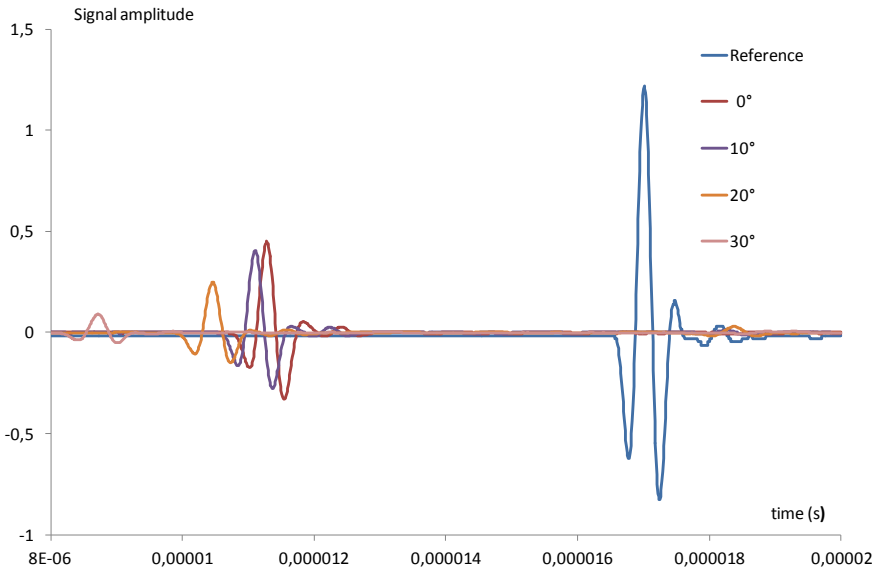

Figure 26 : ultrasonic signal at different angles for GSEP (20 mm thick)

From right to left can be noted:

- The reference signal (without any specimen between the two sensors) (amplitude reduced by 100)
- 10° angle incidence signal,
- 20° angle incidence signal,
- 30° angle incidence signal.

Two examples of speed measurements are reported on Figure 27 & 28. The speeds are reported in polar coordinates.

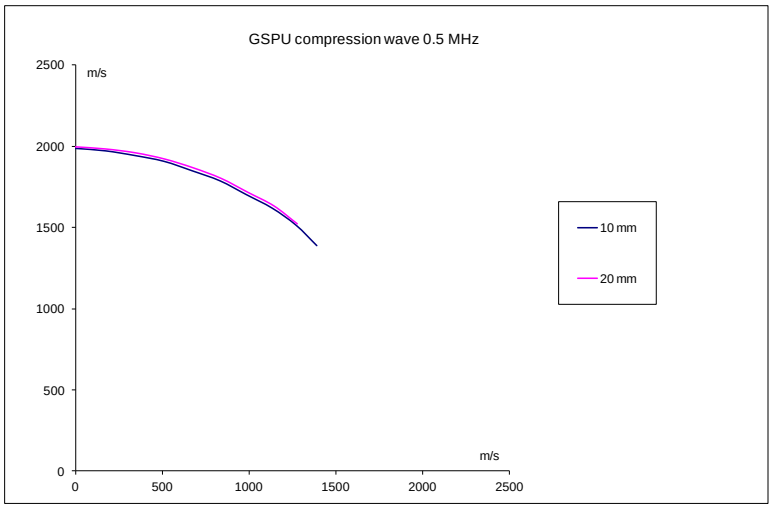

Figure 27 : polar diagram of compression wave speed for GSPU

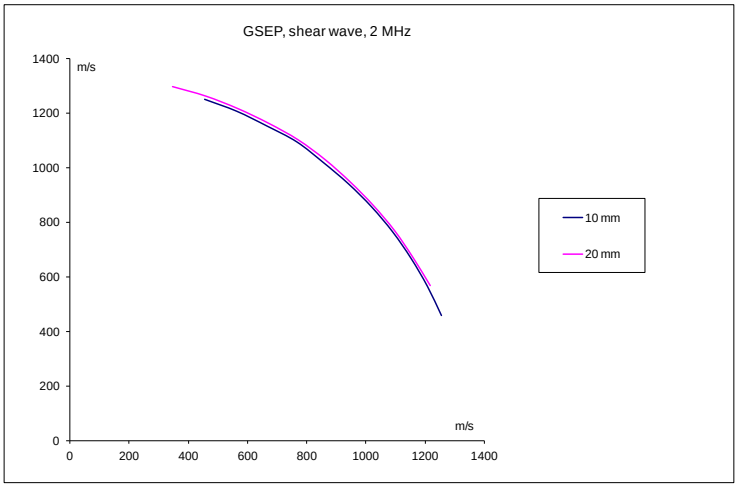

Figure 28 : polar diagram of shear wave speed for GSEP

In direct incidence, the change of amplitude between the signal and the reference signal can be used to estimate the damping of the material. The immersion technique guarantees constant coupling between the sample, the coupling media (here water) and the sensors. Investigations of this amplitude change have been performed, but the results obtained are very difficult to analyze to evaluate the damping of the material. A significant influence of the surface state of the specimen has been noted. The machining of the surface induces local breakage of the microspheres, which generate an imperfect interface polluting the wave transfer.

2.1.8 Results

The wave speed measurement results are reported on table 6.

These results are the means of three measurements performed on samples of 10 and 20 mm. The Cv (Coefficient of variation in %) obtained for the 5 mm specimens were very high (>20%) and are not reported.

GSEP	**Speed (m/s)**	**Cv (%)**
Compression 0,5 MHz	2492	2
Compression 2 MHz	2535	9
Shear wave 0,5 MHz	1325	6
Shear wave 2 MHz	1337	4

GSPU	**Speed (m/s)**	**Cv (%)**
Compression wave 0.5 MHz	1949	0.7
Compression 2 MHz	2008	10
Shear wave 0.5 MHz		N/A
Shear wave 2 MHz	390 *	> 10

Table 6 : Wave speed measurements

* The results from wave speed measurements of the shear wave for GSPU are only reported for the 2 MHz sensors. The damping of the wave is very important and time delay is difficult to evaluate at 0.5 Hz.

From these results the elastic properties of the material can be calculated (see method in 6.5) and the results are reported on Table 7.

	GSEP	GSPU
Young's modulus E	3 GPa	393 MPa

Coefficient Poisson ν	0,3	0,48
Shear modulus G	1.15 GPa	133 MPa
Bulk modulus K	2.56 GPa	3.3 GPa

Table 7 : mechanical properties from ultrasonic evaluation

The accuracy of the value calculated is mainly governed by the homogeneity of the material. For the same piece of material repeatability of ultrasonic speed measurement is generally better than 0.3%.

2.1.9 Conclusions

Determination of elastic constants of syntactic foams has been performed using ultrasonic speed measurements.

The measurement was performed by immersion using the through-transmission technique.

To use this technique specimens of thickness greater than 10 mm are necessary.

2 MHz is the optimum frequency for this measurement. At higher frequency the wavelength of the signal is small in comparison with the dimensions of the material and internal diffraction of waves in the material makes it difficult to recover a proper signal. At lower frequency the accuracy obtained on the determination of wave speed is not sufficient.

For GSEP material the method is suitable for shear and compression waves and for the determination of the elastic constants

For GSPU material, taking into account the damping of the signal, the method is not suitable for determination of shear wave speeds so the accuracy on the determination of the Coulomb modulus is low. For materials with high damping other techniques have to be developed [68].

The use of this method to evaluate the damping of these materials is not straightforward and requires more study. The machining of the specimens results in a surface roughness state which is incompatible with accurate measurement of damping due to a variable interface (broken glass microspheres).

An original method coupling cross correlation and Hilbert transform has been implemented for the determination of time delay and then for the determination of wave speed.

2.2 Uniaxial compression test

Uniaxial compression tests are frequently used to provide information on the behaviour of syntactic foams.

2.2.1 Test specimen

Different standard tests are available, for example, ASTM D695M (compressive properties of rigid plastics) [69], and ASTM D1621 (compressive properties of rigid cellular plastics) [70], but considerable liberty is left in terms of sample geometry.

From ASTM 695 it is specified: "the standard test specimen shall be in form of a right cylinder or prism whose length is twice its principal width or diameter. Preferred specimen sizes are 12.5 by 12.5 by 25 mm (prism) or 12.5 mm in diameter by 25 mm (cylinder). Where elastic modulus and offset yield-stress data are required, the test specimen shall be of such dimensions that the slenderness ratio is in the range of 11 to 16:1. In this case, preferred specimen sizes are 12.5 by 12.5 by 50 mm (prism), or 12.5 mm in diameter by 50 mm (cylinder). When testing syntactic foam, the standard test specimen shall be in the form of a right cylinder 25 mm in diameter by 50 mm in length."

The ASTM D1621 specifies: "The test specimen shall be square or circular in cross section with a minimum of 25.8 cm^2 and maximum of 232 cm^2 in area".

Considering these points and the facility to machine cylindrical samples the following test samples have been chosen (Figure 29) here.

Figure 29 : Uniaxial compression samples

Type	Shape	Diameter (mm)	Length (mm)	Calibrated Length (mm)
1	Right cylinder	12.5	25	25
2	Right cylinder	30	25	25
3	Dog bone cylinder	13	65	27
4	Dog bone cylinder	13	90	50

Table 8 : compression sample geometry

The type 1 sample is homothetic to the recommended specimen for syntactic foam from the standard.

The type 2 sample has been retained to limit the eventual buckling of the sample.

Types 3 (Figure 30) and 4 were designed in order to limit the “barrel effect” and to be close to the sample proposed by the standard for thick samples. This shape aims to localize the deformation in the calibrated part of the specimen, and to limit the edge effects at the load introduction area.

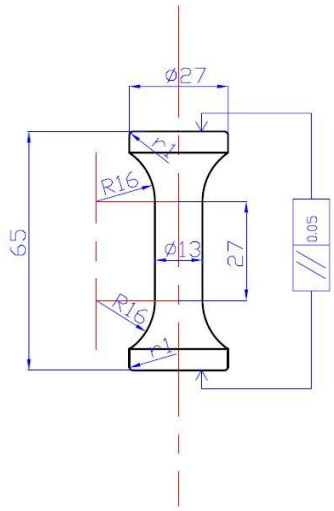

Figure 30 : Type 3 compression sample

All the tests were performed at 20°C +/-1°C at 50RH%. Loading rate was 2 mm/min.

2.2.2 Results

Examples of the results obtained from preliminary tests on the two materials are reported below, both in terms of stress-displacement and stress-strain.

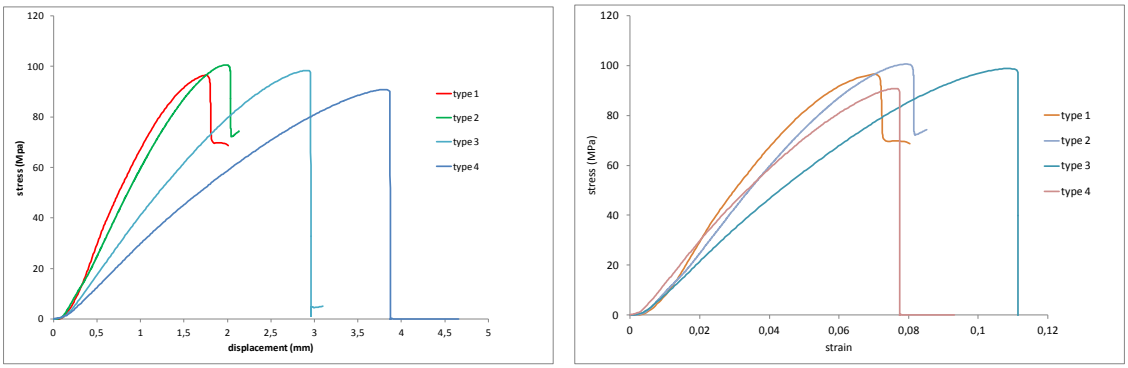

Figure 31 : GSEP uniaxial compression

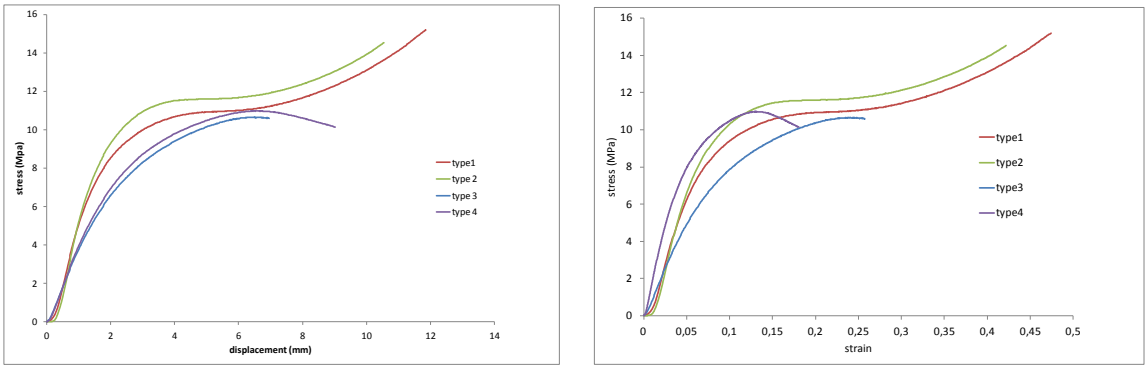

Figure 32 : GSPU uniaxial compression test

The curves reveal non linear behaviour, so it is difficult to determine a single compression modulus.

Significant barrelling is observed for GSPU for samples 1 and 2 while buckling occurs for specimens 3 and 4.

For GSEP it should be mentioned that the shape of the curves is significantly different from the shape of the stress-strain curves generally reported in the literature (Figure 33).

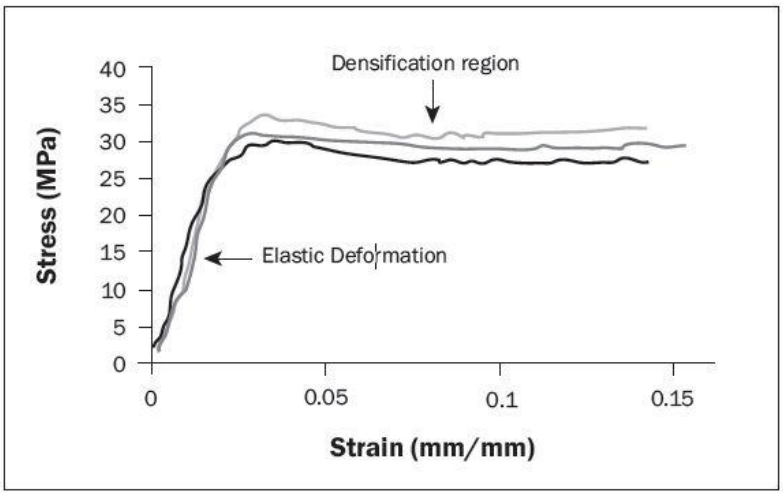

Figure 33 : Classical compression curve for syntactic foam (from [46])

The material tested in our study is significantly stronger than the material classically encountered. The nature of the microspheres, the ratio microsphere/matrix, and the stiffness of the matrix all influence the stress at break and here the densification region which is generally mentioned is not observed. In addition the part which is often termed elastic is here notably non linear and must be investigated in more detail.

Samples equipped with strain gauges have then been tested in order to evaluate the Young's modulus and to evaluate Poisson's ratio of the materials (Figure 34).

Figure 34 : Instrumented specimen

In addition an axial extensometer was used to complete the measurement.

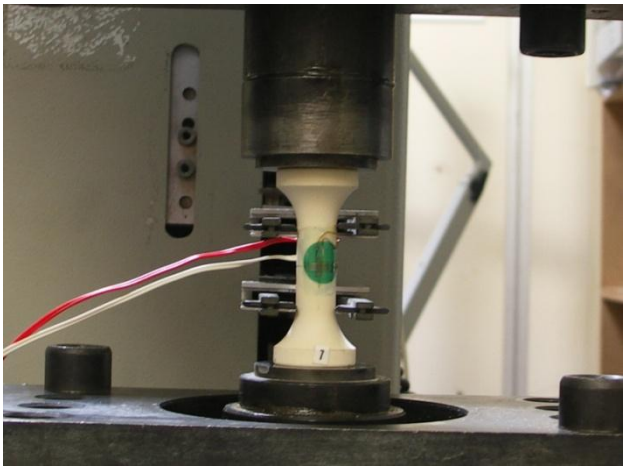

Figure 35 : Specimen with extensometer and strain gauges

Indications noted from strain gauges and extensometer are mainly comparable for type 3 and no real conclusion can be emitted on the most pertinent sample geometry to perform the test.

Load-unload cycles have been performed in order to characterize the behaviour of the material with samples type 3.

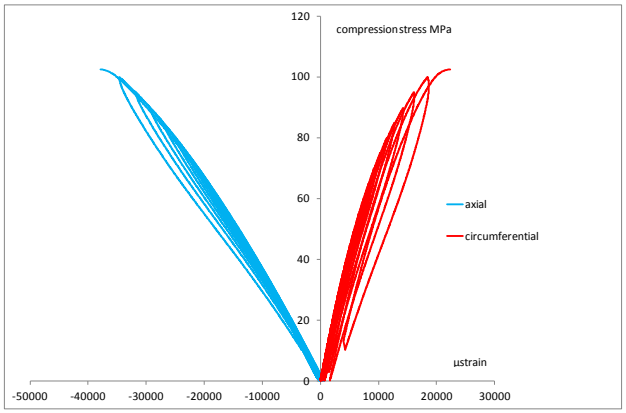

Figure 36 : GSEP load unload compression test

The behaviour of GSEP under uniaxial compression is not purely linear elastic. Small residual deformations after loading, in particular in the circumferential direction, are noted revealing damage occurrence.

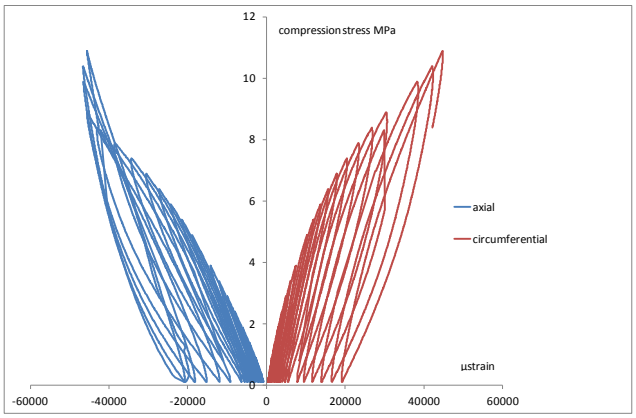

Figure 37 : GSPU load-unload compression test

For GSPU, the material exhibits complex visco elastic damageable behaviour followed by a densification phase. Taking into account the low rigidity of the sample type 4 is not suitable for this material (buckling occurs) and in order to avoid "barrelling" on the calibrated area sample type 3 seems to be more suitable.

The apparent initial elastic parameters (linear regression between 0.001% and 0.01%) of the materials are reported in Table 9 (mean of 3 samples type 3).

	GSEP	GSPU
E comp (MPa)	3340 +/- 6.1%	432 +/-8.4%
Poisson's Coefficient ν	0.34 +/- 2%	0.49 +/- 8%
Stress at break (MPa)	97.8 +/- 5.3%	11.7 +/- 7.5%

Table 9 : Uniaxial compression test

It should be mentioned that the evaluation of the modulus for GSPU, by following the standard (measure of the global displacement) will provide a Young's modulus value around 250 MPa. Early damage occurs in the specimen, particularly on the edges of the sample, and then the measured global strain will be overestimated.

2.2.3 Conclusions

The uniaxial compression behaviour of the syntactic foam tested in the present study is slightly different to that generally presented in the literature.

Non linear behaviour of the material is apparent and for the material with low stiffness (GSPU) buckling can govern the collapse of the specimen.

Pertinent uniaxial compression tests are not easy to perform for syntactic foam. Damage initiated at specimen edges will pollute the results if the standard is followed.

Instrumented specimens are needed to in order measure appropriate data, and a new type of sample is proposed (specimen type 3)

2.3 Hydrostatic compression test

Hydrostatic compression is the main loading condition for submarine structures. In the case of buoyancy, the material is purely loaded hydrostatically, but when the material is used as a coating or bonded onto a surface, (pipeline, doghouse...) it is also subjected to deviatoric stresses which must then be taken into account. However, for an underwater structure made of syntactic foam, to a first approximation, it is of primary interest to evaluate its hydrostatic compression behaviour.

No standards are available for hydrostatic compression testing. Previously some standards (ASTM D2736 and D2926) addressed this topic but these standards have since been withdrawn.

The ASTM standard D2736-78(1982) proposed a practice for determination of hydrostatic compressive strength of syntactic foam and was withdrawn in 1984.

The ASTM standard D2926-70(1976) proposed a method of test for bulk modulus of elasticity of syntactic foam (Piston-Cylinder Method) and was withdrawn in 1987.

Currently most of the studies concerned by this type of loading are related to soil mechanics, foam behaviour, and polymeric materials (for example, the influence of pressure on crystallinity [71-73]). Classically load at break is studied via confined pressure or triaxial testing. Extensive studies by Pae and colleagues [74, 75] examined the influence of hydrostatic pressure on a wide range of solid polymers in a pressure vessel allowing mechanical loads to be applied to specimens under pressure.

Ifremer has extensive experience of pressure testing, operating a hyperbaric test facility in Brest for over 20 years. Pressures up to 240 MPa can be applied in a range of pressure vessels. A device similar to that of Pae, the CHEM, has been developed to study how pressure up to 1000 bar affects material properties [76, 77], but most studies to date have focussed on solid polymers and composites.

Recently some published studies have addressed the volume variation of material versus pressure and then the hydrostatic compression behaviour of the material [78-81]. These papers refer to polymeric foams (polypropylene foams and foams used in the automobile industry) and concern relatively low pressures <10 MPa where gas is generally used as the loading medium. For low pressure in gaseous atmosphere instrumentation problems can be solved more easily than at higher pressure, where tests are generally performed in liquids for safety reasons.

The range of pressures of interest for syntactic foams and deep sea applications is notably higher, and pressures up to 60 MPa have to be considered.

One of the aims of the present study was to develop a hydrostatic compression test which would allow the volume variation of the material to be followed during the pressure increase. There is also a need to perform such tests at different temperatures. Taking into account the application of syntactic foams as passive insulation, a range of temperatures extending from 2°C to 160°C has to be addressed.

The requirements for the test are summarized in Table 10.

Maximum pressure	100 MPa
Minimum temperature	2°C
Maximum temperature	160°C
Measurement of volume variation	continuous
Sensitivity of volume change measurement	better than 1%

Table 10 : Hydrostatic compression test requirements

Different methods have been envisaged, which will be developed in this chapter.

First, water has between chosen as the compressive medium for the following reasons:

- the physical properties of water are relatively well known,
- water is readily available, and
- for short duration tests the chemical resistance of the materials to water is generally good.

Concerning this last point, the behaviour of syntactic foam materials with respect to water has already been reported [27, 60] and the water uptake by diffusion can be estimated. However, considering the quite significant sample sizes of interest here (from a few tens of cm^3 to 1 dm^3 for test specimens) and the test duration, generally short with regards to the time constant for diffusion and degradation processes, the water uptake can generally be neglected.

For short mechanical tests the nature of the water has no significant influence on the result, so tap water can be used. For long term behaviour the nature of the water has to be taken into account however [56].

Prior to describing the methodology, a short reminder of the physical properties of seawater and the relation between depth and pressure is presented.

2.3.1 Physical properties of water

To perform accurate analysis of hydrostatic compression tests using water as the loading medium, knowledge of the specific gravity and of the compressibility of the water is of primary importance.

The compressibility of a liquid is a measure of the relative volume change as a response to a pressure change.

The compressibility of water has been studied by Fine [82] and is given to be maximum 2.05 $\times 10^{-10}$ Pa^{-1} at 400 bar and 5 °C and equal to $5.1*10^{-10}$ Pa^{-1} at 0°C.

The compressibility can also be defined from the change of density:

$$K = -\frac{1}{V}\frac{\partial V}{\partial p} \equiv \frac{1}{\rho}\frac{\partial \rho}{\partial p}$$

The bulk modulus, corresponding to the inverse of the compressibility, is generally given equal to 2.2 GPa.

The properties of sea water are generally defined from the state equation of seawater provided by Unesco under the reference EOS 80, published in 1981. This equation has recently been replaced by the TEOS-10, the International Thermodynamic Equation Of Seawater – 2010 (http://www.teos-10.org) which allows all the thermodynamic properties of pure water, ice, seawater and moist air to be evaluated in a self-consistent manner.

Seawater is a system fully defined by 3 state variables which are the salinity, the temperature and the pressure. For a pure water (salinity = 0) the density of the water can then be reported as a function of pressure and temperature. The EOS definition limits the temperature to 50°C, data from other has been identified for higher temperatures.

The values of density of pure water versus pressure for different temperatures are reported on (Figure 38).

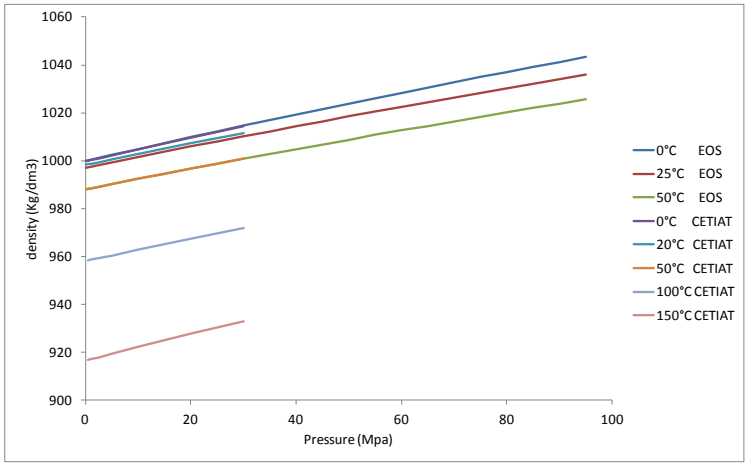

Figure 38 : pure water density versus pressure

The data from CETIAT are limited to 30 MPa and the data from OES (equivalent to TEOS-10) limited to 50°C. However a good correspondence between the data over their common range allows extrapolating the CETIAT curve up to 60 MPa.

The Cetiat data available are reported on table 11

	pressure (bar)								
temperature (°C)	0.1	1	5	10	25	50	100	200	300
0	999.8	999.8	1000.03	1000.28	1001.03	1002.28	1004.75	1009.66	1014.49
10	999.8	999.8	1000	1000.22	1000.93	1002.1	1004.44	1009.04	1013.57
20	998.3	998.3	998.5	998.7	999.4	1000.54	1002.78	1007.19	1011.52
30	995.7	995.7	995.9	996.1	996.8	997.9	1000.1	1004.4	1008.6
40	992.3	992.3	992.5	992.7	993.3	994.4	996.6	1000.83	1004.97
50		988	988.2	988.4	989.1	990.2	992.4	996.6	1000.72
60		983.2	983.4	983.6	984.3	985.3	987.5	991.8	995.9
70		977.7	977.9	978.1	978.8	979.9	982	986.4	990.6
80		971.6	971.8	972.1	972.8	973.9	976.1	980.5	984.7
90		965.2	965.3	965.5	966.3	967.4	969.7	974.2	978.6
100			958.3	958.6	959.2	960.4	962.8	967.4	971.9
110			950.8	951.1	951.8	953.1	955.6	960.2	964.9
120			943	943.2	944	945.3	947.8	952.7	957.4
130			934.7	934.9	935.7	937.1	939.7	944.7	949.7
140			925.9	926.3	927	928.4	931.2	936.4	941.5
150			916.8	917.1	917.9	919.4	922.3	927.7	933

Table 11 : pure water data density (from Cetiat)

2.3.2 Relation between depth and pressure

To a first approximation it is often considered that the pressure increases by 1 MPa for every 100 meters of immersion depth.

To be more accurate, taking into account the compressibility of water and the dependence of the Earth's gravity on latitude and depth a formula is provided, derived from the method developed by Saunders & Fofonoff [83], giving the relation between pressure and depth [84]. Following this method, knowing the salinity and the temperature of the water and the considered pressure the following relationship is obtained:

$$z = \sum_{\Delta p, p=0}^{p=p} \bar{\alpha} \, . dp \, / (g_{\emptyset}^{o} + \frac{1}{2} \gamma' . \, p)$$

With

z = depth

γ' = 2.184 * 10-6 $m.s^{-2}.dbar^{-1}$ as a corrective factor

$g_{\emptyset}^{o}$ = 9.7080318 . (1+ 5.2788 . 10^{-3} $\sin^2 \emptyset$ + 2.36 . 10^{-5} $\sin^4 \emptyset$) giving the relation of the Earth's gravity to the latitude $\emptyset$.

As an example, for a homogenous ocean (t=0°C and salinity =35) the relation between pressure and depth (m) is reported on Table 12 [84]. This example reveals the relative influence of the parameters.

P (MPa)	Latitude (°)				
	0	30	45	60	90
5	497	496	495	495	494
10	992	991	989	988	987
20	1980	1977	1974	1972	1969
40	3941	3936	3930	3925	3920
60	5885	5877	5870	5862	5854
80	7813	7803	7792	7782	7772
100	9725	9713	9700	9687	9674

Table 12 : Relation pressure - depth

An approximate correspondence between depth and pressure is provided in the oceanographic equipment qualification standard [85].

2.3.3 Hydrostatic compression tests based on the measurement of volume change of compression fluid

The first test developed (figure 39) was based on the measurement of the volume of water necessary to increase the pressure of the hyperbaric chamber containing the sample to be evaluated. Knowing the compressibility of water, the deviation of the theoretical volume change of a chamber without a sample with pressure increase can be attributed to the volume change of the specimen.

To a first approximation in a hyperbaric chamber, considered as non deformable, holding for example 1 dm^3 of water and a specimen to be evaluated, to increase the internal pressure by 10 MPa it is necessary to add $10/(2.2 * 10^3)$ dm^3 of water (4.55 cm^3). The excess of water to be added corresponds to the volume change of the specimen.

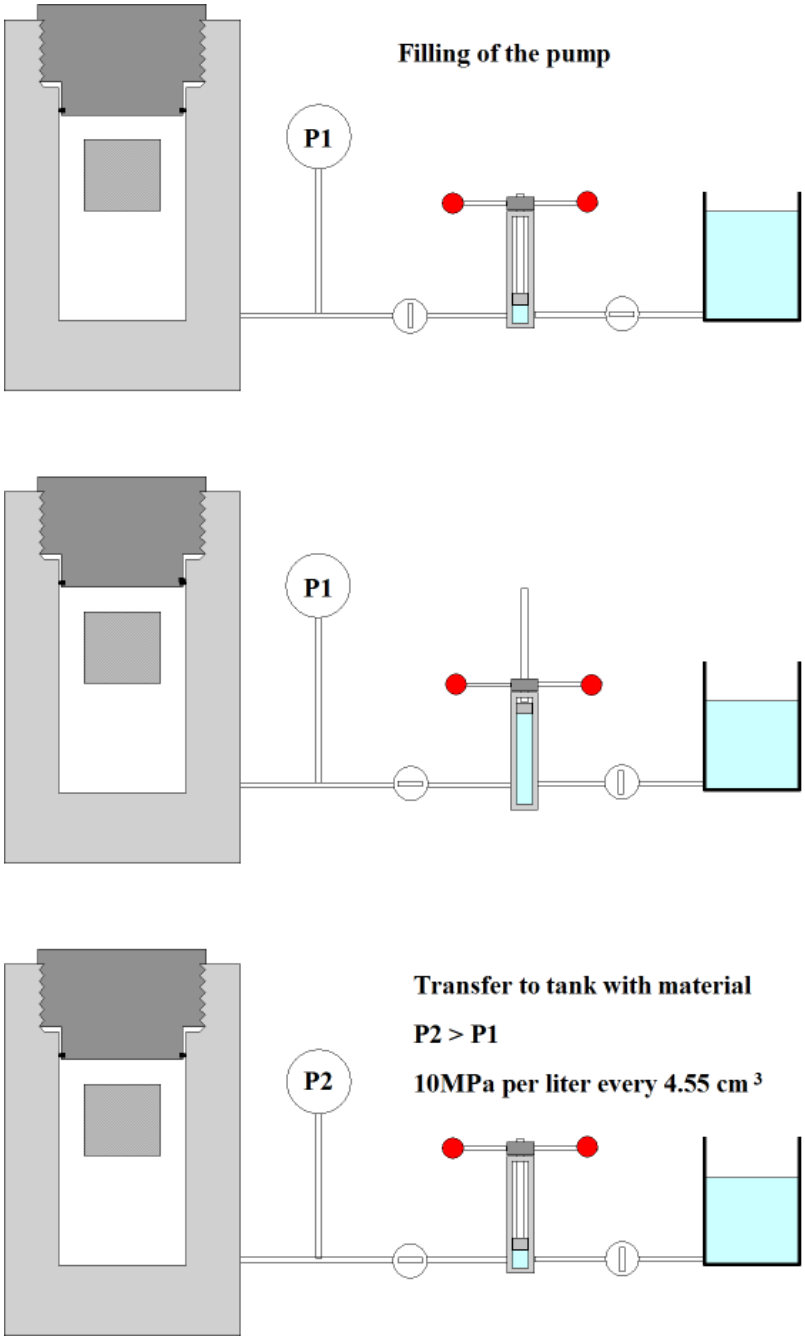

Figure 39 : Schematic diagram of hydrostatic compression test using measure of transferred volume

A 1000 bar hyperbaric tank has been designed (Figure 40, drawing see 6.6) and different trials have been performed with both a pneumatic volumetric pump and a manual volumetric pump.

Figure 40 : Hydrostatic compression test based on volume change

However, after testing different sizes of specimen the results obtained were not accurate enough to allow volume change versus pressure plots to be drawn. The main problems identified were:

- The volume change of the pressure circuit and chamber with the increase of pressure.
- The difficulty to eliminate all the air in the circuit. Air in the circuit significantly modified the pressure response due to air compressibility.
- The influence of temperature. A high level of temperature control is needed.
- The difficulty to determine the volume of water transferred. With a manual pump , only a visual indication of the position of the piston of the pump is available.
- Difficulty to control the pressure increase.

A second test was therefore evaluated, based on the use of a classical tensile-compression testing machine. The principle is to record the displacement a piston generating the increase of pressure in a hyperbaric tank as shown on (Figure 41).

A drawing of the tank is given in Appendix 6.7

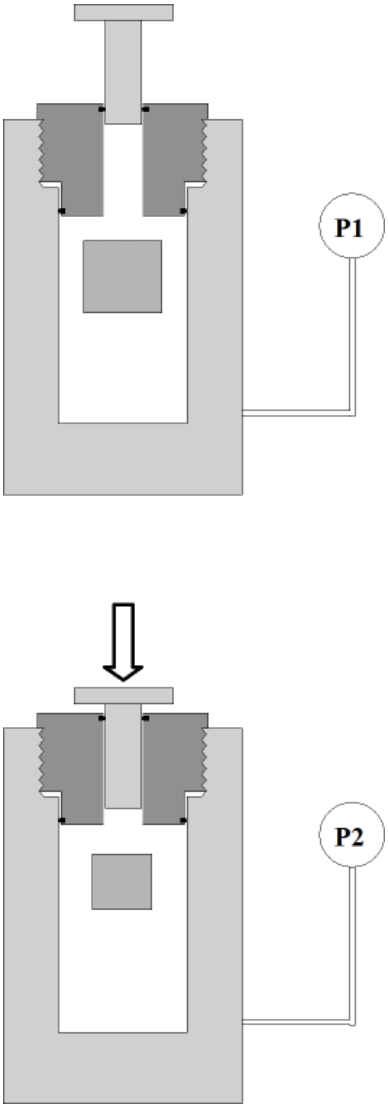

Figure 41 : Hyperbaric compression test based on piston displacement

The design of such equipment has to take into account; the volume of the hyperbaric chamber, the capacity of the testing machine, the size of the sample, and the potential volume variation of the samples.

The volume variation of the sample can be expressed as follows:

$$\Delta V_{mat} = \pi . R^2 . d - P . K_w . V_w$$

With:

ΔV_{mat} = volume variation of the sample

d = piston displacement

P = pressure

K_w = compressibility of water

V_w = volume of water in the chamber

A 1000 bar hyperbaric tank dedicated to this application has been designed (Figure 42), it can be mounted on a standard test machine.

Figure 42 : Hydrostatic compression test based on piston displacement

Different tests have been performed at room temperature and an example of the curves obtained is reported on figure 43.

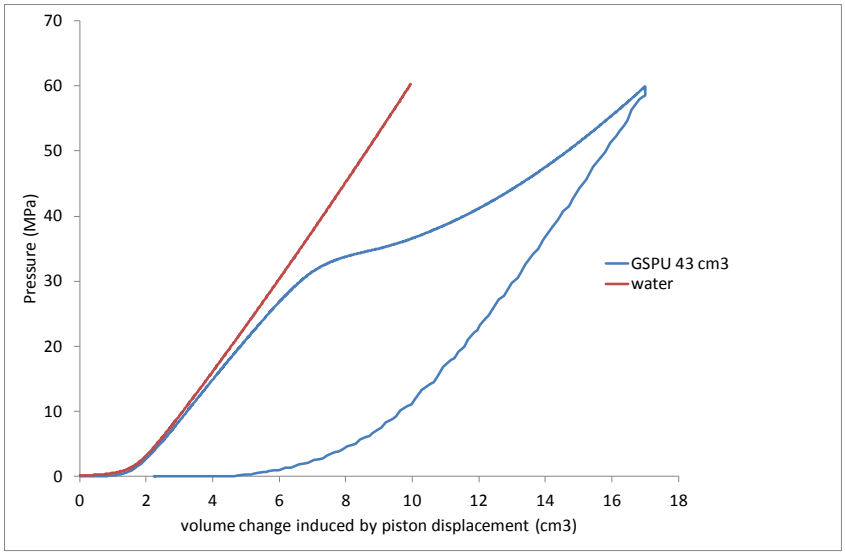

Figure 43 : Hydrostatic compression curve for GSPU at 20°C

The following conclusions can be made on the pertinence of this test device:

- Loading speed can be controlled easily and tests at different loading speeds can be performed over a large range of loading rates.

- Level variations along the pressure circuit have to be eliminated in order to avoid air in the tank. This air pollutes the displacement versus pressure response, and makes analysis difficult at low pressures.
- It is difficult to perform tests at elevated temperatures, in particular for temperature >90°C. Thermal dilatation of all the components has to be taken into account in order to obtain valid data in terms of volume change.
- For high pressures, deformation of the tank has to be taken into account. This problem can be solved by performing tests with no sample which can be used as a reference.

If only room temperature data are needed this approach is quite attractive. However, taking into account the difficulty to perform tests over a range of temperatures and in particular above 90°C, this approach was not pursued further here, and it was decided to develop a new approach to perform hydrostatic compression testing.

2.3.4 Instrumented hydrostatic compression based on buoyancy measurement

The experience gained in developing the tests described previously, using volume change measurements, indicated that an alternative approach was needed. A new test has therefore been developed based on the measurement of the buoyancy of sample during pressure increase.

This test development required a waterproof balance, a weighing device compensated in temperature and in pressure. The requirements of this device have been established and are reported in table 13.

Load Range (N)	+/- 5N
Sensitivity	0.01% of FS
Temperature range	2°C – 160°C
Pressure	Up to 60 MPA

Table 13 : balance requirement

The principle (Figure 44) of the test is to apply a hydrostatic pressure to a specimen through a loading fluid and to follow its buoyancy throughout the duration of the test. The sample is placed in a hyperbaric tank which is temperature and pressure controlled. The buoyancy is directly measured by means of a weighing device specially designed to be temperature and pressure compensated. The loading fluid is generally water.

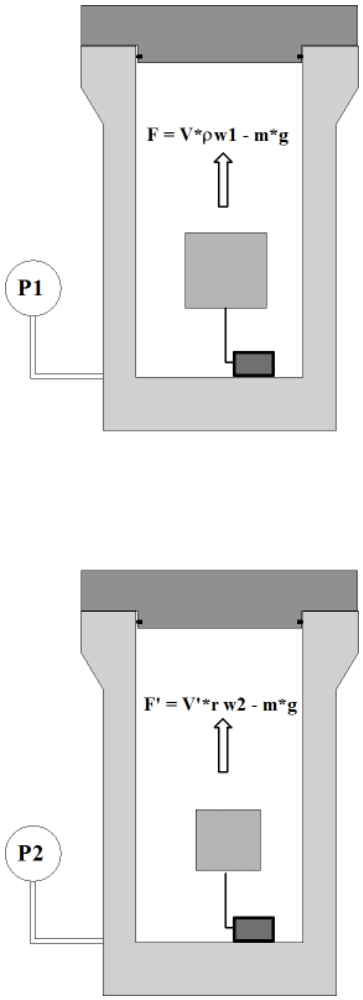

Figure 44 : Principle of hydrostatic compression test using waterproof balance

From the buoyancy change and knowing the specific gravity of water in the range of temperature and pressure considered, it is possible to evaluate the volume change of the material versus pressure.

The Archimedes' principle states that an object fully immersed in a liquid is buoyed upward by a force A equal to the weight of the liquid displaced by that object.

In the test configuration the measured force corresponds to:

F = A – W (Weight) which may be reported as

A(i) = W + F(i) or V(i)* ρ(i) water * g = M*g + F(i)

The volume of the sample can be evaluated at any time whatever the pressure and the temperature.

It must be noted that the load range of the balance has been chosen to be the minimum range available from the manufacturer. In order to be properly compensated a special design of the load cell has been developed, based on foil strain gauges bonded and placed in oil and using a low rigidity metallic substrate. In addition particular attention has been paid to the choice of an adapted high pressure – high temperature electric connector.

The load range of the cell imposes the use of specimens with about 4N of buoyancy, at atmospheric pressure and room temperature, in order to obtain the maximum accuracy for the measurement (Figure 45).

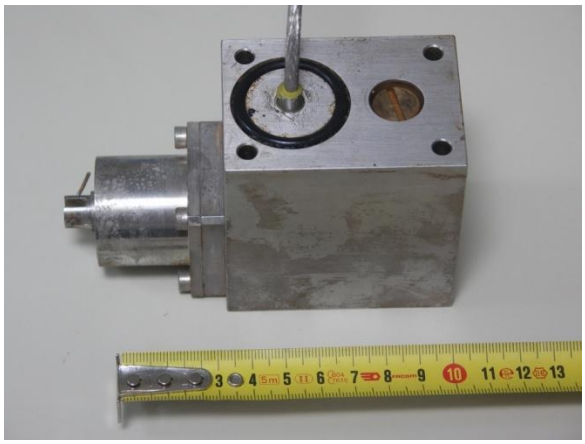

Figure 45 : waterproof balance

Specific equipment has been designed, and is described on the figure 46. A drawing of the tank is given in Appendix 6.8

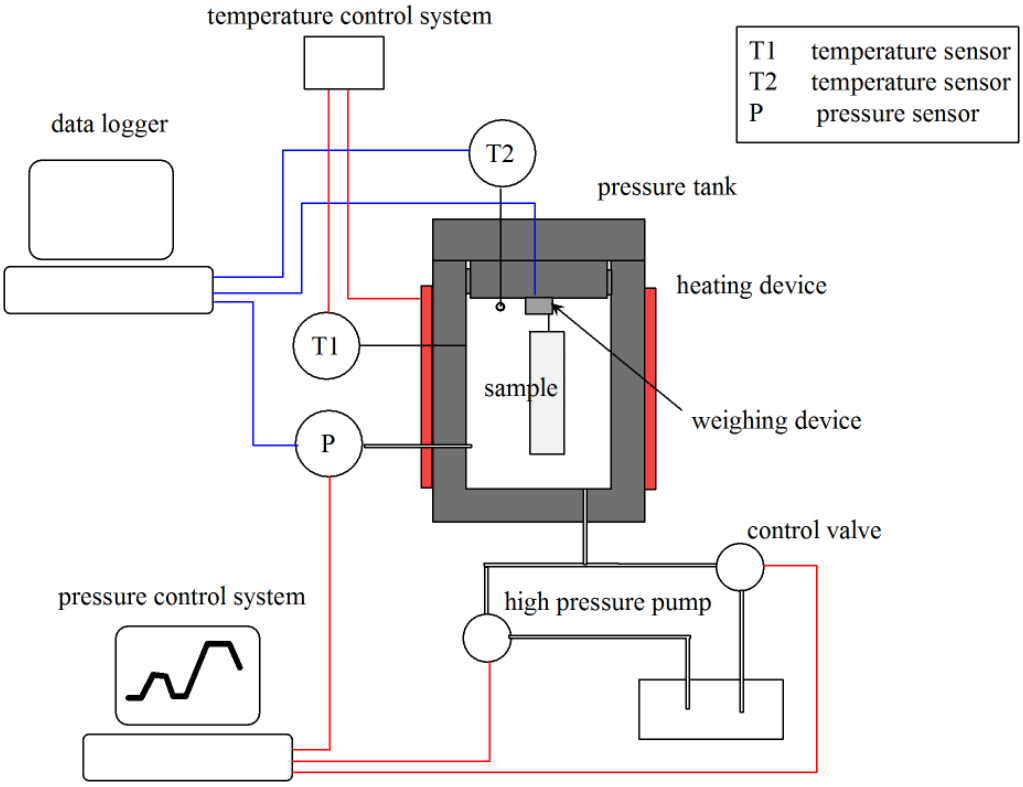

Figure 46: Schematic diagram of hydrostatic compression test using waterproof balance

Figure 47: Picture of hydrostatic compression test system

Upper left: pressure control system

Upper right: hyperbaric tank

Bottom: data logger

The system is composed of different elements (table 14). An in-house control system of the pressure has been developed which allows both quasi static and creep tests to be performed by maintaining constant pressure over a fixed time (so far creep tests have been performed for up to 7 days).

Data logger	HBM type AB22
Hyperbaric weighing device	Sixaxes 5N - 150°C – 1000 bars
Pressure sensor	FGP P101 1000 bar
Temperature sensor	Pt 100 Radiospare
Heating device	Articulated ceramic band heater 3 Vulcanic type 4030
Heating controller	Thermostat control unit Vulcanic 32060-13
Pressure control system	In-house control system based on PC board and high pressure control valve.

Table 14 : equipment used for hydrostatic compression test

Before reporting results on material behaviour some typical results will be analyzed.

To highlight the importance of taking into account the evolution of water density with pressure increase in the analysis of results, a comparison of change of buoyancy and change of volume was performed and reported on (Figure 48).

The variation of buoyancy is directly obtained from the balance, and normalized by the initial volume of the sample.

The change in volume is obtained by taking into account the change of water density as expressed above.

A result is given below for the epoxy syntactic foam at room temperature, Figure 48.

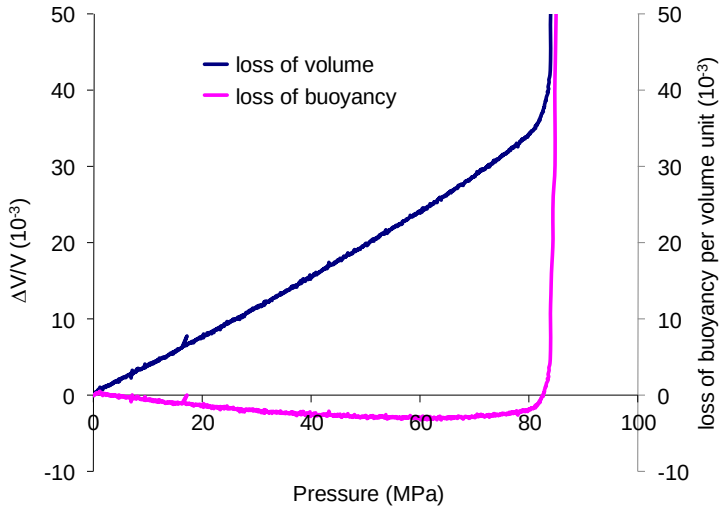

Figure 48 : GSEP hydrostatic compression test

It can be noted that initially (pressure < 60 MPa) the buoyancy of the material increases with the pressure increase whereas the volume of sample decreases quite linearly. The initial increase of buoyancy explained by a bulk modulus of the material higher than the bulk modulus of the water (2.2 GPa at room temperature). It should be noted that for a material with a bulk modulus > 2.2 GPa, when submitted to pure hydrostatic compression, its buoyancy will increase with the pressure or nominally with immersion depth.

Following discussions with other groups developing hydrostatic compression tests (Herriot Watt University, Trelleborg offshore, …) and in order to verify the pertinence of the method, tests have been performed on samples of different sizes of parallelepiped shape. Specimens in a volume range of about 1 to 10 have been machined out of a 0.47 kg/m^3 epoxy syntactic foam (developed by SNPE during a previous collaborative program). The results are reported on Figure 49 and reveal a very good correspondence between the curves obtained on specimens of different sizes.

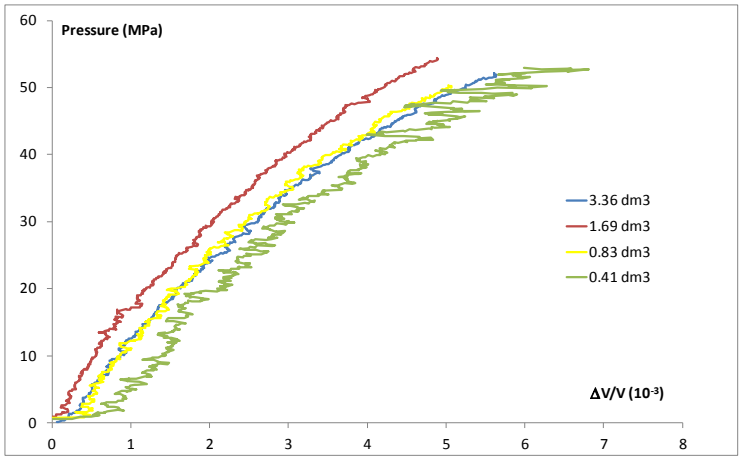

Figure 49 : Influence of volume of sample on hydrostatic compression test tesults

A test procedure has been established and is reported in 6.9

Typical curves are reported on Figure 50.

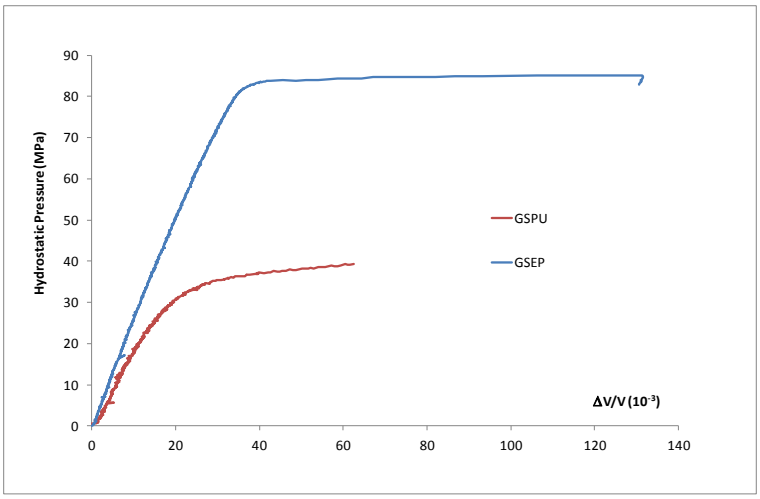

Figure 50 : hydrostatic compression test at 20°C

Tests have been performed at different temperatures to verify the performance of the equipment, tests up to 150°C are possible. As an example, results from tests on GSEP material at temperatures up to 100°C are shown below.

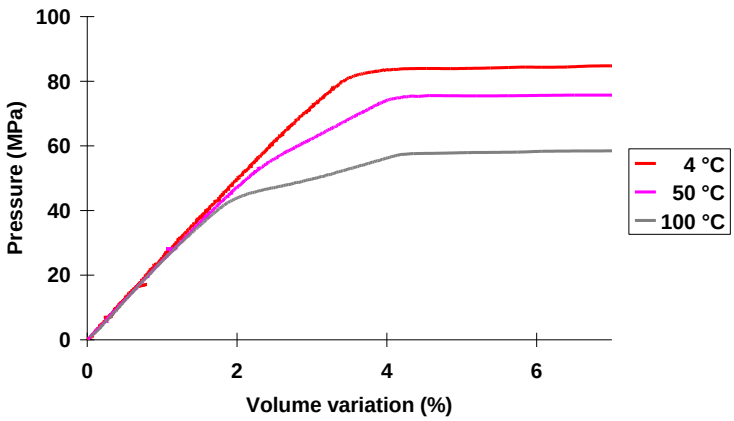

Figure 51 : GSEP hydrostatic compression test at different temperatures

2.3.5 Results

The behaviours of the two materials shown in Figure 50 are slightly different.

For the GSEP, the material exhibits initially a linear behaviour up to 80 MPa followed by a sudden collapse of the material. The block of material is cracked and the material is then no longer buoyant.

For the GSPU, the initial slope of the curve is not linear from the beginning and a plateau is noted at about 40 MPa.

From these curves the following parameters can be established:

- The bulk modulus, corresponding to the slope of the ΔV/V versus pressure plot.
- The crush pressure corresponding to the pressure at the plateau.

It must be mentioned that for a material such as the GSPU, given the non linear behavior additional indications have to be provided in order to standardize the values.

The bulk modulus has been chosen to be the secant modulus at 1% strain (linear part of the curves for the two materials).

The crush pressure is defined to be the pressure corresponding to the intersection between the bulk modulus slope and the slope of the plateau.

Results at 20°C are reported on table 15 (mean of 3 tests for each material).

	GSEP		GSPU	
	value	CV	value	CV
Bulk modulus (GPa)	2.62	0.01	1.93	0.03
Crush pressure (MPa)	83	0.02	32	0.05

Table 15 : Hydrostatic compression test at 20°C

Tests at 50 and 100°C, Figure 51, reveal the effect of temperature on the behaviour of GSEP. Crush pressure drops with increasing temperature but there is no significant change in initial bulk modulus. An intermediate slope change, between the initial slope and the plateau, is also noted. Further study of the thermo-mechanical behaviour of this material is needed to clarify the mechanisms responsible for this change in behaviour.

Considering the non linear behaviour of the GSPU material a special loading spectrum, including load-unload cycles and creep periods, has been performed at 20°C (Figure 52).

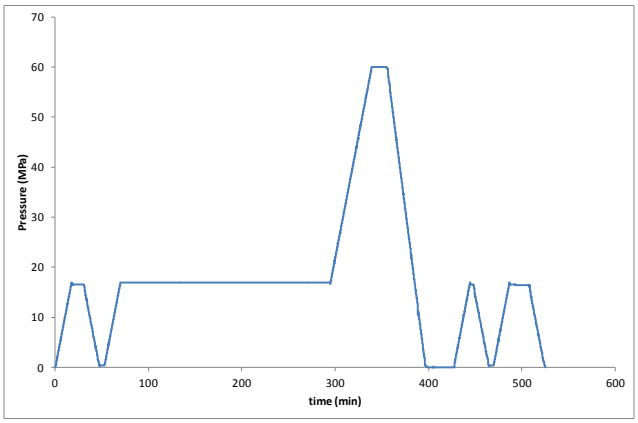

Figure 52 : loading spectrum

This loading sequence reveals the particular behaviour of this GSPU material (Figure 53).

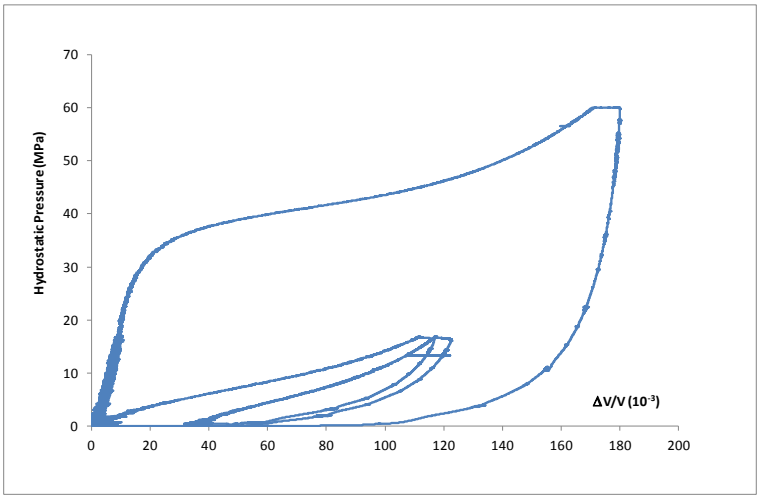

Figure 53 : hydrostatic compression on GSPU (load – unload cycles)

The behaviour can then be decomposed in different phases.

Up to 17 MPa, the load - unload cycles generate little residual deformation and the behaviour can be considered as elastic with no significant creep deformation during the creep period.

From 30-35 MPa large volume deformation occurs. Between 35 and 45 MPa the volume strain increased significantly, from 2% to 12%. This 10% increase of volume strain can be compared with the volume of microspheres included in the material. Collapse of microspheres has to be considered at these pressures.

From 50 MPa densification of the material occurs. It can be noted that the creep period at 60 MPa generates volume creep deformation. At this stage volume creep deformation can be considered as a non classical mechanical behaviour. For a classical viscous material creep, hydrostatic loading will not induce any volume change, contrary to the behaviour shown here.

The release of load reveals viscous residual deformation.

Re-loading highlights significant damageable behaviour of the material.

2.3.6 Confined pressure test

Finally in this section on hydrostatic compression testing it should be noted that confined pressure tests are sometimes used [86], and a procedure dedicated to syntactic foam has been proposed for the oil and gas industry [53]. This test has not been used in the present study due to the difficulty in evaluating the real loading condition of the material during this test. The loading conditions are strongly affected by the accuracy of the machining of the samples. Thus, the boundary conditions for confined pressure tests are not easily defined, and friction effects will pollute the results. It must be mentioned that in the literature [44] views of syntactic foam under confined pressure have been presented (figure 54). These clearly reveal an anisotropic damage process, which is not comparable to damage induced by pure hydrostatic compression (see 3.1)

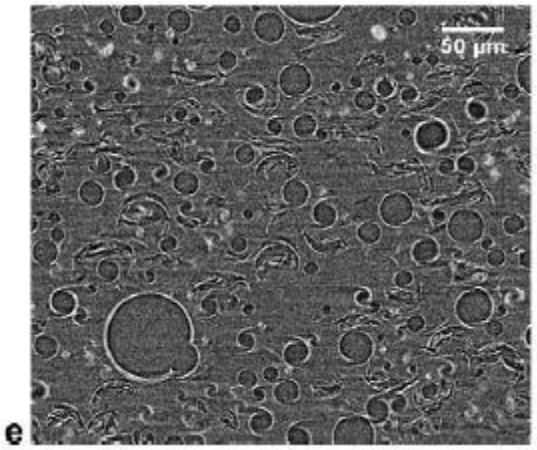

Figure 54 : X-ray microtomography view of syntactic foam under confined pressure

2.3.7 Conclusions

A new hydrostatic compression test has been developed, which can be considered as purely hydrostatic.

The equipment developed allows tests to be performed under different conditions of loading rate and temperature (up to 150°C) [87].

The test equipment is fully documented, and can be proposed to other institutes.

This test can be proposed as a standard, considering that currently no standard is available to obtain the pressure-volume change data needed to design underwater buoyancy structures. A proposal will be made to the standardization organizations.

The test is adapted for all types of syntactic foam and can also be applied to other polymeric foams.

It can be used to evaluate quasi static as well as creep behaviour. Cyclic loading can also be envisaged.

A volume of sample about 1 dm^3 is needed to guarantee accuracy better than 1% on the results.

The specific behaviour of two types of syntactic foam has been identified, and significant differences between GSEP and GSPU have been noted.

Damageable behaviour of GSPU syntactic foam has been revealed. A non-classical behaviour, volume hydrostatic creep deformation, was observed, which will require the development of an adapted model.

Additional tests are now needed to identify the damage processes in the material. These will be discussed in the next chapter, but first some methods to determine shear properties will be discussed.

2.4 Shear testing

2.4.1 Standard tests

There have been few previous studies describing shear testing of syntactic foams. Classically short beam flexure testing is used, and results have been reported on the characterization of sandwich foams [88]. The information provided by this test is limited to the shear stress at break .

In the field of composite materials different tests in use have been widely discussed [89-95] The short beam shear test (three point bending of a specimen with a distance between supports of 4 or 5 times the thickness, ASTM D2344) is frequently used to provide an indication of interlaminar shear strength but does not allow elastic properties to be determined.

To obtain elastic properties, 3 or 4 point bending on specimens with different length to thickness ratios can be used but given the weak properties of syntactic foam in tension the range of application of such tests is limited.

Double lap shear test have been used but Doleski has encountered difficulty in reaching shear failure of an epoxy syntactic foam [96]

Another approach to obtain the shear properties is to use the rail shear test, which is widely used on foam materials for sandwich construction. However, taking into account the stiffness of the material (in particular for epoxy syntactic foam) the standard ASTM C273 / C273M - 11 Standard Test Method for Shear Properties of Sandwich Core Materials is not very suitable in our case. Previous work performed at Ifremer has identified difficulties in bonding the specimen to the metallic support and premature failures can occur at the ends of the specimen generated by important stress concentrations. Nevertheless this test can provide stiffness data.

An interesting approach has been described by Chavez [34] who used a triaxial shear test to obtain the failure envelope of carbon micro balloon syntactic foam, however this approach has been mainly employed to provide yield surface data.

At the start of the present project the most promising way to obtain shear data of polymer materials appeared to be the method described in ASTM D5379 (Shear Properties by the V-Notched Beam Method), also known as Iosipescu method.

No previous references to the use of this test on syntactic foam were found so this test has been evaluated.

2.4.2 Iosipescu test.

The Iosipescu test is a shear test using the test set up described in figure 55.

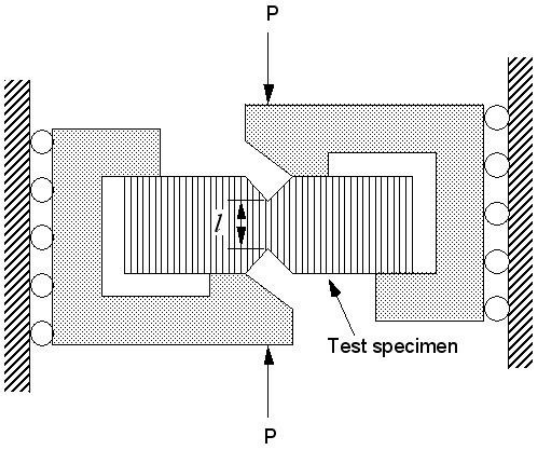

Figure 55 : Iosipescu shear test

This test has been studied in detail for composite materials in order to access interlaminar shear properties but it can also be used for isotropic materials.

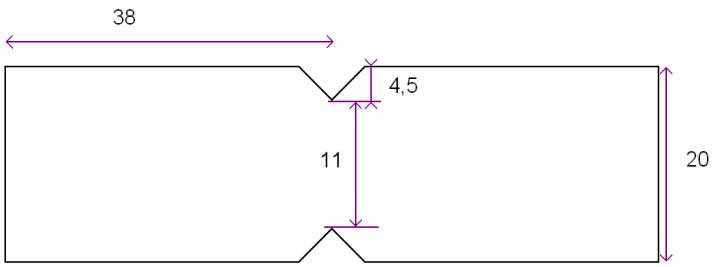

Figure 56 : sample size (in mm)

Two clamps hold the specimen horizontally and then one of these two fixtures is moved vertically in order to generate shear loading of the specimen. A V shaped specimen is used, Figure 56.

In order to examine the response of syntactic foams in this test configuration some preliminary finite element (FE) analyses were performed (2D and 3D models),) which confirm a quasi homogenous shear strain in the central part of the specimen as visualized on figures 57 & 58 . The parameters of the model were E = 3 GPa, ν = 0.4, elastic material.

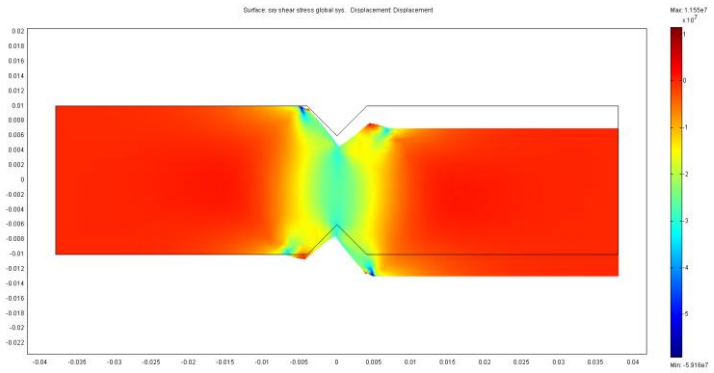

Figure 57 : 2D FE model Iosipescu test

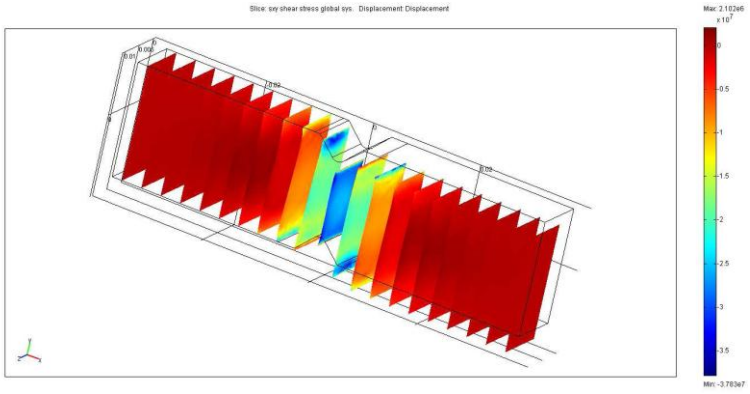

Figure 58 : 3D FE model Iosipescu test

In terms of specimen thickness the standard states: “A wide range is allowed in the requirement for specimen thickness to allow the user some flexibility in unusual cases. When possible, however, the specimen thickness should be kept in the range from 2 to 5 mm”.

In order to evaluate the potential use of the Iosipescu test for syntactic foam, samples of two difference thicknesses (3 mm and 10 mm) have been machined in GSEP and GSPU, strain gauged and tested at 2 mm/min.

Typical response curves are reported on figures 59 & 60.

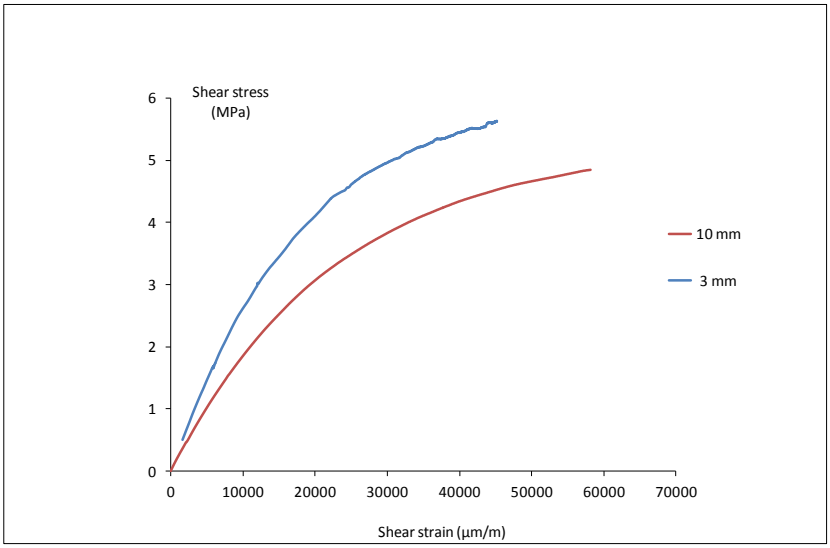

Figure 59 : Iosipescu test on GSPU

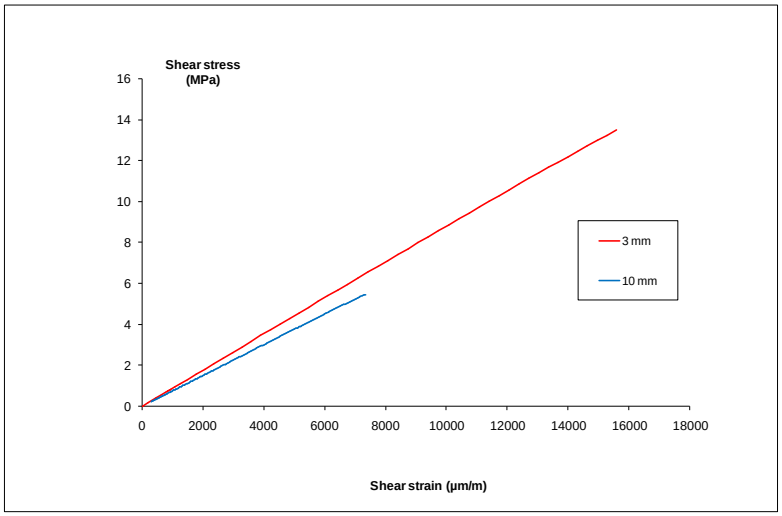

Figure 60 : Iosipescu test on GSEP

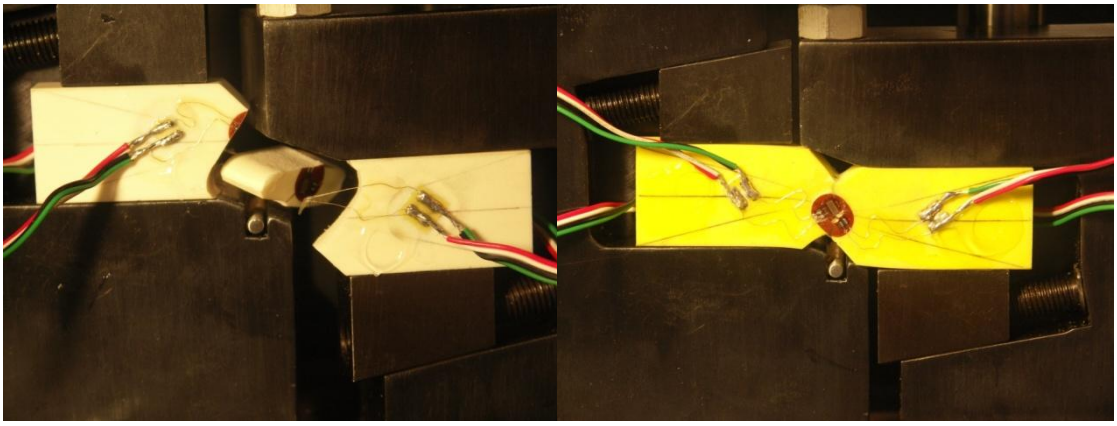

Figure 61 : Pictures taken during Iosipescu tests, right GSEP, left GSPU.

Samples have been equipped as recommended in the ASTM standard by two strain gauges on each face, and the differences observed between the two faces of the samples have been noted. For 3 mm GSEP samples the relative difference between the results was always lower than 3 %. For 3 mm GSPU samples two specimens exhibit differences lower than 3% but the other one presents a relative difference of 12%. However the latter result is retained because it is comparable to the other results. The relative difference obtained on 10 mm samples is 9.7% and 4.3% respectively for GSEP and GSPU, so all are outside the ASTM validity limits.

The results are summarized on table 16 (tests performed on 3 samples of 3 mm thick and 1 sample of 10 mm thick for each material)

material	Thickness	G (MPa)	τ (MPa)
GSEP	3 mm	870 +/- 90	13.7 +/- 2
GSEP	10 mm	750	5.46
GSPU	3 mm	292 +/- 40	N/A
GSPU	10 mm	198	N/A

Table 16 : Iosipescu test results

From the first results it may be noted that:

- The GSPU exhibits non linear behaviour while the GSEP response is linear
- Large deformations are noted on GSPU
- There is a strong specimen thickness effect on failure of GSEP samples.

It must be mentioned that a recommendation is given by the standard that the difference between values provided by the gauges bonded on the two faces of the specimen should be below 3 % otherwise the specimen should be rejected. Even with particular attention paid to the machining of samples and conducting the tests, the results obtained are not always really satisfactory. Small strain gauges are difficult to align precisely, and difficulty in fixing the 3 mm GSPU samples in the test set up has also been encountered. The early break of 10 mm thick GSPE specimen has been noted and may be explained by the more brittle behaviour of the material and then its high sensitivity to stress concentration. All these points confirm the difficulty to conduct Iosipescu tests properly on this type of material. Since early work by Pierron and colleagues [97] various papers [98, 99] have highlighted the many parameters affecting the results obtained with this test.

Load-unload cycles have been applied to 3 mm GSPU samples and reveal apparently damageable behaviour of the material (Figure 62).

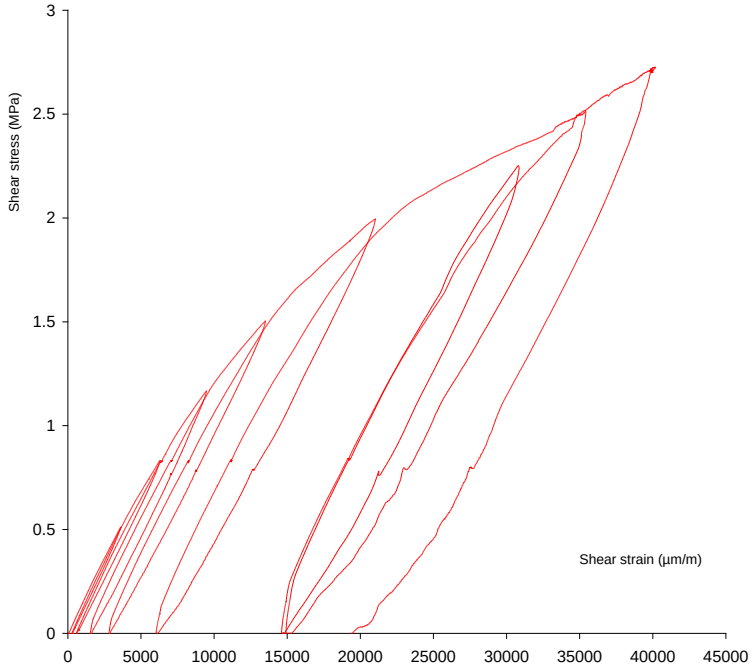

Figure 62 : load – unload cycle on GSPU

Thick samples are not well adapted for the evaluation of the shear strength of the material, although they can provide the shear modulus of the material. However, 3 mm thick samples are difficult to test, in particular for low shear stiffness materials (GSPU) due to the limited surface of sample in contact with the test set up and the risk of buckling.

GSPU samples also exhibit non linear behaviour. In addition the shear deformation allowed by the standard loading device is too small to allow the shear behaviour to be performed to failure.

In order to look for a more satisfactory test for GSPU-type materials an alternative shear testing approach was therefore examined.

2.4.3 Modified ARCAN test.

A modified Arcan test set up has recently been proposed for the study of out plane loading of adhesive bonds and composite materials [100, 101]. This test is based on an Arcan set up

[102] which allows specimens to be loaded under different conditions (pure shear, coupled shear-tension, shear-compression) and then to identify the yield and failure envelopes. Taher has recently used this test to determine PVC foam mechanical properties [103].

Modification of the specimen fixtures by local machining of the metallic specimen supports, as proposed by Cognard et al. [95,96] limits the stress concentrations at the edges of the specimen (Figure 63).

Figure 63 : detail of modified Arcan specimen (from Cognard)

Digital Image Correlation (DIC) is used to evaluate the displacement on the whole surface of the specimen. DN, the normal displacement, and DT, the tangential displacement is measured and provides information on the behaviour of the specimen. These values are normalized by the thickness of the sample and are reported versus load.

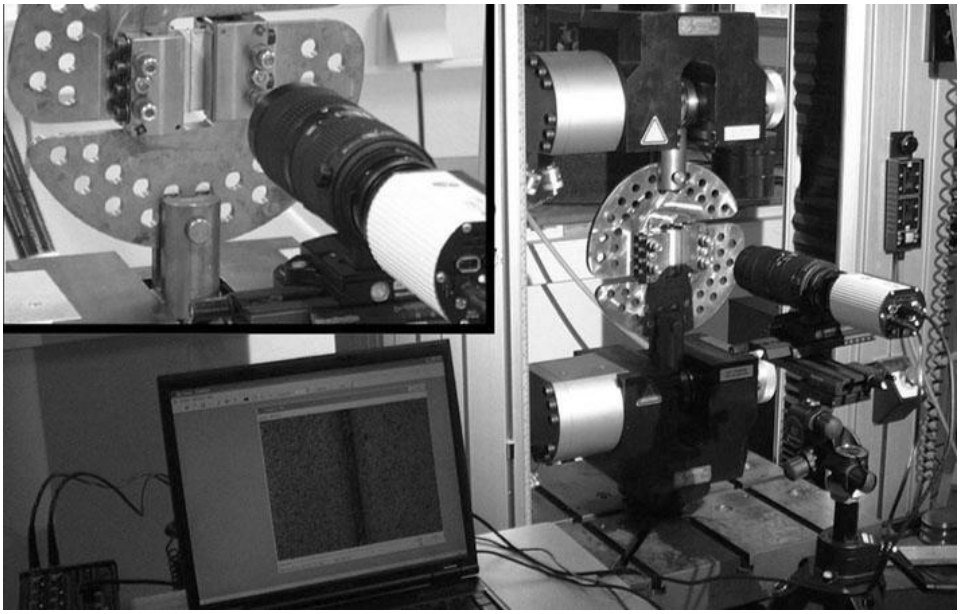

Figure 64 : Modified Arcan set up and DIC equipment

The modified Arcan test has been performed on GPSU syntactic foam in collaboration with the LBMS laboratory in Brest, to evaluate the shear behaviour of the materials.

Based on the equipment available with a loading surface of 7.6*66 mm different specimens (3 types) have been machined and tested with 2 types of U shaped aluminium supports as shown on figure 65. The specimens were bonded onto the support using Hunstman Araldite™ 420 A/B adhesive.

A first series of specimens was loaded under pure shear loading.

Figure 65 : Three types of syntactic foam modified Arcan specimens

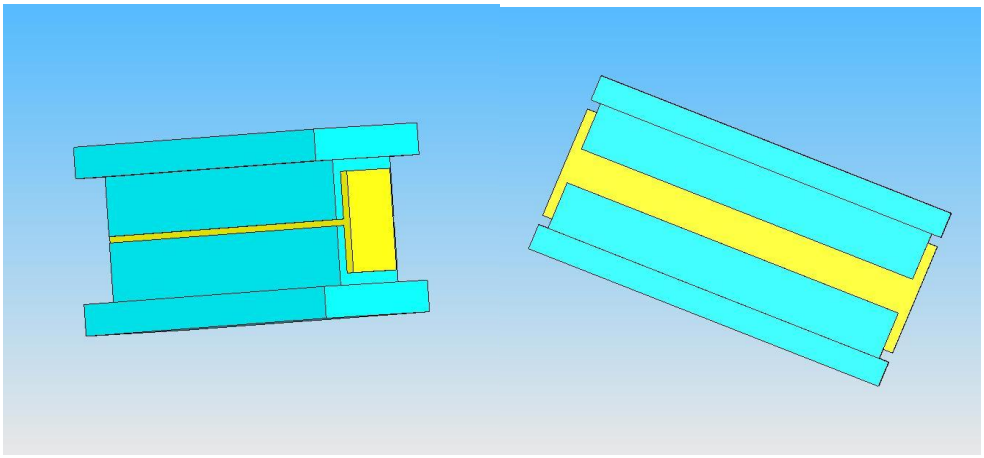

Figure 66 : 2 and 6 mm thick initial shear specimen

Load versus shear displacement curves have been obtained and again revealed a non linear behaviour of the GSPU material. However with this geometry it was not possible to obtain the failure in the central part of the specimen. The failure of the specimen occurs near the free edge of the specimen in all cases (Figure 68).

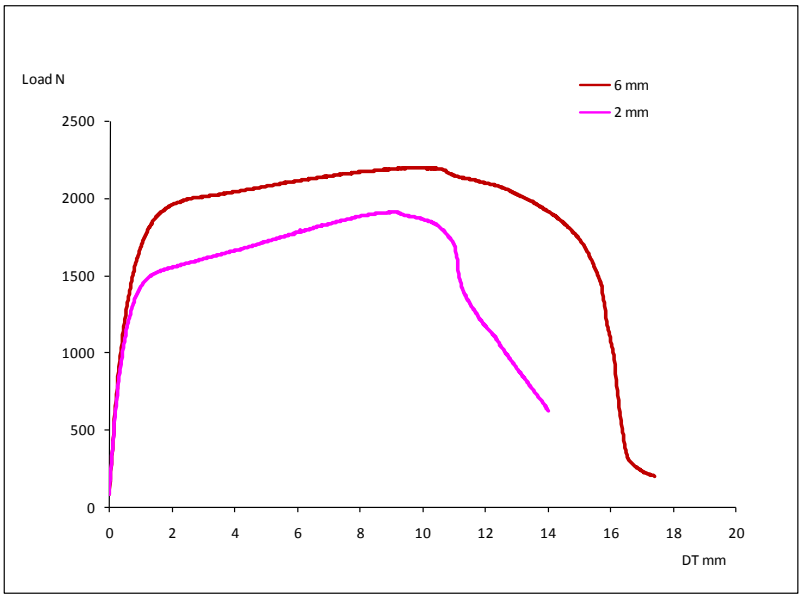

Figure 67 : initial modified Arcan test (pure shear), DT tangent displacement

Figure 68 : 2 mm Arcan modified failure (GSPU)

Based on these results it was decided to re-design the samples in order to be closer to the study of the thin films used in the studies performed on bonded joints. Small plates (2*7.6*66 mm^3) have been manufactured and bonded onto the aluminium substrates and tested. Particular attention was paid to the machining of the samples, to limit the local degradation of the material. Considering the diameter of the larger microballons (about 100 µm for S38HS 3M grade) the minimum thickness considered for the test was 0.7 mm. Based on the experience of testing of adhesive joints, local chamfers (1 mm at 45°) of the aluminium fixture (figure 69), aiming to localize failure in the median plane of the specimens, were machined. In addition supports with beaks were also machined, and a comparison of results is reported on figure 69. The global loading speed was 1 mm/min, corresponding to a shear deformation rate of of 0.0083/s. In this case both GSPU and GSEP samples were tested.

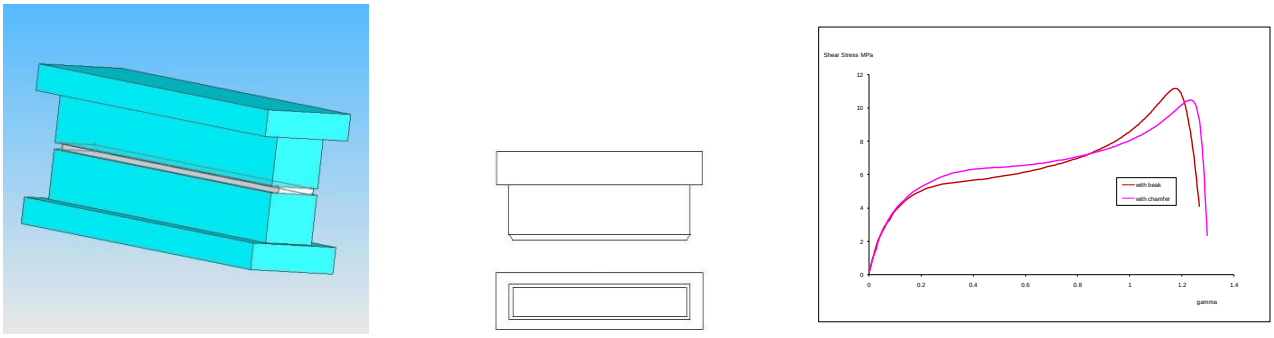

Figure 69 : retained Arcan modified specimens

In order to evaluate the influence of the bonded joint on the global response of the specimen, comparisons have been made between the curves obtained on:

- The bonded specimen
- The adhesive alone

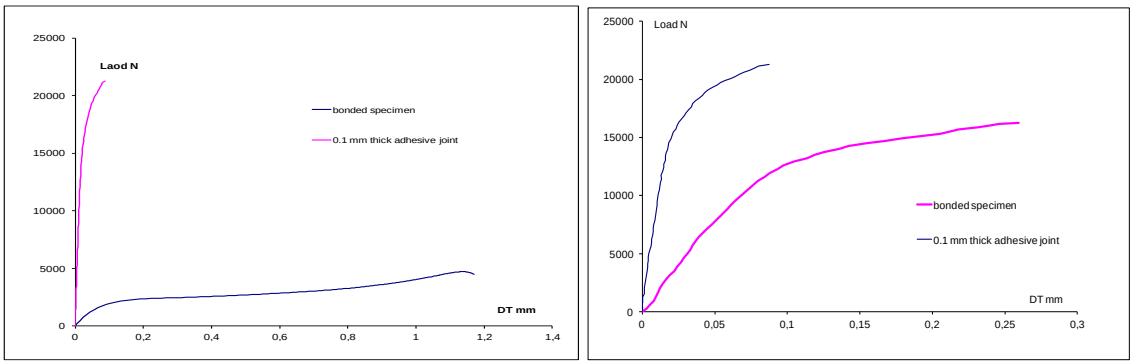

Figure 70 : comparison of tangent displacement response observed for syntactic foam specimen + adhesive and adhesive alone (left GSPU, right GSEP)

The comparison between the two curves indicates that for GSPU the deformation induced in the adhesive joint is very low in comparison to the deformation noted in the material itself. The tangent displacement can be mainly attributed to the tangent strain of the material.

For the GSEP material, some remarks can also be made. Cracks occur in the material and not in the adhesive joint (Figure 71). The plasticity of the adhesive joint occurs close to the break load of the specimen. For accurate analysis an inverse method would be needed to reveal the real material behaviour [104]. At this stage this inverse method has not been developed.

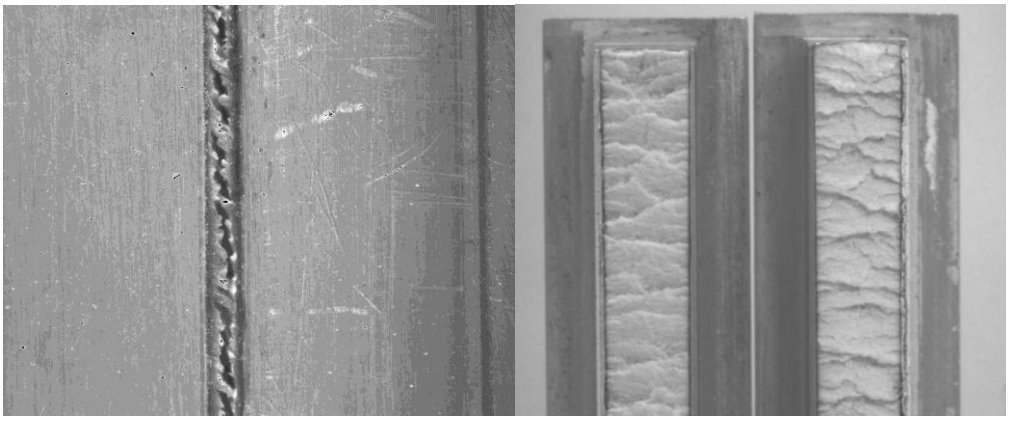

Figure 71 : GSEP fracture surfaces

Normal displacements have also been measured for the two materials on 2 mm thick samples. The results are presented on figures 72 & 73

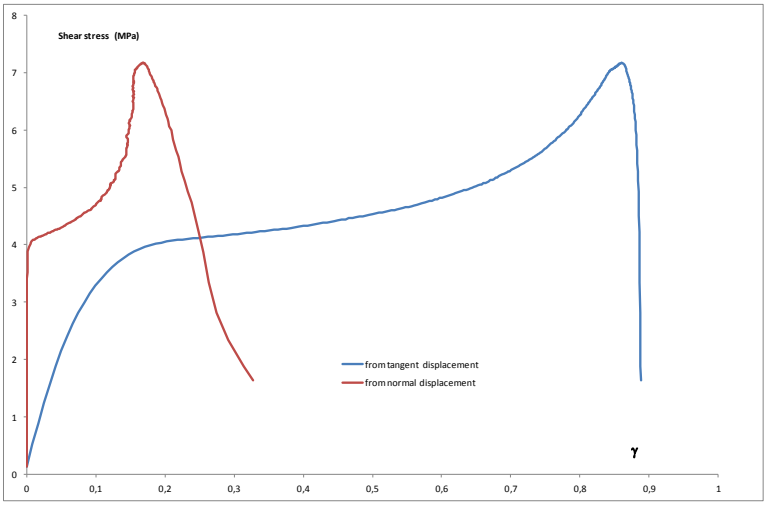

Figure 72 : modified ARCAN stress strain curve for GSPU

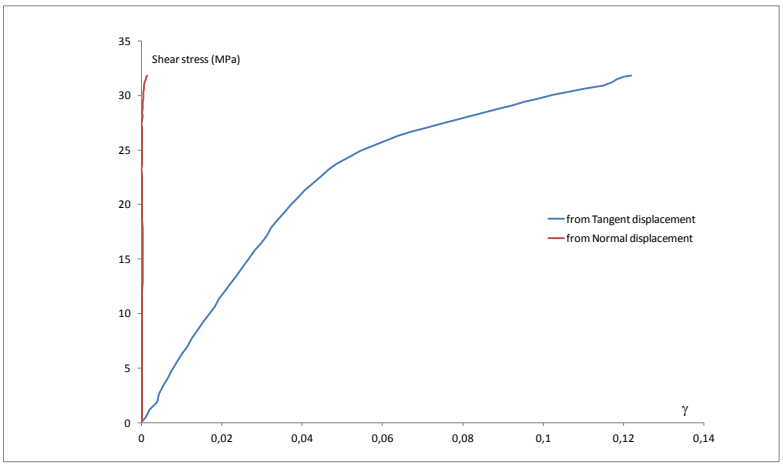

Figure 73 : modified ARCAN stress strain curve for GSEP

In the first part of the plots up to yield a very low normal displacement is noted. This low normal displacement underlines the pertinence of the test.

These tests highlight the shear behaviour of these materials and significant levels of strain are obtained for GSPU (strain up to 100%) and for GSEP.

From these tests the following values (Table 17) of the shear modulus and failure stress can be estimated (mean of two tests). An improvement in displacement measurements is still needed and for GSEP the inverse method has to be developed to take into account the strain in the adhesive.

At this stage the accuracy obtained on the normal displacement does not allow the normal displacement field to be estimated with precision. An indication is provided on the normal displacement between the two metallic parts of the specimen and through thickness normal displacement is considered to be constant. However, in terms of shear properties at break or shear at the plateau for GSPU, the values obtained are significantly higher than the values obtained by the Iosipescu test. This suggests that the former is inducing premature failure. In

the modified Arcan specimen edge effects are limited by the use of specimen machining, which is not the case in the Iosipescu test where a stress concentration is deliberately introduced in order to localize failure in the centre of the specimen.

material	G (MPa)	τ (MPa)
GSEP	630	32
GSPU	55	4*

Table 17 : Modified Arcan results

* Value at the plateau

Additional tests have been set up to highlight the potential of the modified ARCAN tests to characterize shear properties of syntactic foams.

On GSEP, samples of different thickness 2 mm and 0.7 mm have been tested with the same strain rate. To maintain the same strain rate it is necessary to consider the thickness of the sample and to adjust the crosshead speed rate proportionally to the thickness. The shear strain rate was here chosen at 0.0119 / s.

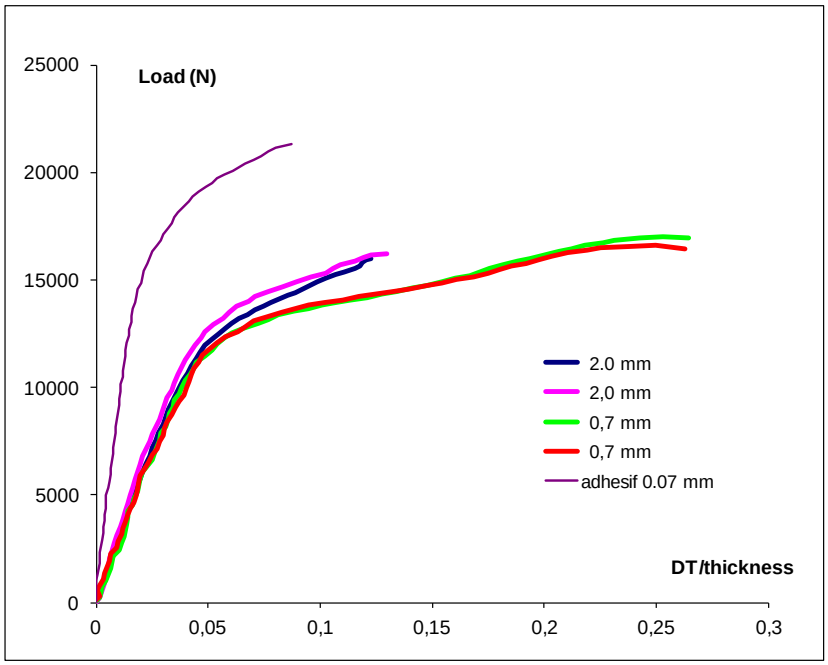

Figure 74 : Modified ARCAN influence of specimen thickness on results for GSEP

Based on the results of these tests the following comments can be expressed:

- There is very good reproducibility of the test, the two samples of the same thickness show identical behaviour.
- In the linear part of the curves, the behaviour of samples of different thickness seems similar.
- Differences occur in the non linear part of the curves.

The same comments can be made for the GSPU samples.

For GSPU, tests have been performed on samples of the same thickness (0.5 mm) at different shear strain rates.

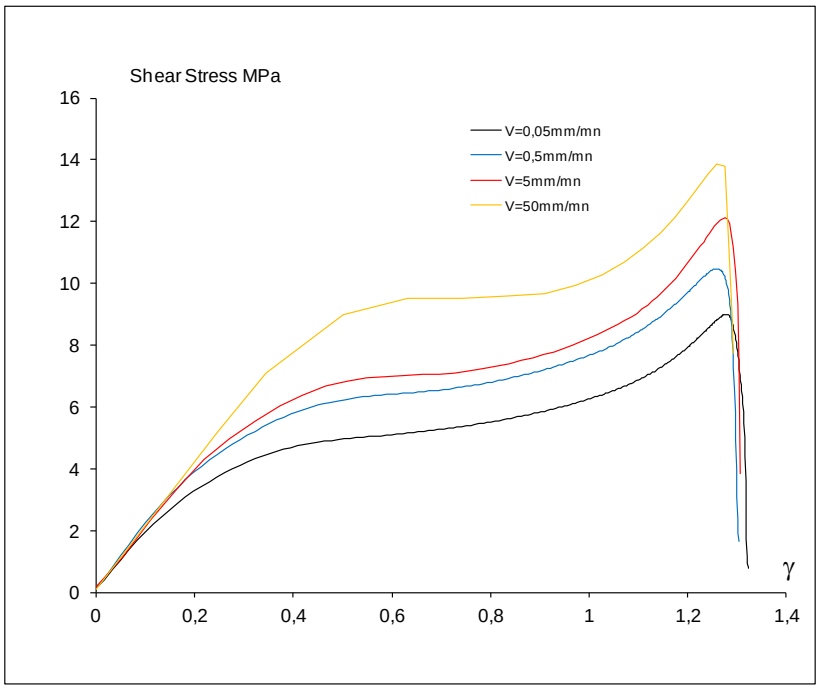

Figure 75 : Modified ARCAN influence of loading rate on results for GSPU

Whatever the shear strain rate the initial linear slope is similar but the loading rate strongly affects the non linear part of the curve, with an increase in plateau level as the rate increases. It can also be noted that the strain at break is constant for all the tests.

Finally, load–unload cycles have been performed on GSPU on 1.2 mm thick specimens at a crosshead displacement rate of 2 mm/min. These curves are compared with a curve obtained on a sample of the same thickness under monotonic loading

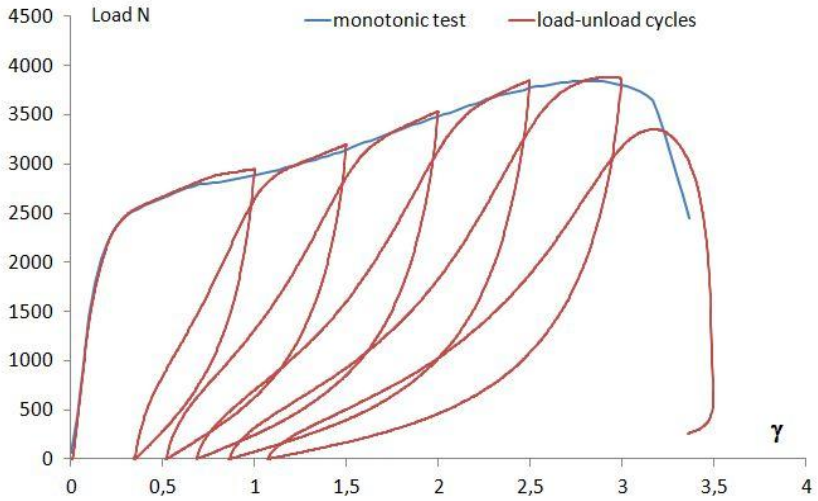

Figure 76 : Modified ARCAN load – unload cycles GSPU

These curves confirm the damageable visco elastic behaviour of the material, which is comparable to the behaviour of the material under hydrostatic compression (see 2.3).

2.4.4 Conclusions

Shear tests have been performed on syntactic foam. The Iosipescu test was considered initially as a standard method exists. It is appropriate to determine modulus but premature failures occurred in the more brittle material while for the more ductile foam strains were too large to allow failure to be reached.

In order to reach larger shear deformations, and based on the developments previously carried out to study shear of adhesives, a modified Arcan test has been developed.

Using this test a larger shear deformation range has been investigated and significantly higher shear properties at break have been obtained. This test reveals the behaviour of the materials over a large range of shear strain.

This test has to be improved in order to provide pertinent initial shear deformation values. Deformation of the adhesive pollutes the result obtained (in particular for GSEP). Analyses of through thickness deformation have also to be developed. Recent DIC developments should significantly help for this purpose.

An additional advantage of the Arcan test is that it enables the behaviour of the material to be characterized under biaxial loading (shear + tension, shear + compression …) and this will probably provide interesting information on the behaviour of syntactic foam for other applications.

2.5 Digital Image Correlation

Following the recent acquisition in the Materials and Structures group of a commercial Digital Image Correlation system, complementary uniaxial compression and shear Iosipescu tests have been carried out in order to examine the potential of such a system to improve the quality of the results obtained from these tests.

2.5.1 DIC System

The available equipment is an Aramis 5M system from GOM company. This system is a non contact optical 3D deformation system. The system is based on the use of 2 cameras placed in front of the specimen to be analysed with an adapted angle of view. A speckled pattern is deposed on the sample by spraying with paint.

The measurement is performed in 3D mode and the the calibration panel used for this experiment was a 90*72 mm^2 panel (reference 90 CP 20/MV). This is important to specify as defining appropriate calibration procedures is one of the issues to be addressed when proposing DIC in a standard test procedure.

2.5.2 Uniaxial compression

The four types of specimen tested in 2.2 were evaluated, Figure 77, in order to verify the strain distribution along the length of the samples.

The results are reported on figures 78 to 85.

For each type of specimen and for each material, the stress-strain curve is drawn from the information collected in the centre of the specimen (reference point).

The axial strains collected on a central generator of the specimen are also reported. For specimen types 1 and 2 the line covers the whole length of the specimen. For specimen 3 the line covers half of the specimen, position 0 corresponds to the central part of the sample. For specimen 4, the data are collected over 28mm along the central calibrated part of the sample.

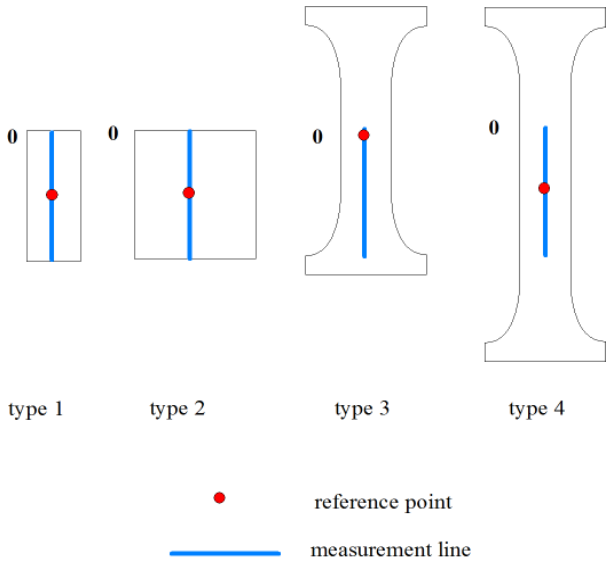

Figure 77 : compression sample geometry and location of measurement

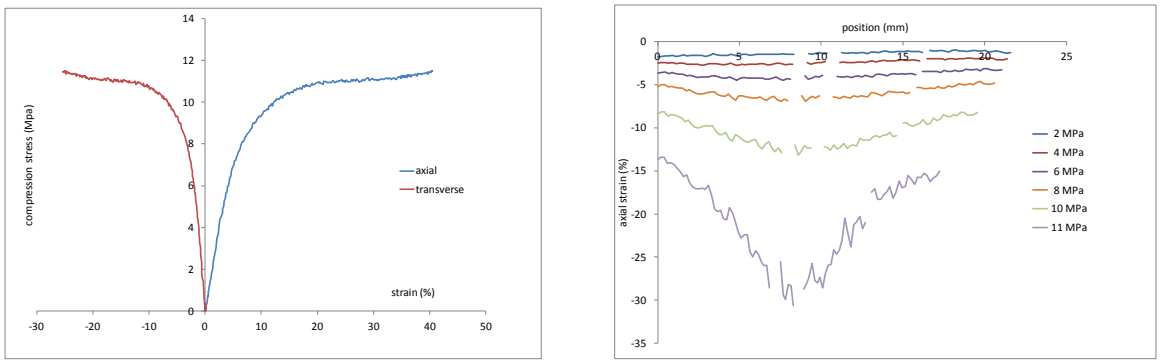

Figure 78 : compression curve and strain distribution on GSPU type 1 specimen

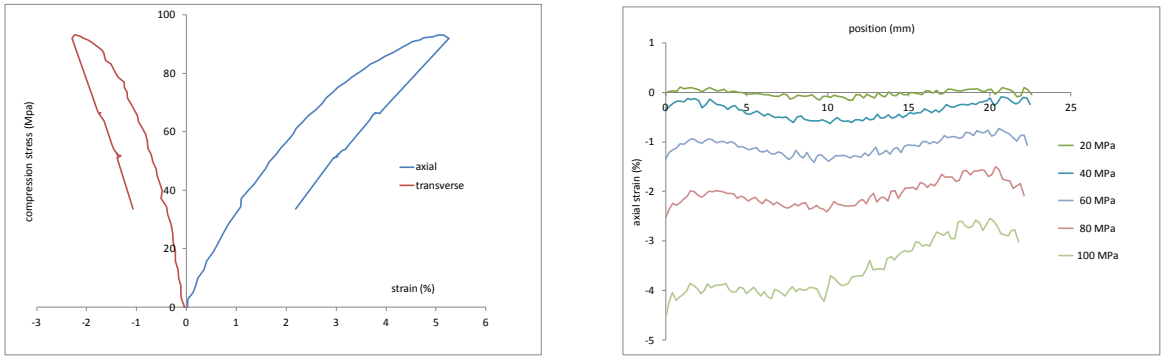

Figure 79 : compression curve and strain distribution on GSEP type 1 specimen

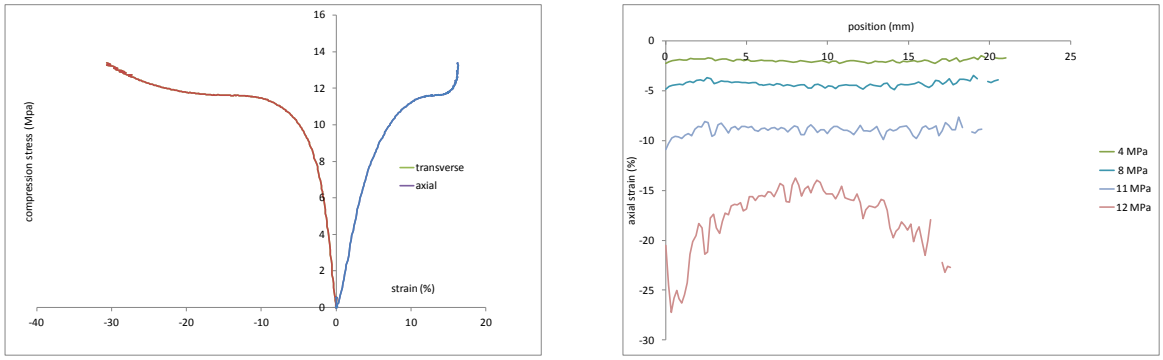

Figure 80 : compression curve and strain distribution on GSPU type 2 specimen

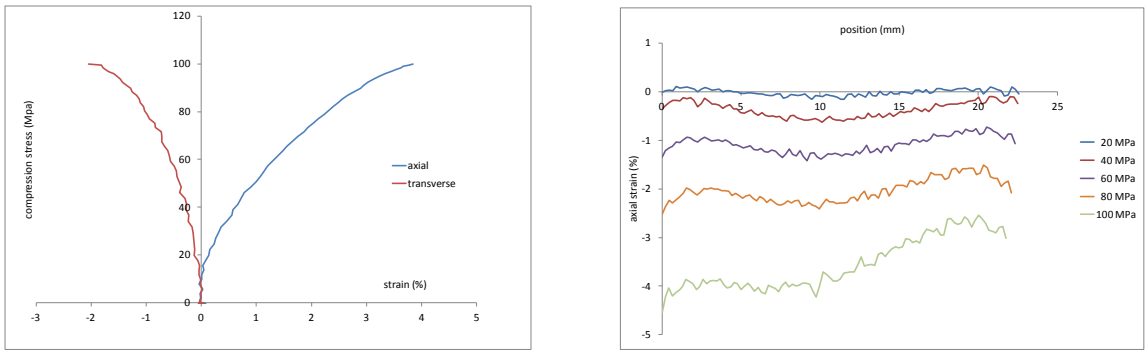

Figure 81 : compression curve and strain distribution on GSEP type 2 specimen

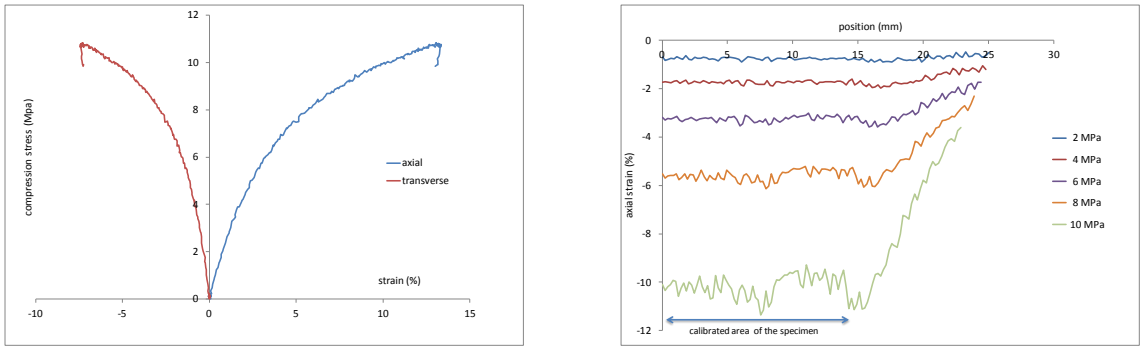

Figure 82 : compression curve and strain distribution on GSPU type 3 specimen

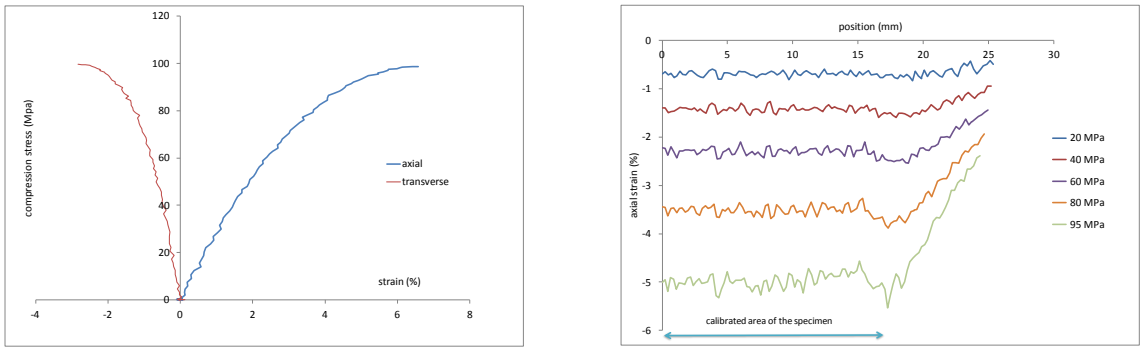

Figure 83 : compression curve and strain distribution on GSEP type 3 specimen

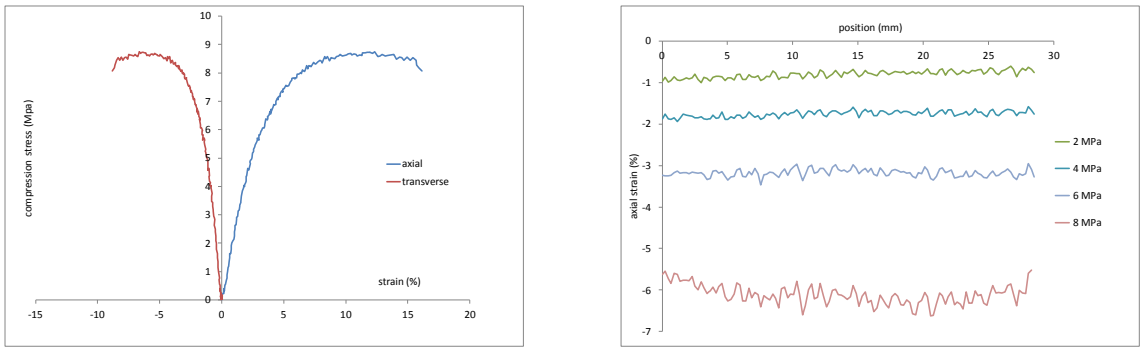

Figure 84 : compression curve and strain distribution on GSPU type 4 specimen

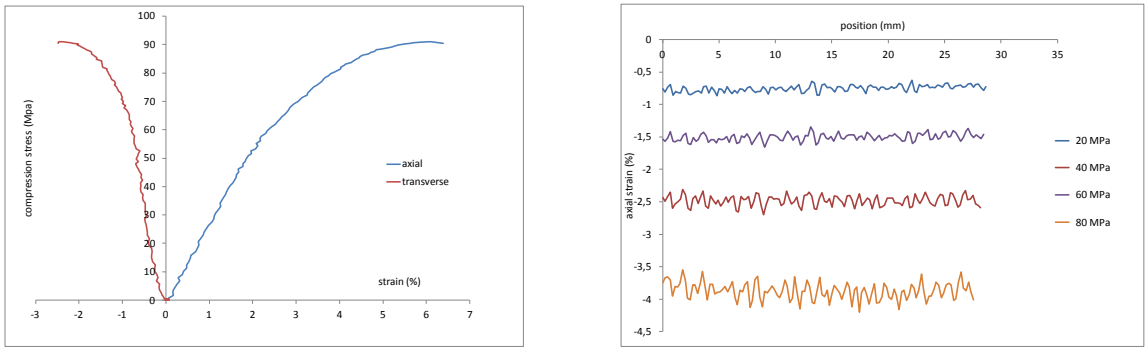

Figure 85 : curve and strain distribution on GSEP type 4 specimen

These different results are particularly instructive. It is demonstrated that for specimen types 1 and 2 the strain distribution is not homogeneous along the length of the specimen whichever the nature of the material. This heterogeneity is particularly highlighted at high strain level. Considering this point, the Saint Venant principle is far from respected with the specimen types 1 and 2 so analysis of results obtained on such specimens is very debatable. Even with the use of an extensometer or strain gauge placed on the centre of the specimen the results obtained are strongly affected by the strain gradient along the length of the sample.

Specimens type 3 and 4 exhibits more homogeneous results. For specimen 3 the strain distribution on the calibrated part of the specimen appears to be quite constant. The strain distribution on the central part of specimen 4 is also constant. The results presented in 2.2 coming from type 3 specimens can thus be considered to be pertinent.

Based on these measurements specimens 3 and 4 can be proposed for measuring uniaxial compression properties. However, for GSPU, which exhibits a lower stiffness, buckling of specimens can occur and this will limit the range of use of the longer type 4 specimen.

2.5.3 Iosipescu shear test

A series of tests on 6 mm thick specimens has been carried out with DIC on each type of material. The thickness of the sample has been chosen taking into account the remarks made on 2.4.2.

3 samples of GSPU and 2 samples of GSPE were tested in the same condition (2 mm/min cross-head speed) and a pattern was applied to the surface of the material (Figure 86) in order to perform DIC measurements.

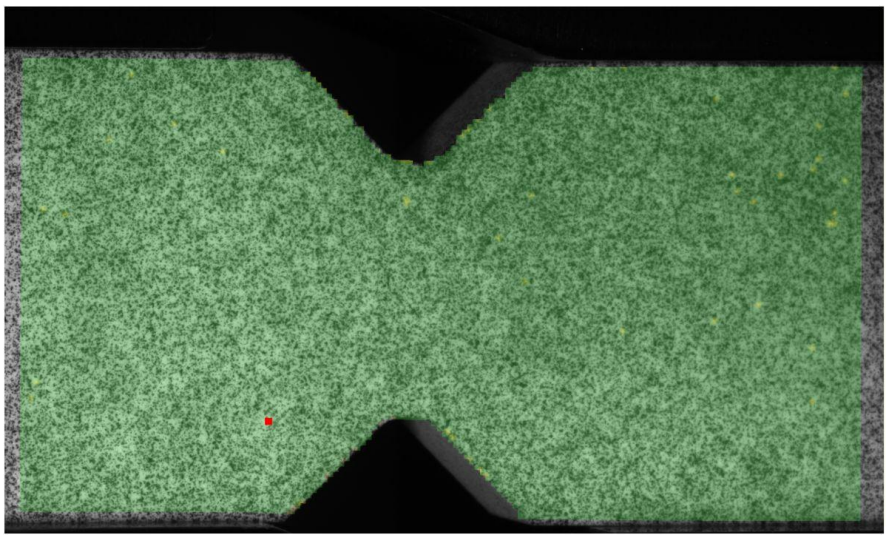

Figure 86 : pattern on Iosipescu sample

Considering the recommendation of the standard, observations should be made on the two faces of the specimen to verify the concordance of the results obtained on the two faces and to guarantee symmetry of loading. Due to the availability of only one DIC system the observation was limited to one face here, but no significant Z displacements were detected during the measurements.

Examples of results obtained are presented hereafter.

For GSPU, the stress strain curves at the central point of the specimen are reported for the three samples (Figure 87).

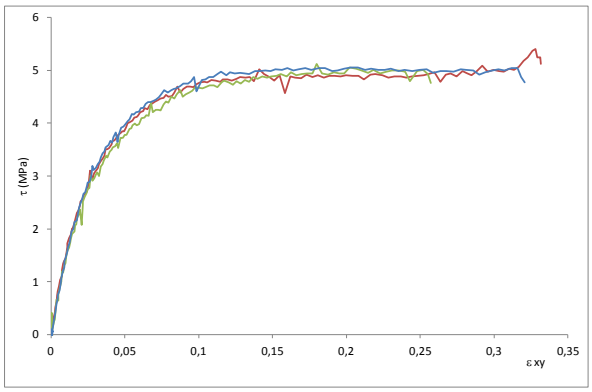

Figure 87: GSPU shear stress-strain curve from DIC

These results indicate:

- the very good reproducibility of the results,
- a curve shape which is slightly different to that of the curves obtained in 2.4.2

From these observations it can be suggested that the discrepancy observed on 2.4.2 could be attributed to a measurement problem. Measurements were performed using 5 mm long strain gauges there. The positioning of the strain gauge in terms of location and orientation is delicate and is a critical point of the measurement. In order to confirm this point, on Figure 88 the evolution of the strain in the central part of the specimen at different loading steps is reported.

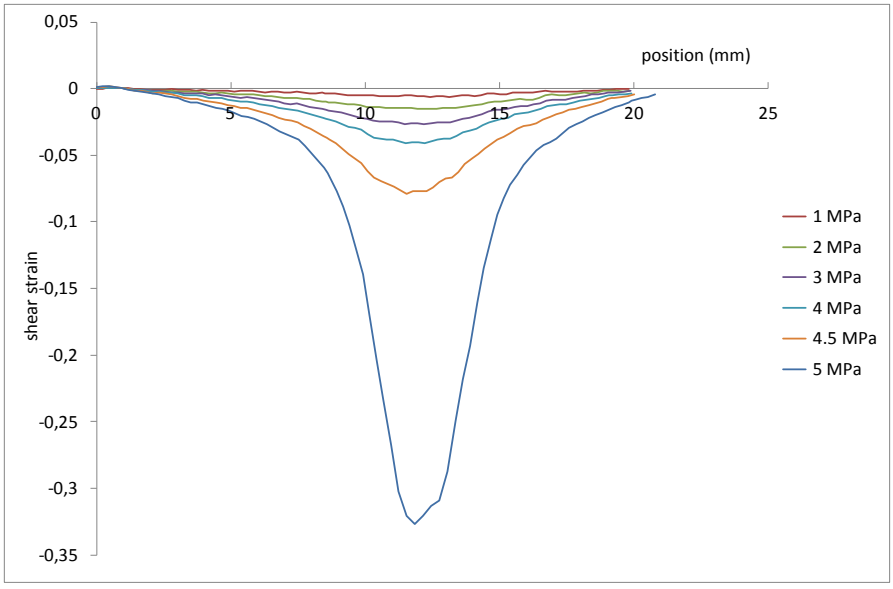

Figure 88 : shear strain profile GSPU (centre of the specimen)

The high gradient of strain reveals the limited zone of constant strain in the central part of the specimen. This gradient depends on the stiffness of the specimen and may be further

increased considering the damageable behaviour of the material. Complementary analyses (e.g FE analysis using a material model including shear damageable behaviour) may be useful to confirm this point.

The results on the two samples of GSEP are reported on figure 89. Considering the acquisition speed of the available DIC system the crosshead speed has been reduced from 2 to 0.5 mm/min for the second specimen (in blue). Dots have been used to draw the curve for better readability due to the small number of measuring points at higher loading rate.

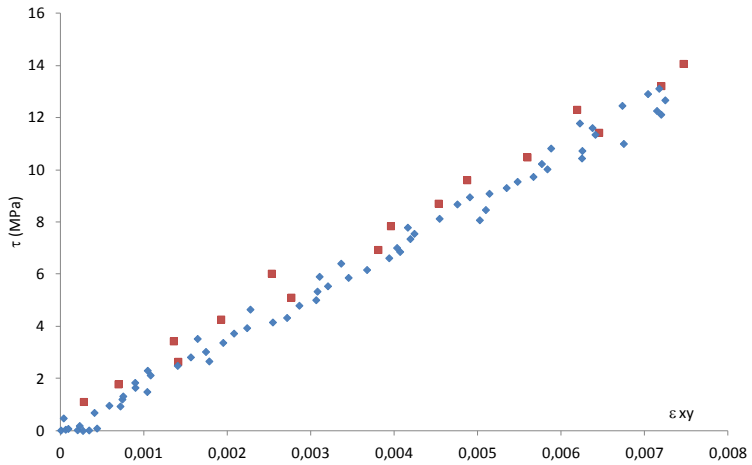

Figure 89 : shear stress-strain curves on GSPE

Once again the two results are very close. The material exhibits elastic behaviour and the deformation at break is very low, 0.008. It may also be noted that for the two materials there is no significant rate effect, confirming elastic behaviour of the material over this range of loading rates

On Figure 90 for GSEP and Figure 91 for GSPU DIC shear strains are reported, at the maximum shear stress reached during the test. On the left side the distribution of the shear strain, and on the right side the longitudinal strain are shown.

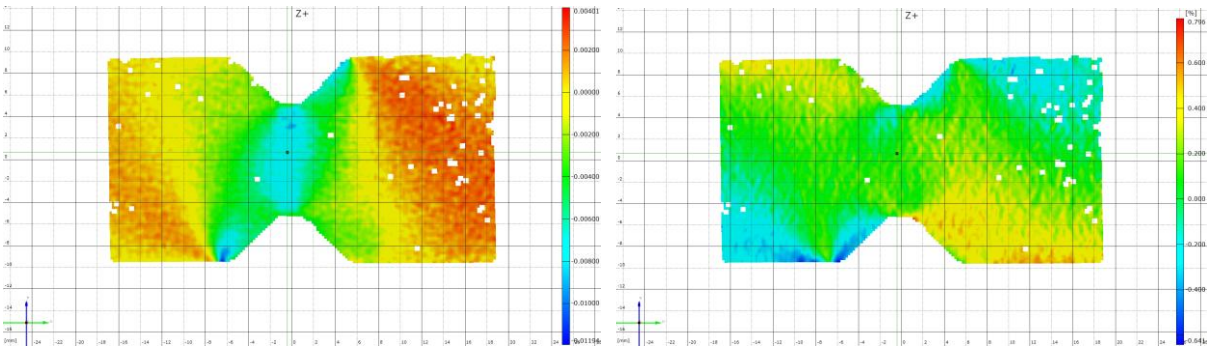

Figure 90 : GSEP material, left, shear strain and right, longitudinal strain at 13 MPa

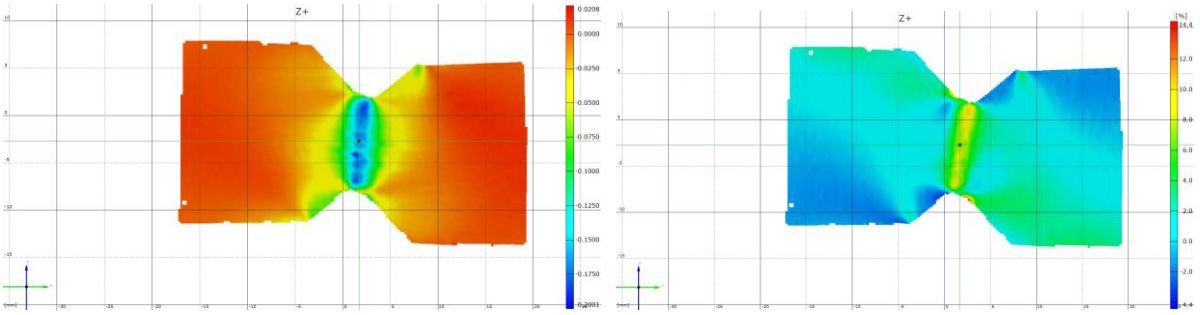

Figure 91 : GSPU material, left, shear strain and right, longitudinal strain at 5 MPa

For the GSEP material, the area of homogenous shear strain is quite large, about 4 mm and strong edge effects are noted close to the V notched indicating overloading and generating early failure of the specimens. This material is brittle and very sensitive to edge effects. The machining of samples may introduce local degradation or local overstressing which can induce the early break of the specimen.

For GSPU specimen, the localisation of an overstrain zone is highlighted, corresponding to the observation made on Figure 88. Quite significant longitudinal strain is noted which indicates at this load level a non-pure shear stress in the centre of the specimen.

However, the shear mechanical properties of the material can be determined from these Iosipescu tests, and are reported on table 18. These values are preferred to the value noted in 2.4.2, considering the difficulty in obtaining valid strain values on this material with the measurement system used (strain gauges).

2.6 Synthesis of experimental characterization

A summary of the results obtained is reported on table 18

method	properties	GSEP	GSPU
US	E (MPa)	3000	393
	G (MPa)	1115	133
Uniaxial compression	E (MPa)	3340	432
	ν	.34	.49
	σ (MPa)	98	12
Hydrostatic compression	K (MPa)	2620	1930
	P (MPa)	83	32
Shear test ARCAN	G (MPa)	630	55
	τ (MPa)	32	4
Shear test Iosipescu	G (MPa)	1800	175
	τ (MPa)	14	5

Table 18 : results from test

From these results additional values can be calculated using the isotropic material assumption. The value of the Young's modulus issued from the uniaxial compression test is used for the calculation when one input is missing. The results are reported on table 19. Some clearly suspect results are placed in grey cells.

method	properties	GSEP	GSPU
US	K (MPa)	3230	2904
	ν	0.34	0.48
Uniaxial compression	G (MPa)	1246	145
	K (MPa)	3479	7200
Hydrostatic compression	G (MPa)	1297	147
	ν	.28	.46
Shear test ARCAN	K (MPa)	-438	-29
	ν	1.65	2.92
Shear test Iosipescu	K (MPa)	972	270
	ν	-.07	0.23

Table 19 : indirect calculated properties

The following points can be noted:

- Mechanical tests on this type of material are delicate to perform. Data obtained on this material has to be used with great care. These materials exhibit complex behaviour with early damage initiation, which must be considered when test results are analysed.
- The moduli obtained from US and uniaxial compression measurements are close. However difficulty in obtaining shear waves makes measurement of shear properties very difficult for GSPU.
- Hydrostatic collapse pressure and uniaxial collapse stress have the same value for GSEP and are totally different for GSPU. At this time there is no micromechanical approach which would allow us to investigate this difference of behaviour. GSPU collapse is controlled directly by the collapse of microspheres whereas the collapse of the GSEP is controlled by the compression failure of the matrix skeleton.
- The new hydrostatic compression test proposed here exhibits perfectly controlled boundary conditions and the value of collapse pressure can be considered as pertinent. The curve of volume change versus pressure reveals the behaviour of the material correctly and will be considered as the reference value.

- Uniaxial compression is a delicate test to perform, and although elastic properties may be reliable when a suitable sample is used, the value of stress at break should be used with utmost care. It must be mentioned that a wide literature is available on this type of material and many results are presented from tests which do not satisfy validity criteria.
- Bulk modulus (K) obtained from hydrostatic compression seems slightly lower than the value determined by uniaxial compression. At this time no clear explanation on this point can be given, it may be related to damageable behaviour of the material. The confrontation of results with results obtained from numerical analysis would be interesting but such numerical micromechanics analysis has to be performed with realistic input data (diameter and thickness distributions).
- Elastic properties issued from shear tests are at this time unreliable. Improving the test methods is clearly necessary for this type of material.
- Shear deformation obtained with a modified Arcan test is significantly higher than shear deformation obtained with the Iosipescu test. This was a preliminary study of shear loading but in the future the former may enable failure envelopes to be generated for a range of combined loadings.

Chapter 3. DAMAGE EVALUATION

The different tests described in chapter 2 have allowed a damageable behaviour of the materials to be identified. The nature of this damage must now be identified, as well as its kinetics. Considering the main loading of the structure this identification will be carried out under hydrostatic compression loading. This identification is facilitated by the possibility to load a specimen under hydrostatic pressure with no significant edge effects, promoting a homogeneous mechanical response of the specimen under this type of loading.

For other type of loads, uniaxial compression, shear, biaxial loading ... the damage identification is much more complicated as edge effects are present and it is difficult to identify an area of homogenous loading.

Three types of techniques have been used for this identification:

1. The development of in situ evaluation of damage kinetics under pure hydrostatic compression has been performed by using X ray micro tomography. This measurement is at this time unique, and has needed specific design in terms of equipment.
2. Considering the cost of X ray microtomography inspections, ex situ evaluation of damage has been performed by measurement of microsphere specific gravity after hydrostatic loading. This measurement is based on the use of accurate specific gravity measurement using a gas pcynometer.
3. Finally acoustic emission measurement has been performed. This technique is well known in the damage evaluation domain, and its application potential for syntactic foam studies has been evaluated.

3.1 X ray tomography

3.1.1 Presentation

X ray tomography is an attractive method to visualize and quantify internal damage of materials [105-108]. Tomography combines information from a large number of X-ray radiographs taken with different viewing angles of the sample. The technique contains a calculation step, i.e., it includes a step during which a 3D map of the local absorption coefficients in each elementary volume of the sample is calculated from the set of absorption radiographs. This map gives an indirect image of the microstructure.

This technique has been previously used to visualize the structure of syntactic foam [109] and imaging under in situ confined pressure has recently been performed. This has demonstrated a very interesting potential. However, as the results from such tests are difficult to interpret due to the inhomogeneous loading of the material in a confined pressure test, (as described previously in chapter 2), in the present study the in situ examination of syntactic foam under pure hydrostatic compression has been developed.

This study has been performed in collaboration with the Mateis INSA Laboratory in Lyon.

3.1.2 Test equipment

Internal observation of damage during the compression tests was carried out by means of a three-dimensional (3D) non-destructive technique, high-resolution X-ray tomography. Using this technique, disturbance-free information about the microstructure throughout the volume can be obtained. Very detailed descriptions of this technique can be found in [110, 111]. In the present study, the samples were scanned using a high-resolution X-ray tomography located at the ESRF (European Synchrotron Research Facility beam line ID 19) in Grenoble (France).

Based on equipment previously developed by the MATEIS laboratory of INSA and on the experience gained during their previous experiments a test set up has been designed allowing a sample of about 2*2*5 mm^3 to be hydrostatically loaded in an x-ray transparent tube to a pressure up to 60 MPa during the X-ray imaging. This equipment uses a stepping motor, which moves a piston in a small hyperbaric tank filled with water. The piston displacement induces a pressure increase. A load sensor indicates the pressure in the chamber.

Considering the step of the motor and the compressibility of water, the diameter of the tank has been calculated to reach a pressure increase of 10 MPa with a piston displacement of 20 mm [112]. The material of the hyperbaric tank has to be chosen to have the lowest possible X-ray absorption level in order to avoid screening of the signal and loss of resolution [112].

The equipment is designed to withstand 5KN and the displacement range of the piston is 25 mm.

Based on these elements the set up has been adapted in order to reach 60 MPa with the possibility to control the pressure by steps of about 1 MPa.

The principle of the equipment is shown in Figure 92.

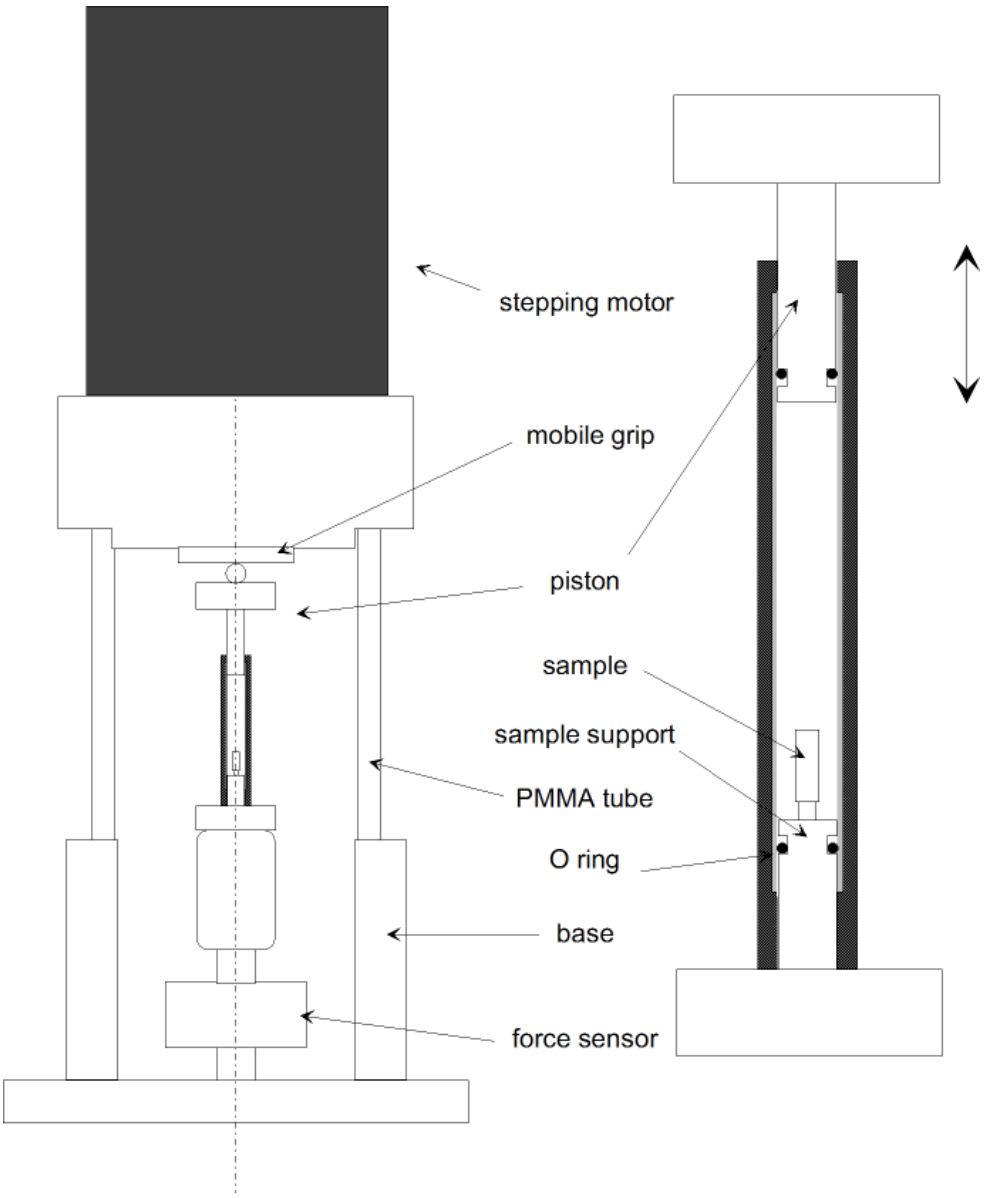

Figure 92 : loading set up for microtomography examination

In a first prototype an aluminium tank was manufactured and adhesive bonding was used to guarantee perfect sealing of the system. The inner diameter of the tube was 6 mm and the thickness of the tube 0.9 mm. The system was limited to 60 MPa due to loss of watertight integrity caused by adhesive failure.

In a second improved system O ring seals were used and gave satisfactory results, still with aluminium tubes. However, aluminium is not optimal with respect to the shielding of the X-ray signal, so a composite tube system was then developed. The Xray absorption coefficient

of carbon fibre/epoxy has been demonstrated to be about 4 times lower than that of the aluminium material.

Considering internal pressure without edge effect a filament wound carbon/epoxy tube was designed with +/- 85° fibre orientation. The thickness was limited to 0.75 mm, for an inner diameter of 6 mm.

Preliminary trials gave unsatisfactory results due to leakage by “weeping” through the tube [113]. This phenomenon has been widely studied and can be solved by using an adapted liner system.

New tubes were therefore designed using a 0.25 mm thick PE liner inside a 0.75 mm thick composite tube. However, further improvements were then needed in order to avoid creep of the inner PE tube due to internal pressure. This was achieved by a new design of the tube (figure 93 et 94)

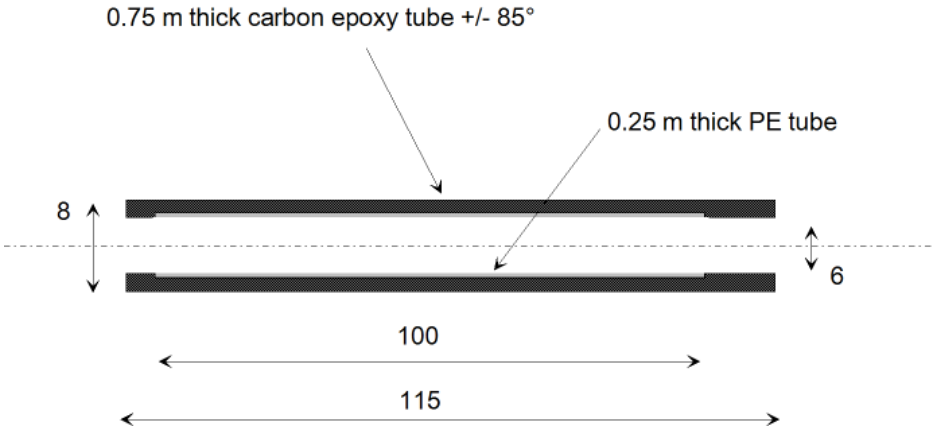

Figure 93 : tube for hydrostatic compression (dimensions in mm)

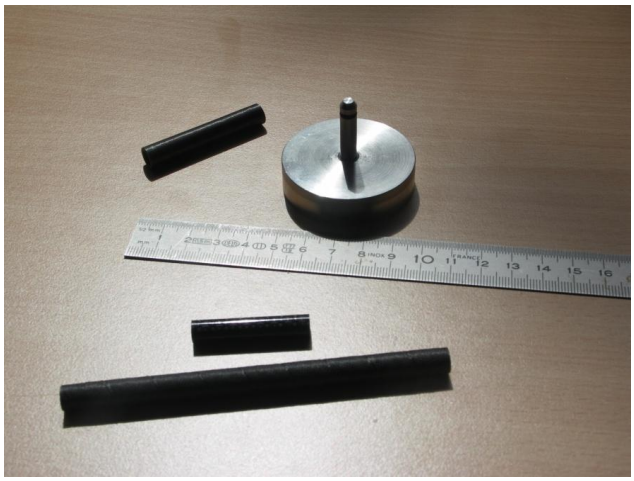

Figure 94 : carbon tubes & loading piston

Satisfactory results were obtained at internal pressures up to 60 MPa, with low X-ray shielding by the tube.

The loading equipment was placed on the rotating table of the beam line ID19 of the ESRF. X-ray tomography was performed at a voxel size of $(3.5\ \mu m)^3$. The energy was set to 17.5 keV. The distance between the sample and the detector was ~50mm.

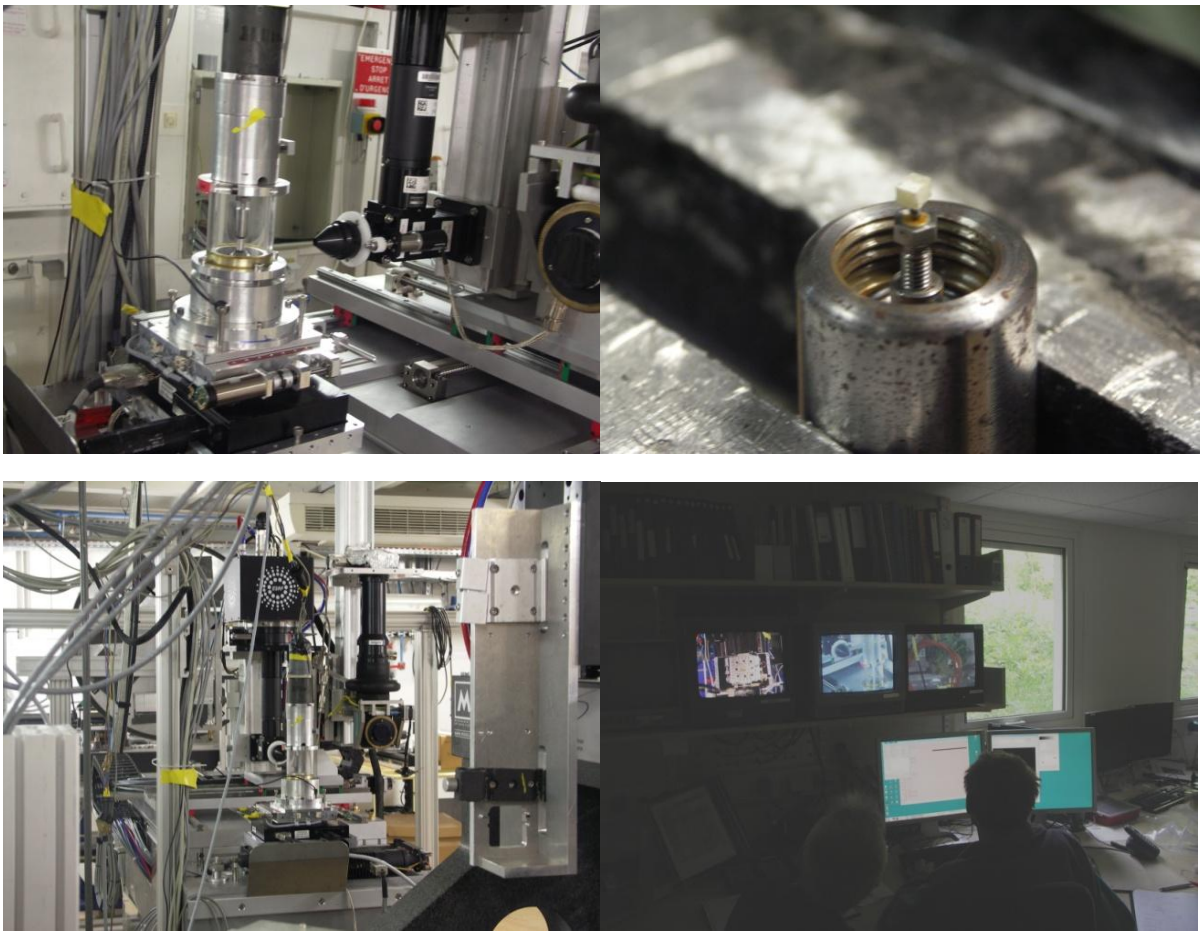

Figure 95 : X-ray micro tomography equipment (upper right shows sample to be tested)

By means of the equipment described above the pressure is increased in the chamber step by step. At each step of measurement the sample is scanned. From the pictures collected, the ESRF software reconstructs slice by slice the volume of the specimen. These slices are then visually analysed to evaluate the damage kinetics.

3.1.3 Results

A campaign of tests was performed on GSPU and GSEP samples. Specimen size was about 2 * 2 * 4 mm^3 and samples were scanned during pressure increase. The loading media was tap water. The GSPU sample was initially coated by PU material in order to avoid water ingress.

The duration of one scan to collect the set of slices to describe a volume of 1*1*1 mm is about 5 minutes.

The test conditions are reported on table 20.

material	GSPU	GSEP
Loading media	water	water
No. of slices	821	971
Image size	550*600	430*520
Steps of measurement (MPa)	0 6 11 22 22 30 37 42 50 0	0 6 11 22 26 38 0

Table 20 : X-ray microtomography test conditions

The test on GSEP was stopped at 38 MPa due to a technical problem.

Typical slice views of each foams are shown on figure 96.

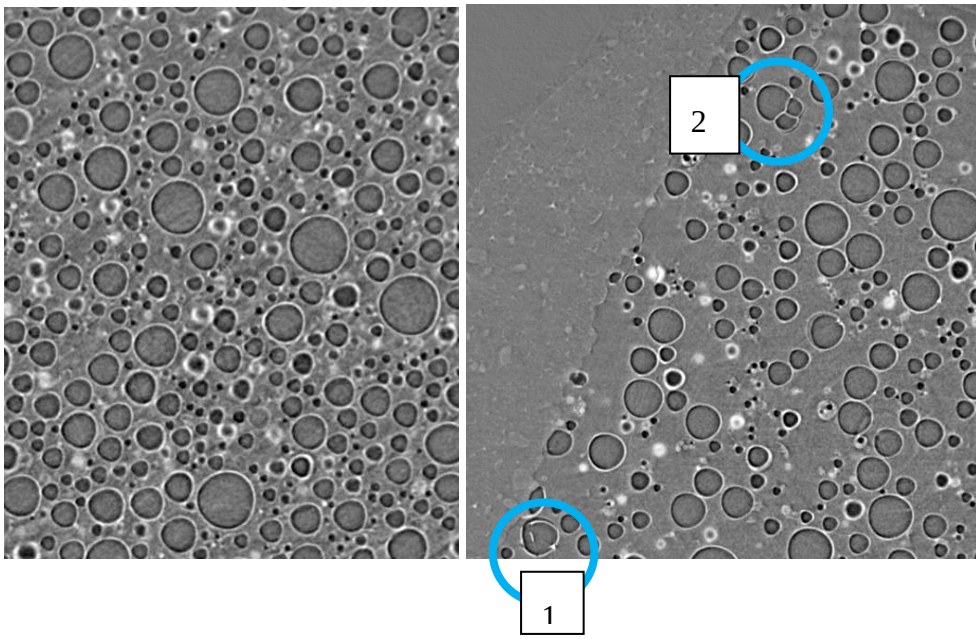

Figure 96 : typical slice view from microtomography, unloaded specimen (left GSEP, right GSPU)

On this view the microsphere distributions can be observed and the higher filler content of the GSEP is clearly noted.

On GSPU it has been chosen to analyze the edge of the sample. In a first analysis, some initially cracked bubbles can be noted (detail 1) close to the surface, as well as non spherical fillers (detail 2).

Taking into account the resolution in terms of gray level it must be noted that it is difficult to distinguish between matrix and gas contained in the microspheres. Previous work performed ex situ, without any water or tube around the sample, gives higher contrast images and then allows a more discriminating analysis to be performed so quantitative analysis could be made. In the case of in situ examination the exposure time has to be limited in order to avoid creep deformation during scanning.

We have limited our analysis here to a qualitative description of the material behaviour under hydrostatic pressure.

Typical slice views at different loading steps are reported in Appendix 6.10.

3.1.4 Analysis

Some representative images are reported hereafter to reveal the behaviour of the material

GSPU

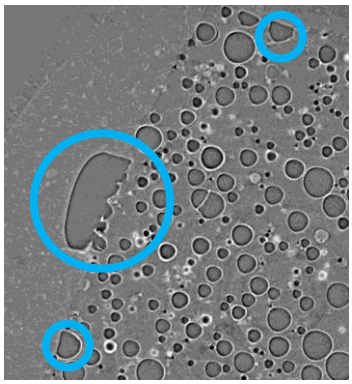

0 MPa

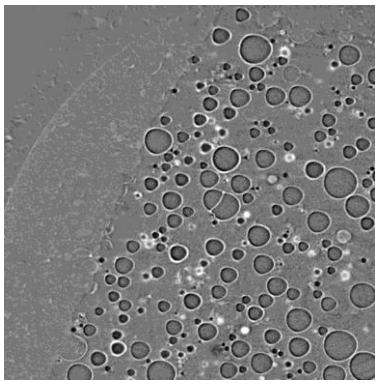

6 MPa

the increase of pressure collapses all the open voids

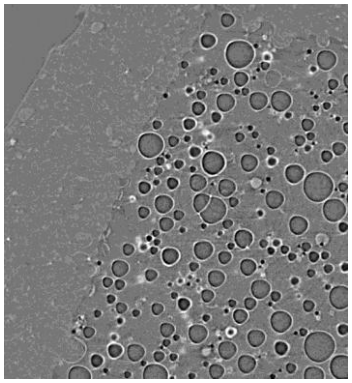

23 MPa

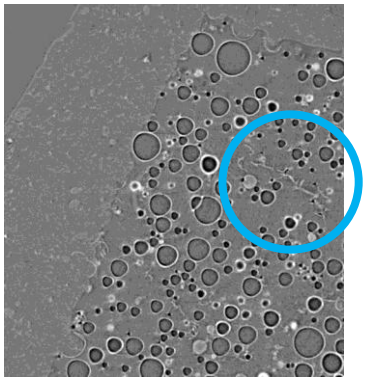

30 MPa

Start of collapse

Collapse of microspheres and filling of the open voids by matrix deformation

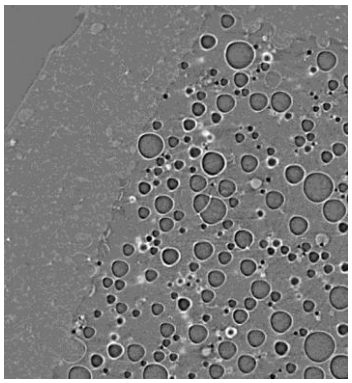

23 MPa

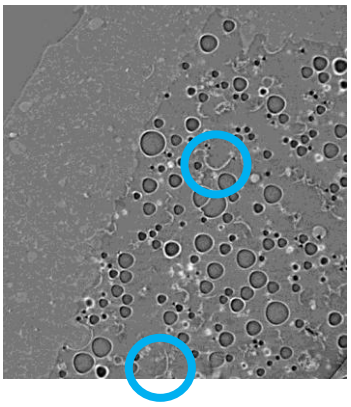

43 MPa

Significant increase of collapsed microspheres.

Visible broken glass wall of microsphere

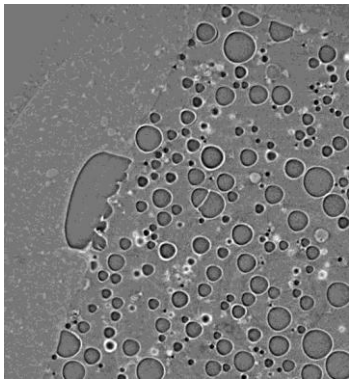

0 MPa

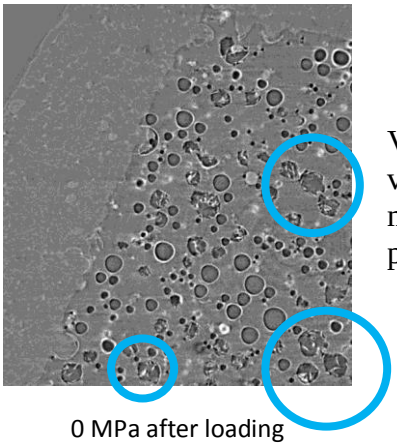

0 MPa after loading

Visco-elastic opening of the voids generated by collapsed microspheres when the pressure is released

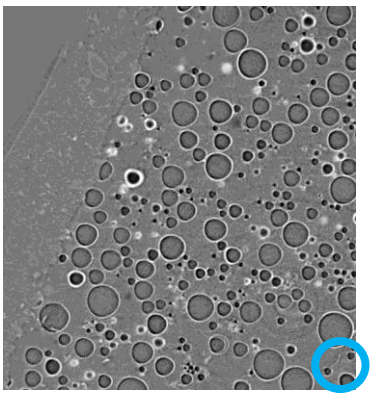

0 MPa

Visible broken glass wall of microsphere. For GSPU the manufacturing process may induce initial collapse of some micro balloons.

These images allow visualization of the damage occurring in the material when pressure increases. Some remarks can be made:

- The collapse of spheres induces a global volume reduction of the material. The volume of collapsed microspheres is filled by visco elastic matrix deformation. Considering the matrix behaviour this deformation is apparently very fast.
- The damage generated could be considered as isotropic. There is not the preferred direction of the damage shown during confined pressure tests.
- The damage is obviously localized but can be considered as homogeneous at a macro scale.
- When pressure is released, the specimen recovers its initial volume by visco elastic deformation of the voids generated by microsphere collapse. It must be mentioned that initially the microsphere contains gas and it is probably the expansion of the gas due to release of pressure which generates this phenomenon. The term “void” is obviously used abusively here.
- It is not always the bigger spheres which collapse first, the resistance of the microsphere being mainly governed by the thickness/radius ratio. With the definition

level of the images available it is difficult to discriminate the wall thickness of the microspheres.

- Imperfect spheres can still have a good resistance.

GSEP

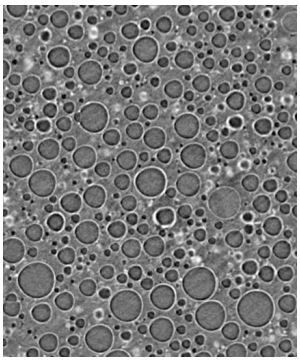

0 MPa

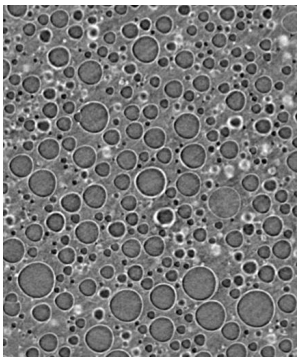

6 MPa

No significant change

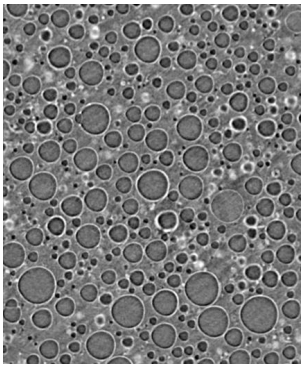

0 MPa

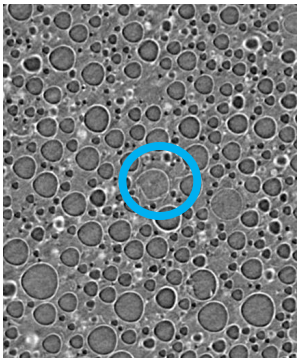

22 MPa

Identification of first collapse.

No volume change. The matrix skeleton remains unchanged

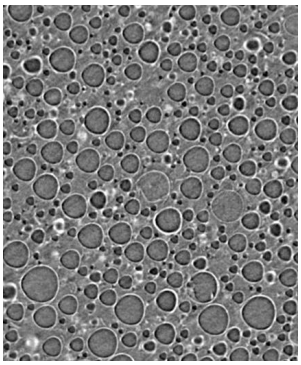

22 MPa

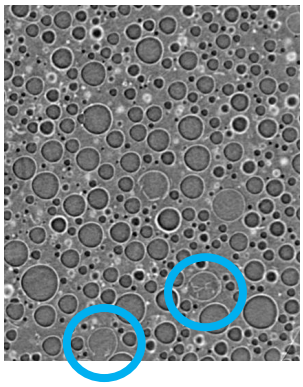

38 MPa

Significant increase of collapse events, always with no significant volume change

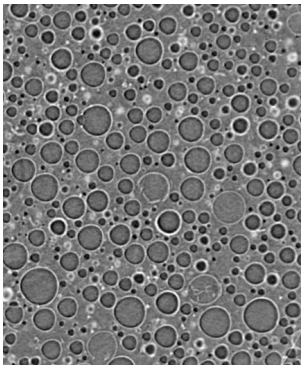

38 MPa

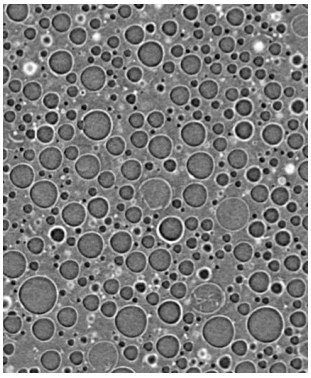

0 MPa after loading

No change

The following remarks can be made for GSEP:

- The collapse of spheres does not induce a global volume reduction of the material. The matrix skeleton remains unchanged even if collapse of microspheres occurs.
- The first significant collapse of microspheres occurs around 25 MPa.
- The geometry of the material remains unchanged after unloading. As mentioned previously maximum pressure was limited to 38 MPa (around 50% of the break stress) for this test. For higher pressure additional investigation is needed.

3.1.5 Conclusions on in-situ damage detection.

The experience gained by the Mateis laboratory with X-ray microtomography has shown that this is a very attractive method for understanding syntactic foam behaviour.

An original experimental set up has been designed allowing in situ examination of syntactic foam under hydrostatic compression up to 60 MPa. This system can be considered at this stage to be unique.

This development has required the design and manufacturing of a very small hyperbaric tank in composite material, in order to limit the X-ray absorption by the equipment which would limit its performance in terms of image quality. Considering the size of the sample tested it could be envisaged to decrease the diameter of the tank further and hence to increase the sensitivity and the resolution of the technique.

The purpose of this test was to verify the feasibility and to provide information on the material behaviour under hydrostatic pressure. At this stage only a qualitative analysis has been performed. Quantitative analysis will require considerable additional time and development and is not the object of the present study.

Hydrostatic pressure induces damage in the material by collapse of microspheres. It is difficult to affirm that the bigger microspheres collapse first, as the wall thickness and the shape (sphericity) of the microspheres influence the collapse pressure of the microspheres.

Damage generated by hydrostatic pressure is isotropic and homogenous at the macro scale.

To a first approach, up to 40 MPa, the kinetics of damage increase (collapse of microspheres) seem quite similar for the two materials with a start of significant damage around 25 MPa. Quantitative analysis on the whole volume of samples is needed to confirm this point

However, GSPU and GSEP exhibit different behaviour. When damage occurs in GSEP the matrix skeleton remains unchanged. For GSPU the collapsed microspheres are replaced by the matrix inducing reorganization of the material. This point confirms the densification of GSPU at high pressure.

When the pressure is released the GSEP material remains almost unchanged while for GSPU the material tends to recover its initial shape.

All these points confirm the behaviour of the material identified previously by hydrostatic compression tests.

The Mateis laboratory has currently developments in the domain of damage quantification [114], but at this time this work is not addressing the syntactic foam materials.

3.2 Ex situ damage measurement.

Micro tomography is a very attractive method to evaluate the damage kinetics (see 3.1) in syntactic foams. However this technique requires expensive equipment, is currently limited to small volumes of material and still needs improvement in particular in the analysis of results in order to provide the unbroken sphere volume ratio and, if possible, their diameter distribution.

An alternative to estimate the volume fraction of broken spheres is to perform ex situ measurements. This consists of analyzing samples after loading, in our case after different steps of hydrostatic loading.

Classically in materials science, SEM (Scanning Electron Microscope) examination of material is performed to evaluate damage (crack, collapse …). In the case of syntactic foam this observation is not recommended as any surface preparation will induce damage at the scale of the microspheres.

It was therefore decided to analyze the microspheres after burning off the matrix of the material. This technique is widely used with composites to evaluate fibre content of the material. For syntactic foam this technique is also used to evaluate the mass content of unburned material. Attention must be paid to the fact that syntactic foam is not only polymer + microspheres. Mineral fillers are added to the material for different reasons (e.g for GSPU a humidity absorber is currently included).

Calcinations were performed at 450°C and the ash content was analyzed. In order to guarantee total removal of the polymeric material a burning duration of at least 24 hours is needed.

The volume percentage of broken microsphere can be estimated by evaluation of the density of the fillers. The density of broken bubbles is equal to the density of the glass, that is 2.7 g/cm^3, while the density of the intact microsphere corresponds globally to the density of the microspheres as given in the manufacturer's datasheets.

In a first attempt to separate broken glass and unbroken microspheres, a decantation technique was used. The decantation was done in different liquids: water, water + surfactant, ethylic alcohol Centrifugation was used to optimize the decantation. After decantation, followed by drying, the weight and volume of floating material were compared with those of the fluid. However, no pertinent analysis could be performed on these results and the method was abandoned.

In a second approach it was decided to perform density measurements of the material. A double chamber gas pycnometer was designed in accordance with EN ISO 1183-3 Methods for determining the density of non-cellular plastics — Part 3: Gas pycnometer method.

3.2.1 Pcynometer principle

A pycnometer is composed of: a gas capacity (helium is generally chosen), a pressure sensor, two chambers, 3 valves and a calibration volume. The operating principle is described in 6.11 and a schematic diagram is reported on figure 97.

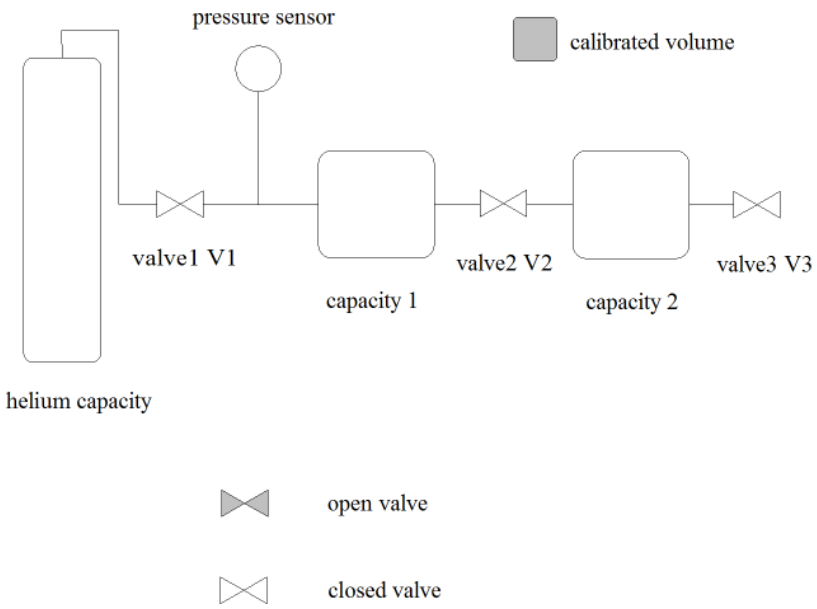

Figure 97 : schematic diagram of pcynometer

The chambers of the in-house designed pycnometer are visualized on Figure 98. The volume of the chamber has been fixed at 0.02 dm^3.

Figure 98 : in house pycnometer

However, after calibration steps and measurements on different materials, the accuracy obtained was considered not to be sufficient. For a 1100 kg/dm^3 material, an accuracy and repeatability around +/-50 kg/dm^3 was obtained and for 150 kg/dm^3 glass bubbles these were reduced to +/-10 kg/m^3.

Given the limits of the results obtained with the in-house pycnometer it was decided to evaluate commercial equipment. This equipment, AccuPyc™ II 1340, is manufactured by the Micromeritics Company and is shown on Figure 99.

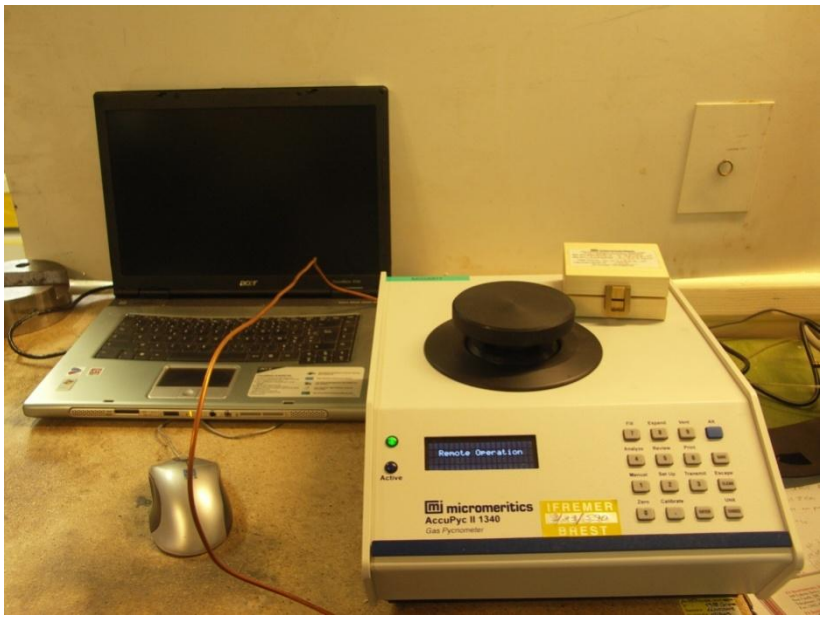

Figure 99 : Accupyc™ pycnometer

The variation coefficient evaluated on 10 measurements on the same sample is about $<5* 10^{-4}$ which is far better than that of the in-house equipment.

Based on the capacity of this equipment it was then decided to evaluate the density of the microspheres after calcination of samples of material which had been subjected to different pressures.

3.2.2 Pycnometer measurement

The measurement procedure was as follows:

Sampling of 20 coupons of material (about 5*5*5 cm).

Two reference samples which were not loaded.

The others samples in pairs were hydrostatically loaded in water at 20°C to different pressures.

The rate of increase of pressure was about 20 bar/min.

The maximum pressure was maintained for 10 minutes.

The samples were then placed in an oven at a temperature of 450°C for a minimum of 24 hours, the time necessary to guarantee complete removal of the resin.

The microspheres were recovered and density measurements were performed using the Accupyc pycnometer. Before placing in the equipment, the mass of the sample was determined, with a 1 μg accuracy balance.

3.2.3 GSPU Results

The results are reported for the GSPU material in 6.13 and presented in Figure 100

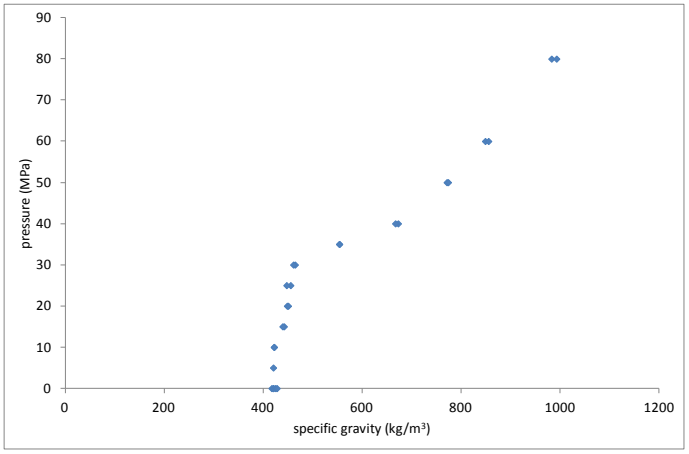

Figure 100 : evolution of filler specific gravity versus pressure for GSPU

There is a good reproducibility of the results (2 samples per pressure) and good accuracy of the measurement. A coefficient of variation better than 1% is calculated. This coefficient integrates the reproducibility of the measurement and the homogeneity in terms of microsphere density. It can be noted that after a pressure increase up to 80 MPa the specific gravity of the filler is about 1000 kg/m^3 which is far below the specific gravity of the glass. This means that all the microspheres are not collapsed.

To go further in the analysis these results have to be expressed in terms of percentage by volume of broken bubbles versus pressure.

The diameter distribution of microspheres of the same grade is not constant so it must be considered that the density of the microspheres is not uniform. For the S38HS grade, 3M gives the following information:

Particle size in volume of 10th % is <19 µm,

Particle size in volume of 50th % is <65 µm,

Particle size in volume of 90th % is <70 µm,

Effective maximum size is 85 µm.

Laser sizing can be used to evaluate the effective particle size of a set of materials, but considering the data provided by the manufacturer, and based on microtomography analysis [44] which mentions a mean thickness of the microspheres of 1.3 µm an estimation of the density of microspheres by size can be made.

The measured specific gravity corresponds to the weight of the bubbles (unchanged whatever the level of loading) divided by the sum of the volume of uncollapsed bubbles with the volume of glass of collapsed bubbles.

In order to estimate this parameter for this analysis some hypotheses have to be made:

- The specific gravity of glass of 2.52 kg/m^3.
- The distribution of the diameters is taken from the commercial information.
- No other mineral material than microspheres is present in the syntactic foam.
- The bigger microspheres collapse first.
- The thickness of the spheres varies from 0.5 for spheres of radius 4.75 to 1.71 for a sphere of radius 38.75, and is proportional to the diameter of the sphere.

The third point leads to an estimation of an initial volume of collapsed bubbles. As mentioned previously some additional mineral filler may be added in the material to ease the manufacturing process, but at this stage this material is not considered.

The last hypothesis is based on results from Gimenez [27] which highlight a dependence of thickness on the diameter, and has been chosen to recover the specific gravity of the non collapsed microspheres provided by the manufacturer.

The relation between volume percentage of uncollapsed bubbles and density of the material is reported on Figure 101.

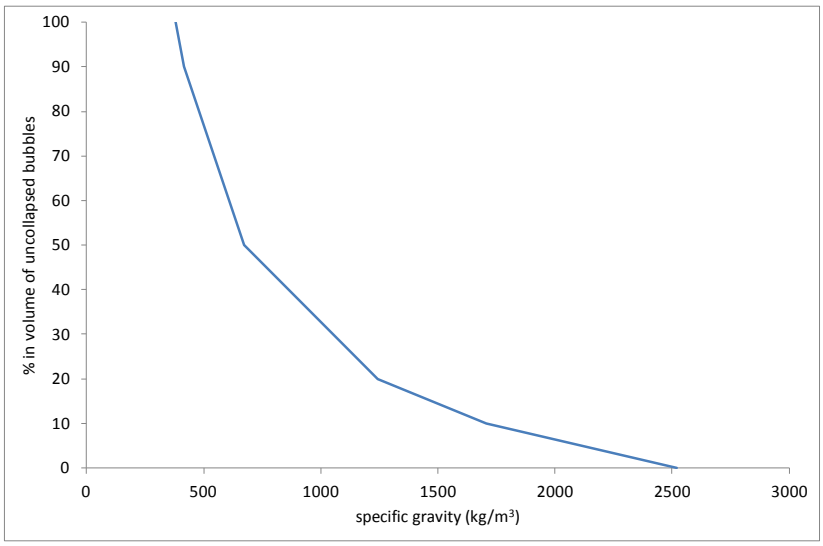

Figure 101 : estimation of the uncollasped volume of microsphere versus filler density

From these results the evolution of percentage of volume of uncollapsed bubbles can be estimated as reported on Figure 102.

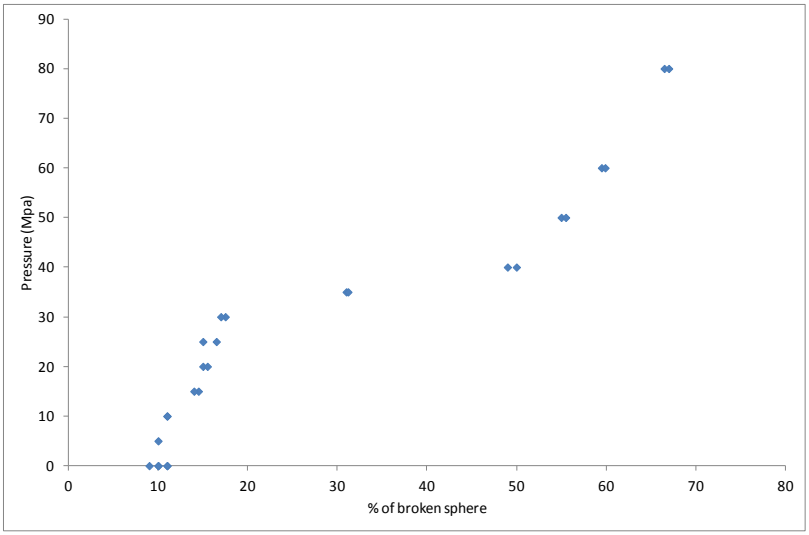

Figure 102 : evolution of the volume of collapsed broken sphere versus pressure

These curves have clearly to be compared to the hydrostatic compression curve for GSPU material (Figure 53).

3.2.4 GSEP Results

Identical tests have been performed on GSEP material.

Unfortunately unexpected difficulties were encountered with the specific gravity measurement. On GSEP it was impossible to reach a stable pressure with the pcynometer.

This difficulty seems to be related to the difficulty in obtaining real powder after burning of the resin. The duration of the calcination was therefore increased to 72 hours to ensure total burning of the resin. Different burning cycles and temperatures were also tested.

However aggregates of microspheres were always present, and considering the weaknesses of the microspheres it was impossible to recover powder from this aggregate without collapsing microspheres. The formation of this aggregate is probably due to the low resin volume content of the GSEP material.

At this stage no procedure has been found to solve the problem, so the method is restricted to GSPU materials.

3.2.5 Conclusions

The use of pycnometer measurement is an attractive method to measure glass microsphere specific gravity. This method is in fact the method classically used during the industrial process to verify the density of the microspheres.

The design of this equipment has to be optimized to provide pertinent information and at this stage the use of commercial equipment is preferred.

This method has been applied to quantify the damage in syntactic material after pressure loading, by an evaluation of the volume of microsphere collapse based on measuring glass microsphere density.

This method was successful for the GSPU material where a correlation between glass microsphere collapse and volume change under hydrostatic pressure has been shown.

However this method seems not to be applicable for GSEP material with high microsphere volume content.

3.3 Use of acoustic emission

Acoustic emission is an attractive method for damage identification and it can be used for damage quantification with adapted methods [115-117].

An attempt to use acoustic emission on syntactic foam under hydrostatic compression loading has already been related [118], which has identified the possibility of using this approach for damage identification. In the present study this method has therefore been applied.

3.3.1 Equipment used

A PCI2 Europhysical Acoustic™ system was used, coupled to 2 R15 sensors and standard Euro Physical 2/4/6 preamplifiers.

The sensors were located on the outer surface of a testing tank in which the sample was placed. The pressure was increased in the tank via a manual piston pump. This system has been chosen in order to limit the mechanical noise which would be generated by an air pump or a hydraulic pump. The schematic drawing is reported on Figure 103.

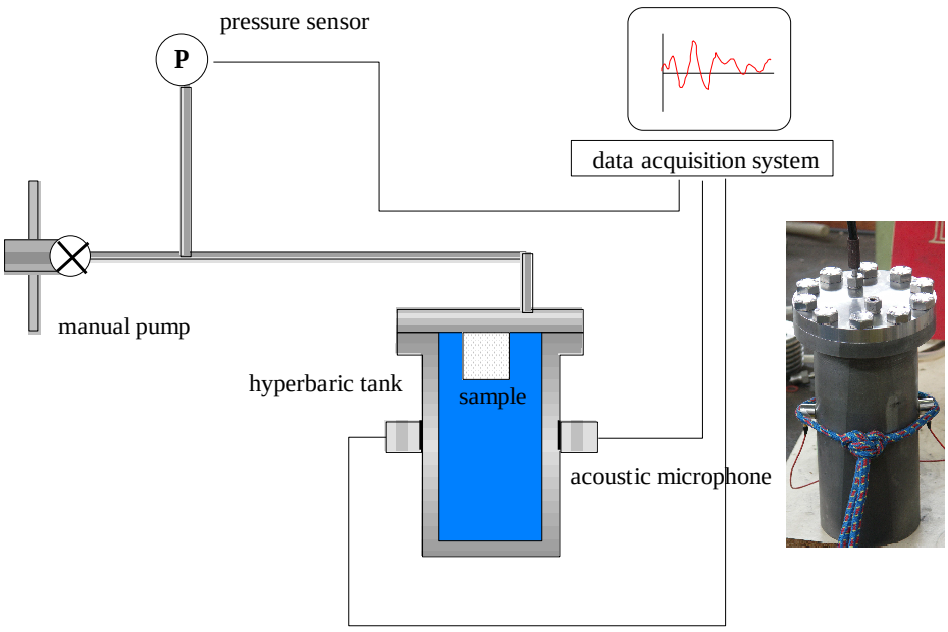

Figure 103 : Acoustic emission measurement during pressure increase

3.3.2 Results

In order to verify the interest of this method it was first tested by applying a load- unload sequence to GSPU samples. The results are reported on Figure 104

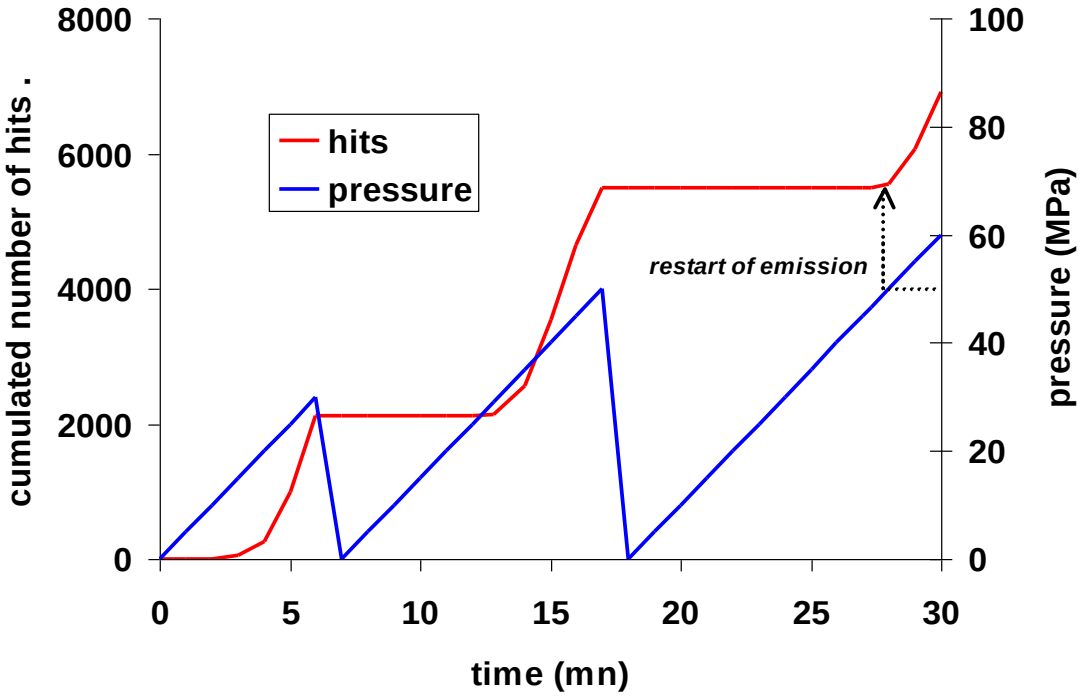

Figure 104 : evolution of hit number and pressure versus time

The analysis is limited to a report of the cumulated number of hits versus time and pressure.

It can be noted that the damage onset is identified by this method, which reveals a classical Kaiser effect with no additional hits between the release of pressure, reloading to the same level, then new acoustic emission beyond the maximum load level previously reached.

It should also be mentioned that the start of emission is about 10 MPa, which represents an early level of damage detection when compared with other methods previously reported.

To investigate this further, tests have been performed on GSPU samples of different sizes (mat C), and compared with the results obtained on GSEP samples (mat E) in Figure 105.

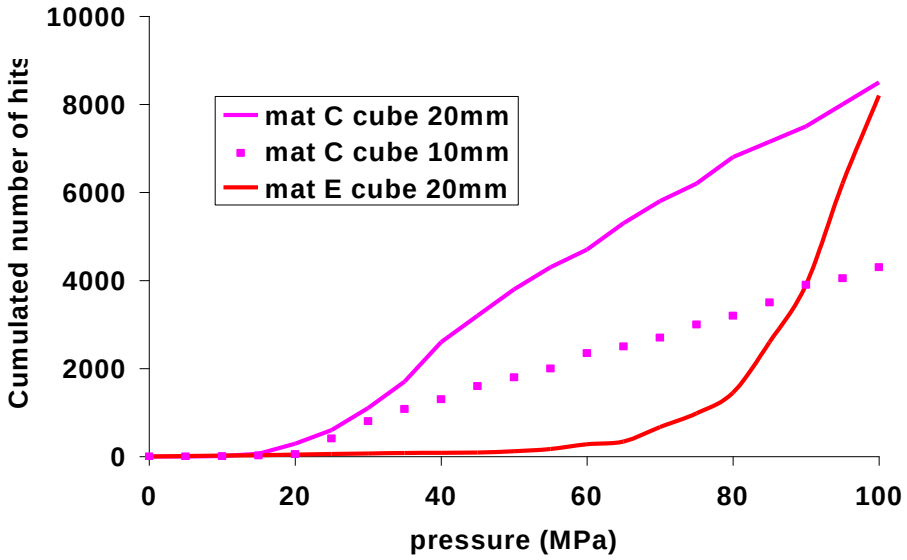

Figure 105 : Evolution of number of EA hits versus pressure

The following points can be noted:

- There is a significantly higher number of hits for GSPU than for GSEP.
- The kinetics of numbers of hits for GSPU is quasi linear while they appear more or less exponential for GSEP.
- For specimens with a volume eight times superior (20 mm edge cube instead of 10 mm) the number of hits is only doubled.

Considering a global damage process, the last remark indicates the limit of this method for a quantification of damage occurrence.

It should be noted that these materials (particularly GSPU) under pressure loading generate a high level of acoustic emission, and that with the equipment available it is difficult to discriminate the different hits properly (almost continuous emission).

3.3.3 Conclusions

Acoustic emission is potentially an interesting method to detect damage initiation in syntactic foams. The syntactic foam under load generates large acoustic signals which may be attributed to the collapse of microspheres. Tests under hydrostatic compression can be performed, but care must be taken to limit the signals generated by the loading device.

However, with the classical tools available a quantification of the damage appears to be very difficult.

Chapter 4. MODELLING APPROACH

The tests performed during this study allow phenomenological models of the material behaviour to be established, and in particular under hydrostatic compression. The behaviour of GSEP and GSPU materials are slightly different but are mainly governed by the collapse of the microspheres Figures 106 & 107.

A mechanical analysis of the microsphere behaviour, taking into account the size distribution in terms of diameter and thickness will be performed first in order to evaluate the parameters governing the collapse of the microspheres.

Then the basis for a more complex mechanical model of syntactic foam under hydrostatic compression will be proposed.

4.1 Effect of broken spheres on the material behavior.

Micro-tomography has revealed the behaviour of these materials under hydrostatic pressure and highlighted that collapse of microsphere occurs when pressure is increased. This collapse of microspheres induces consequences which depend on the nature of the material.

For epoxy syntactic foam, before the global collapse of the material, collapse of microspheres will induce overloading of the residual intact material. The global collapse of the material is governed by compressive collapse of the matrix skeleton. As the collapse of microspheres occurs before the final collapse of the material this reduces the safety factor in terms of capability to withstand the hydrostatic pressure.

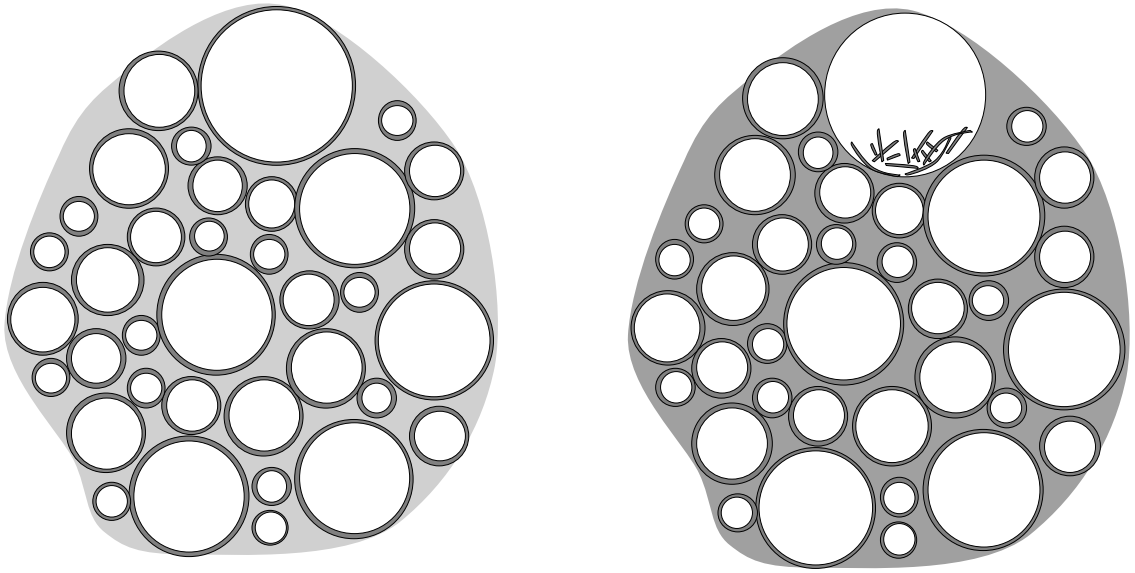

Figure 106 : evolution of microstructure of GSEP with hydrostatic pressure

Left initial condition

Right after pressure increase: collapse of microsphere, no significant volume change – overloading of matrix skeleton and residual microsphere

There is no significant change of volume with pressure increase so the buoyancy of the material is still quasi constant at short term. However, the collapse of microspheres will increase drastically the water uptake potential of the material. The diffusion of water into the material, and filling of the broken microspheres with water can lead to a weight increase of greater than 90% [60]. It should be mentioned that the absorption kinetics are not governed by a single Fickian law and a specific absorption model for syntactic foam has been developed.

For GSPU, considering the low modulus of the matrix and its high elongation capacity, the collapse of a microsphere induces a change of volume of the material. The void generated by microsphere collapse is directly filled by the matrix, as shown in Chapter 3, and then the volume of the material reduces by the same proportion.

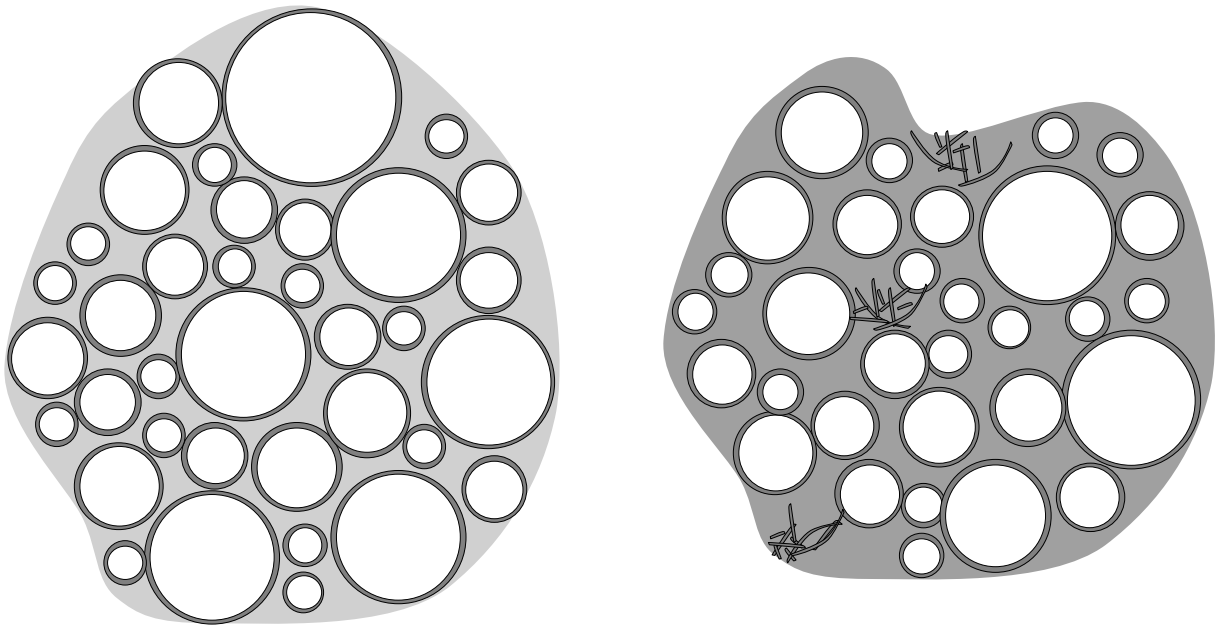

Figure 107 : evolution of microstructue of GSPU with hydrostatic pressure

Left initial condition

Right after pressure increase: collapse of microsphere and significant volume change

This change of volume induces directly a change in density of material and loss of buoyancy capacity.

The water uptake is generally directly correlated with the specific properties of the material. An increase of water uptake will directly decrease the buoyancy properties of the material and the thermal conductivity of material has also been shown to be directly related to the water content [56].

A model has been developed in order to link the water uptake with the evolution of the thermal conductivity. This model is based on the rule of mixtures and can be expressed as follows:

$$\Delta\lambda = vfw * \lambda w$$

with vfw = water volume fraction

λw = water thermal conductivity

On Figure 108 the absolute evolution of thermal conductivity of syntactic foams for different water contents is reported, corresponding to different durations and temperatures of immersion under service conditions.

For large water uptakes, the correlation between $\Delta\lambda$ calculated from the model and $\Delta\lambda$ measured on aged samples is quite good, and is reported on Figure 108.

Knowing the evolution of the water concentration level through a thickness of coating this can allow us to determine the evolution of the thermal conductivity.

The measured values are compared with the calculation.

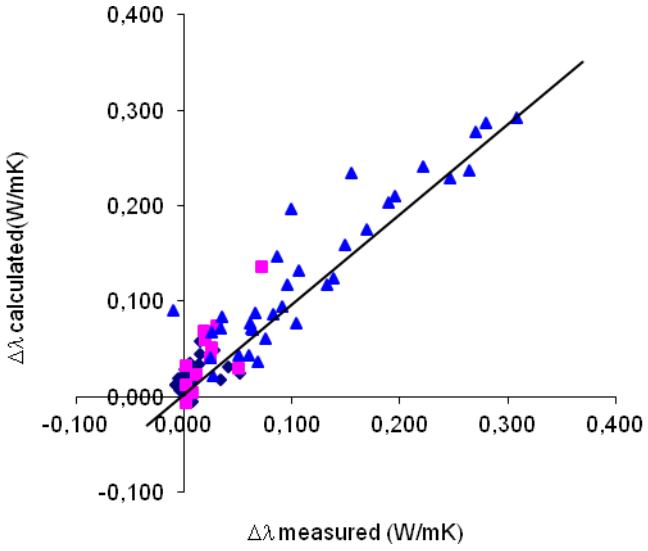

Figure 108 : measured and calculated evolution of thermal conductivity due to water uptake

4.2 Mechanical approach to the collapse of glass microspheres

On Figure 109 an in situ microtomography analysis of syntactic foam under confined compression is reported [44]. This analysis reveals that microspheres of larger diameter tend to collapse first when the material is subjected to confined compression. It can also be noted, and it is the aim in showing this figure, that the wall thickness of larger microspheres is generally slightly greater than the wall thickness of small diameter spheres.

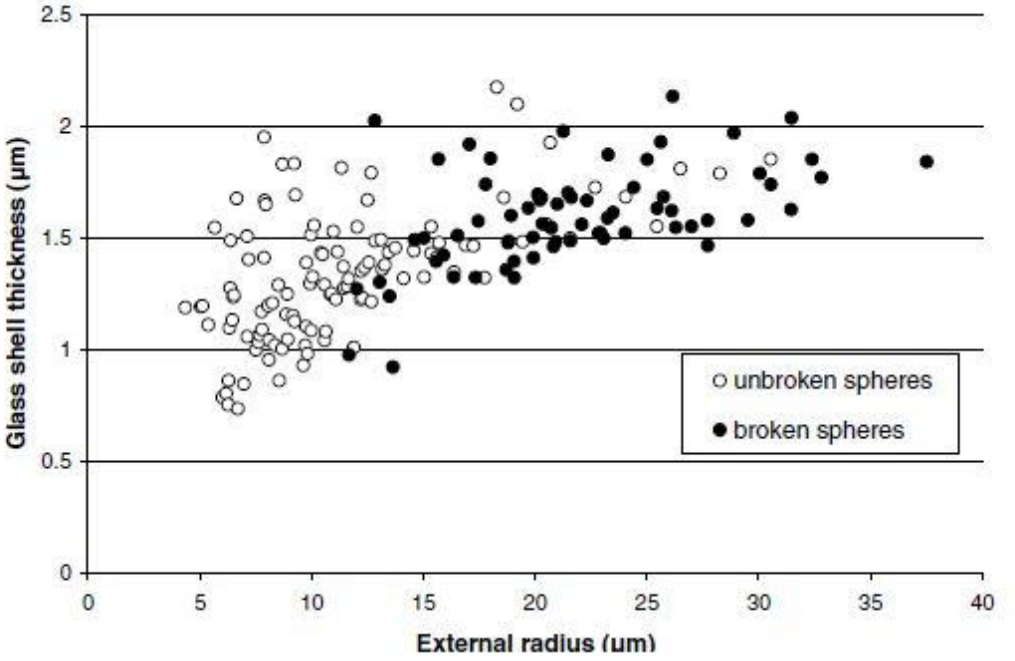

Figure 109 : Correlation between external radius and thickness of microsphere grade S38HS from [44]

From this graph an analysis in terms of diameter and thickness has been made and is reported on Figures 110 & 111. The specimens have been classified by range of radius and thickness.

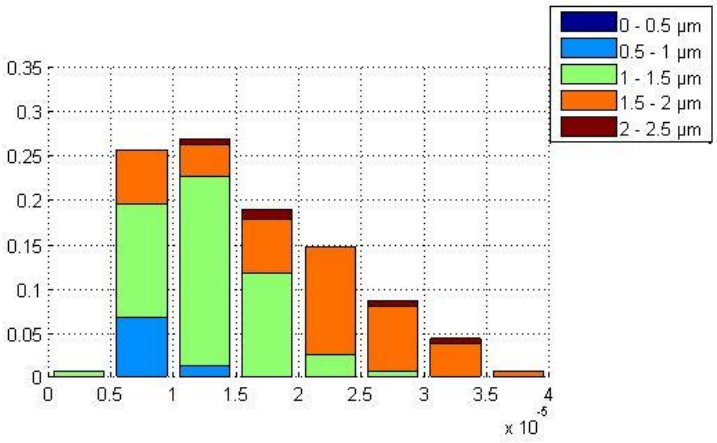

Figure 110 : Histogram of normalized number of microspheres by size distribution of radius (m)

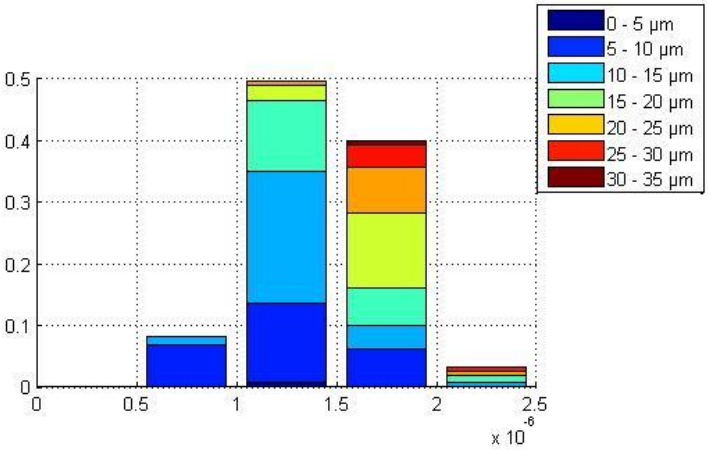

Figure 111 : Histogram of normalized number of microspheres by size distribution of thickness (m)

From these two graphs it can be noted that the range of radius is quite large, globally from 5 to 30 µm, and that most of the microspheres have a thickness between 1 and 2 µm.

To extend this, the analysis has been performed in terms of volume of gas included in each microsphere. This volume accounts for the specific properties of syntactic foam in terms of buoyancy and thermal conductivity. Simple models can be used to calculate these properties from the gas volume in the material [119].

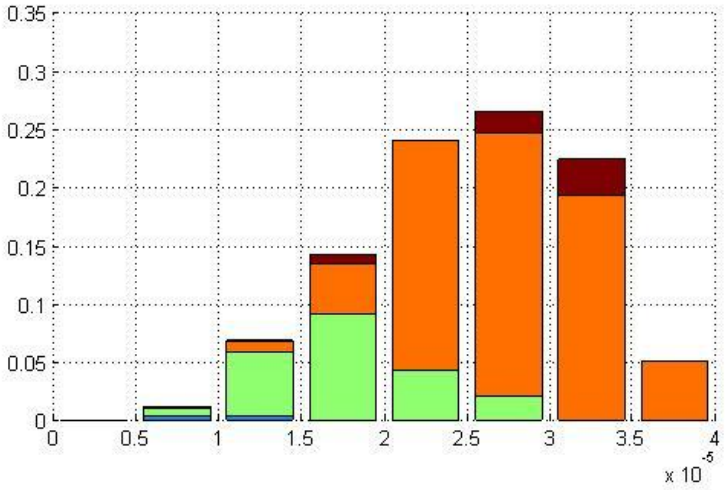

Figure 112 : Histogram of normalized volume of microspheres by size distribution of radius (m)

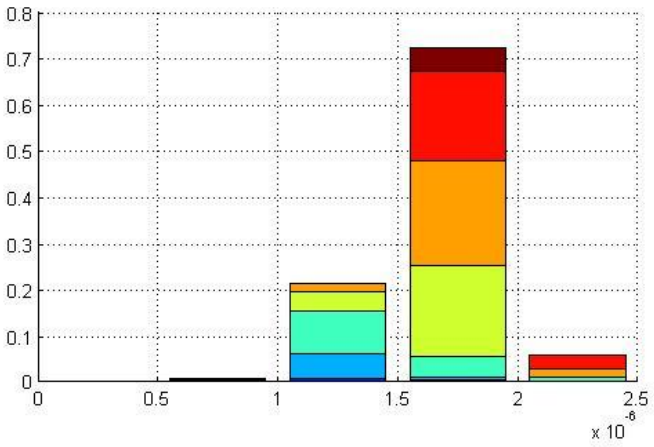

Figure 113 : Histogram of normalized volume of microspheres by size distribution of thickness (m)

These figures reveal that about 75% of the gas volume is included in the microspheres with thickness around 1.75 µm and radius between 20 and 35 µm.

The specific gravity of microspheres in each class has been calculated (Figure 114).

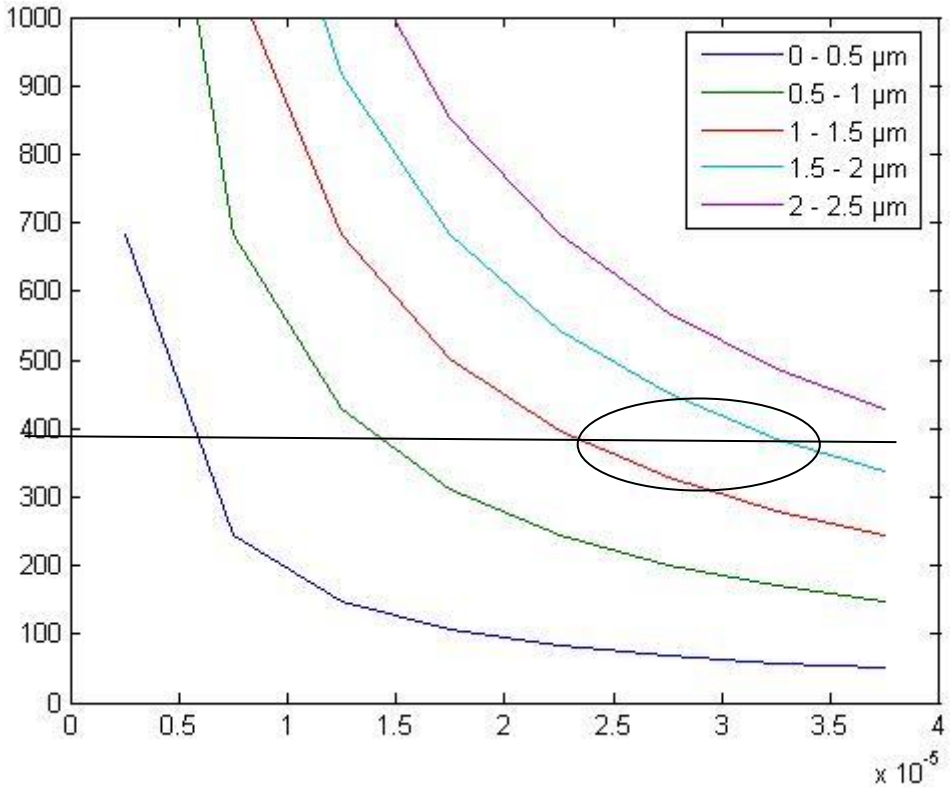

Figure 114 : Volume of microspheres versus radius for different wall thicknesses (m)

The ellipse localizes 75 % in terms of volume of the S38HS 3M glass microspheres.

Considering mechanical behaviour, it is easy, from a simple mechanical analysis, to estimate the capability of microspheres to withstand the hydrostatic pressure for the different classes of microspheres.

The capability to withstand the pressure can be approached in different ways by considering buckling of the sphere and maximum stress in the glass wall.

The ultimate buckling pressure of a spherical hollow tank submitted to hydrostatic pressure uniformly distributed on the surface and a null internal pressure is given by Timoshenko [120] as :

$$P_b = \frac{8 * E}{\sqrt{3 * (1 - \nu^2)}} * (\frac{t}{d})^2$$

Where

P_b : Buckling pressure

E : glass Young's modulus (72 GPa)

t : thickness

d : diameter

ν : Poisson's ratio (0.3)

This formula is limited to thin structures, and does not take into account geometrical imperfections of the microspheres nor buckling restriction effects induced by the polymer around the spheres.

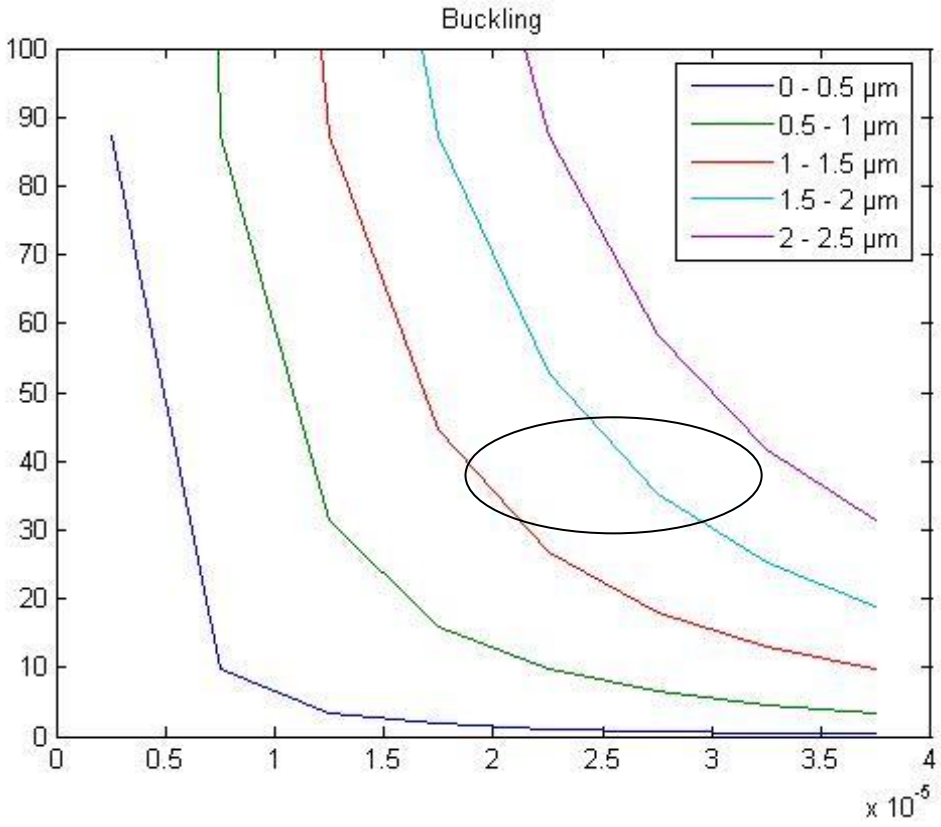

Figure 115 : buckling pressure (MPa) by class of microspheres

The ultimate pressure can also be evaluated by

$$P_y = \frac{\sigma_y * 2 * (d^3 - (d - 2t)^3)}{3 * d^3}$$

which evaluates the maximum compression stress in the glass wall of the microsphere.

Where

σ_y : yield strain (1500 MPa in compression)

It should be noted that the difficulty in using this formula resides in the uncertainty surrounding the evaluation of the σ_y in compression of the material. Values from 700 MPa [8] to 2600 MPa [121] can be found in the literature.

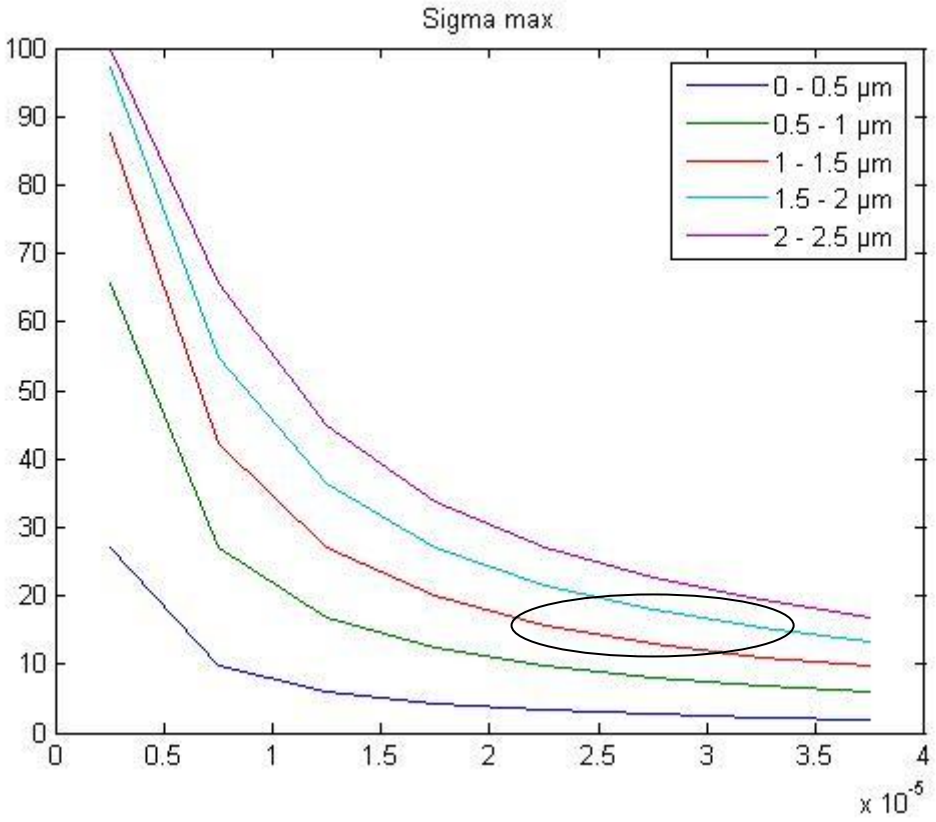

Figure 116 : collapse pressure (MPa) by class of microspheres

For brittle materials (i.e glass), a Tresca criterion is generally used. This criterion is expressed in relation with the compression yield limit of the glass. Considering that under hydrostatic pressure $\sigma_1 = \sigma_2$ and that σ_r max is equal to P at the outer surface of the sphere it can be considered that the Tresca criteria corresponds to the maximum stress criterion here.

This simple approach gives an indication of the behaviour of the material subjected to hydrostatic compression. The capacity to support the hydrostatic pressure of 75% in volume of the microspheres seems to be governed by the maximum stress in compression rather than the buckling. The indications obtained are not so far from the observations in terms of maximum pressure capability of the microsphere grade. Parametric studies in terms of optimization of grade sizing can be performed using this approach.

However limitations to this approach have to be borne in mind.

- Microspheres in the material are not purely hydrostatically loaded as the use of Eshelby's analysis could suggest and interactions between spheres can generate local overloading.
- It is difficult to determine the yield limit of the glass. In general for brittle materials a Weibull approach is used.
- As mentioned previously, the geometry of the spheres is generally not perfect.

- Anti buckling effects will depend on the behaviour of the surrounding polymer matrix material.

4.3 Mechanical modelling of syntactic foam

Mechanical models describing the elastic behaviour of syntactic foams are available in the literature. A classical model, obtained from homogenization, has been enhanced here in order to include a damage process. In order to represent the behaviour of the material revealed by the tests performed during this study, this damage process is represented by reducing the number of hollow spheres. This damage description is completed by a "plastic" strain associated with the compression of the material. This work has been performed with the technical support of Besancon University and the Mahytec Company.

4.3.1 Reminder of the homogenization method

Classical auto coherent models allow the complete description of elastic parameters of an n-phase material to be described.

The auto coherent model consists of two main steps:

- the auxiliary problem, definition of elements

- the effective application of an auto coherent diagram.

In the first step, the initial hypothesis has to be clearly defined: the heterogeneous medium to be modelled is supposed to consist of n families of homogenous elements. Each family (i), I from 1 to n, exhibits known elastic behaviour, fully defined by the strain-stress relation:

$$\underline{\sigma}^{(i)} = \underline{\underline{C}}_i : \underline{\varepsilon}^{(i)}$$

These families are defined by their volume fraction c_i, the shape of the constituents as well as their distribution in the reference macroscopic system.

In each phase the relations between σ(i) and ε(i) and the macroscopic stresses and strains $\underline{\Sigma}$ and $\underline{E}$ applied at infinity to the equivalent homogeneous media have to be established in order to solve the inclusion- matrix auxiliary problem.

The auto-coherent diagram is expressed using the conditions of mean stress and strain by

$$\underline{\Sigma} = \sum_i c_i \underline{\sigma}^{(i)}$$

$$\underline{E} = \sum_i c_i \underline{\varepsilon}^{(i)}$$

The localization tensor linking the strain of each phase with the macroscopic strain as a function of the properties of each phase is expressed from the auxiliary problem by:

$$\underline{\varepsilon}^{(i)tot} = \underline{\underline{A}}^{(i)} : \underline{E}$$

This relation can also be expressed by

$$\underline{\sigma}^{(i)} = \underline{\underline{B}}^{(i)} : \underline{\Sigma}$$

The elastic properties tensor of the equivalent material is given by the auto coherent model as:

$$\underline{\Sigma} = \sum_i c_i \underline{\underline{B}}^{(i)} : C_{eff} : \underline{E}$$

Or by

$$\sum_i c_i \underline{\underline{B}}^{(i)} = \underline{\underline{I}} \qquad \text{and} \qquad \sum_i c_i \underline{\underline{A}}^{(i)} = \underline{\underline{I}}$$

The determination of the localization tensor is solved by two other problems: the Eshelby problem and the heterogeneous inclusion problem, which will not be developed here and which lead in the case of an auto coherent diagram to:

$$\underline{\underline{A}}^{(i)} = \left[\underline{\underline{I}} + \underline{\underline{S}}^{H} : \underline{\underline{C}}^{-1} : (\underline{\underline{C}}^{(i)} - \underline{\underline{C}}_{eff}) \right]^{-1}$$

$$\underline{\underline{B}}^{(i)} = \underline{\underline{C}}^{(i)} : \left[\underline{\underline{I}} + \underline{\underline{S}}^{H} : \underline{\underline{C}}_{eff}{}^{-1} : (\underline{\underline{C}}^{(i)} - \underline{\underline{C}}_{eff}) \right]^{-1} : \underline{\underline{S}}$$

Where $\underline{\underline{S}}^{H}$ is the Eshelby tensor which can be calculated for an ellipsoidal inclusion and which only depends on the inclusion shape and the mechanical properties of the material surrounding the inclusion (the equivalent material in the auto coherent model). Other methods (e.g. the Mori Tanaka method) are available and provide explicit relationships, but are mainly applicable for low dilution of n-1 phases in a main phase.

4.3.2 Elastic behaviour

From the available models, it was decided to use the model proposed by Marur [19] based on the results of Christensen and Lo [11] and allowing the results of Lee and Westmann [122] to be recovered. This model has been recently used by Brini [20], Zaouari[21], and Genna [123].

This model is explicit and can easily be developed to take into account a damage process. The material is represented by a multi phase model of concentric spheres.

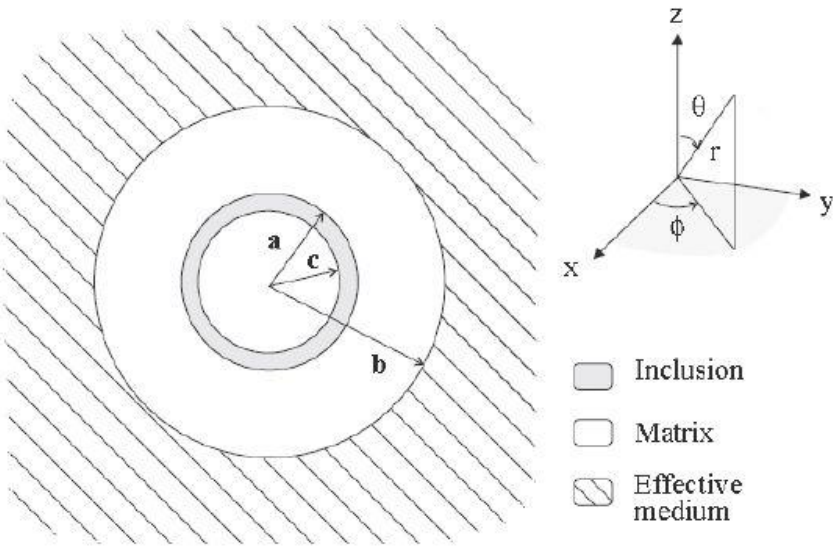

Figure 117 : three phase model

The model consists of one inclusion composed of two concentric spheres (Figure 117).

- One sphere of brittle material (here the glass microsphere) with properties indexed by 1 with inner radius equal to c and outer radius equal to a
- One sphere of polymeric matrix with properties indexed by 2 with inner radius a and outer radius b

placed in equivalent homogeneous material indexed by eff.

In macroscopic terms the medium is isotropic and can therefore be characterized by two constants, for example the bulk modulus and Poisson's ratio. The homogenised properties must be such that under the same loading condition they have the same energy as the material presented in figure 117 which can be reported as:

$$\int_S \left[(\sigma_{rr}^{(0)} u_r^{(c)} + \sigma_{r\theta}^{(0)} u_\theta^{(c)} + \sigma_{r\phi}^{(0)} u_\phi^{(c)}) - (\sigma_{rr}^{(c)} u_r^{(0)} + \sigma_{r\theta}^{(c)} u_\theta^{(0)} + \sigma_{r\phi}^{(c)} u_\phi^{(0)}) \right] dS = 0$$

Where the index r ,θ,ϕ indicates the displacement in a spherical system and the index 0 or c indicates the presence or the absence of an inclusion.

With these hypotheses the bulk modulus can be calculated. By considering a hydrostatic field of pressure P_0 at infinity the displacement field in the r direction (all other components are null by symmetry) can be expressed by:

$$u_r^{(1)} = F_1 r + \frac{F_2}{r^2}$$

$$u_r^{(2)} = G_1 r + \frac{G_2}{r^2}$$

$$u_r^{(eff)} = -\frac{P_0}{3K_{eff}} + \frac{H}{r^2}$$

The Fi, Gi and H constants are determined by the condition of displacement continuity (2 equations) and normal stress to the interfaces (2 equations) and null internal stress (1 equation).

Considering equation (xx) the bulk modulus can be expressed by:

$$K_{eff} = K_2 \frac{\beta(1+\gamma_2\psi)\gamma_1(\eta-1)+\gamma_2(1-\psi)(\gamma_1\eta+1)}{\beta(1+\psi)\gamma_1(\eta-1)+(\gamma_2+\psi)(\gamma_1\eta+1}$$

Where:

$$\beta = \frac{K_1}{K_2} \qquad \gamma_1 = \frac{4\mu_1}{3K_1} \qquad \gamma_2 = \frac{4\mu_2}{3K_2} \qquad \psi = \left[\frac{a}{b}\right]^3 \quad \text{and} \quad \eta = \left[\frac{a}{c}\right]^3$$

In the same way the Poisson coefficient can be calculated. The system is subjected to uniaxial tension. The displacement is given by Marur [124] by

$$\mu_r^1 = -\frac{F_1}{r^2} - 3\frac{F_2}{r^4} + \frac{(5-4\nu_1)F_3}{1-2\nu_1)r^2} + F_4 r + \frac{2\nu_1 F_5 r^3}{7-4\nu_1} + F_6 r + \left[-9\frac{F_2}{r^4} + \frac{(5-4\nu_1)F_3}{3(1-2\nu_1)r^2} + 3F_4 r + \frac{6\nu_1 F_5 r^3}{7-4\nu_1}\right]\cos 2\theta$$

$$\mu_\theta^1 = -\left[-6\frac{F_2}{r^4} + 6\frac{F_3}{r^2} + 3F_4 r + F_5 r^3\right]\sin 2\theta$$

For the media 2 the indexes are replaced and the G constants replace the F constants.

For the equivalent media we obtain:

$$\mu_r^{eff} = \frac{TK_{eff}(1-2\nu_{eff})(1-\nu_{eff})r}{6\mu_{eff}(1+\nu_{eff})^2} - \frac{H_1}{r^2} - 3\frac{H_2}{r^4} + \frac{(5-4\nu_{eff})H_3}{3(1-2\nu_{eff})r^2} + F_4 r + \left[\frac{T_r}{4\mu_{eff}} - 9\frac{H_2}{r^4} + \frac{(5-4\nu_1)H_3}{(1-2\nu_1)r^2}\right]\cos 2\theta$$

$$\mu_\theta^{eff} = -\left[\frac{T}{4\mu_{eff}} + 6\frac{H_2}{r^4} + 2\frac{H_3 r}{r^2}\right]\sin 2\theta$$

The system can then be solved and gives:

$$\nu_{eff} = \frac{3H_1 - 8H_3}{6H_1 + 8H_3}$$

Solving results in a very large expression, so a numerical method is then usually used.

It can be recalled that the knowledge of the bulk modulus and the Poisson coefficient allows the coulomb modulus of the effective material to be determined from:

$$G = 3K * (1-2\nu) / (2*(1+\nu))$$

4.3.3 Viscoelastic behaviour

Considering the behaviour of the matrix of the syntactic foam the hypothesis of linear viscoelastisity can be stated. Then the knowledge of the relaxation spectrum allow the strain rate of the matrix and the stress of the matrix to be linked by

$$\dot{\varepsilon}^{ve} = \sum_i \dot{\xi}_i$$

With

$$\dot{\xi}_i = -\frac{\partial \varphi_{ve}^*}{\partial u \partial v} = -\frac{1}{\tau_i}\left(\xi_i - \mu_i S_{Rm} : \sigma_m\right)$$

The shape of the relaxation time spectrum depends on the nature of the matrix. It has been showed for epoxy matrix that a choice of triangular spectrum can be suitable to predict correctly the viscoelastic strain of a fibre composite material [125].

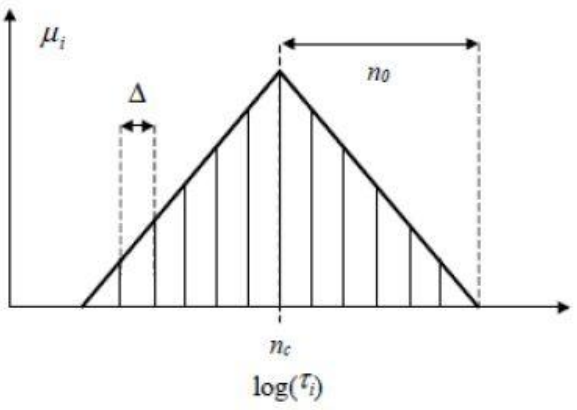

This triangular shape is easy to be implemented and is defined by three parameters.

Taking into account the complexity to introduce this formulation in the previous equation [126] it has been decided to introduce the viscoelastic behaviour directly in the global formulation of the material.

$$\dot{\varepsilon}^t = \dot{\varepsilon}^e + \dot{\varepsilon}^{ve}$$

With

$$\dot{\varepsilon}^e = S_{eff} : \dot{\sigma}$$

And

$$\dot{\varepsilon}^{ve} = \sum_i \dot{\xi}_i$$

With

$$\dot{\xi}_i = -\frac{1}{\tau_i}\left(\xi_i - \mu_i S_{\text{Reff}} : \sigma\right)$$

Then

$$S_{eff} = \begin{bmatrix} \frac{1}{E_{eff}} & \frac{-\nu_{eff}}{E_{eff}} & \frac{-\nu_{eff}}{E_{eff}} & 0 & 0 & 0 \\ & \frac{1}{E_{eff}} & \frac{-\nu_{eff}}{E_{eff}} & 0 & 0 & 0 \\ & & \frac{1}{E_{eff}} & 0 & 0 & 0 \\ & & & \frac{1}{G_{eff}} & 0 & 0 \\ & & & & \frac{1}{G_{eff}} & 0 \\ & & & & & \frac{1}{G_{eff}} \end{bmatrix}$$

$$S_{Reff} = \begin{bmatrix} \frac{A}{E_{eff}} & \frac{-B\nu_{eff}}{E_{eff}} & \frac{-B\nu_{eff}}{E_{eff}} & 0 & 0 & 0 \\ & \frac{A}{E_{eff}} & \frac{-B\nu_{eff}}{E_{eff}} & 0 & 0 & 0 \\ & & \frac{A}{E_{eff}} & 0 & 0 & 0 \\ & & & \frac{C}{G_{eff}} & 0 & 0 \\ & & & & \frac{C}{G_{eff}} & 0 \\ & & & & & \frac{C}{G_{eff}} \end{bmatrix}$$

Where A, B, and C are three constants to be determined.

4.3.4 Damageable behaviour

Considering the phenomenological material behaviour model (for GSPU material as well as GSEP material) it can be considered that the material behaviour is governed initially by the collapse of microspheres which induces a global loss of rigidity of the material. The collapse of the microspheres at a macroscopic scale can be expressed as the presence of damage which can be expressed in the homogenized form in the Representative Elementary Volume of the material by a decrease of the average thickness of the spheres, which is indirectly represented by the parameter:

$$\eta = \left[\frac{a}{c}\right]^3$$

A damage parameter can be introduced in the following form:

$$D = \frac{\eta - \eta_0}{1 - \eta_0}$$

Where η_0 is the value of η at the initial step (before loading). D represents the reduction in the number of hollow microspheres or the global decrease of the volume included in the microspheres. By introducing this parameter in the formula giving the bulk modulus coefficient:

$$K_{eff} = K_2 \frac{\beta(1+\gamma_2\psi)\gamma_1(\eta-1)+\gamma_2(1-\psi)(\gamma_1\eta+1)}{\beta(1+\psi)\gamma_1(\eta-1)+(\gamma_2+\psi)(\gamma_1\eta+1}$$

That can be expressed as:

$$K_{eff} = K_2 \frac{\beta(1+\gamma_2\psi)\gamma_1(D(1-\eta_0)+\eta_0-1)+\gamma_2(1-\psi)(\gamma_1(D(1-\eta_0)+\eta_0)+1)}{\beta(1+\psi)\gamma_1(D(1-\eta_0)+\eta_0-1)+(\gamma_2+\psi)(\gamma_1(D(1-\eta_0)+\eta_0)+1)}$$

or

$$K_{eff}(D) = \frac{A_1 - A_2 D}{B_1 - B_2 D}$$

The damage kinetics has then to be determined.

Damage has been identified both during pure hydrostatic compression test and during pure shear tests (Modified Arcan). So it was decided to introduce a criterion in relation with the

hydrostatic compression and the Von Mises equivalent stress defined as the second invariant of the stress deviator.

$$\sigma_{VM} = \frac{1}{\sqrt{2}}\left[\left(\sigma_{xx}-\sigma_{yy}\right)^2+\left(\sigma_{yy}-\sigma_{zz}\right)^2+\left(\sigma_{zz}-\sigma_{xx}\right)^2+6\left(\sigma_{xy}^2+\sigma_{yz}^2+\sigma_{xz}^2\right)\right]^{1/2}$$

The hydrostatic pressure is defined by

$$P_H = \frac{Trace(\sigma)}{3} = \frac{\sigma_x+\sigma_y+\sigma_z}{3}$$

The general criterion for damage occurring can be expressed by:

$$F = R_H P_H + R_S \sigma_{VM} - Y_{thr} \le 0$$

Where R_H and R_S are two constants which reveal the sensitivity of the material to damage according to the loading type (shear or hydrostatic) with $R_H + R_S = 1$ and Y_{thr} the damage threshold.

The damage kinetics can be written:

$$\left.\begin{aligned}\dot{D} &= \lambda \frac{\partial F}{\partial \sigma}\\ \dot{Y}_{thr} &= -\lambda \frac{\partial F}{\partial D}\end{aligned}\right\}$$

With λ a Lagrange multiplicator, given by the consistency equation (F=0,dF=0) in the damage process.

The evolution of the damage threshold with the damage is controlled by

$$Y_{thr} = Y_0 + R_{D1} D^{R_{D2}}$$

Where , R_{D1}, R_{D2} are constants to be determined and Y_0 the initial threshold.

The damage is also associated with a "plastic" strain linked to the collapse of the wall between microspheres after failure due to compression of the material.

A non linear strain can be associated with the damage, in order to represent the presence of a permanent residual strain after unloading. For hydrostatic loading the relationship between the stress and strain tensors can be expressed as:

$$K_{eff}\ Trace(\varepsilon_{elastic}) = \frac{Trace(\sigma)}{3}$$

To introduce plastic strain, the total strain is partitioned into elastic and plastic strains:

$$\varepsilon_{elastic} = \varepsilon_{total} - \varepsilon_{plastic}$$

To be consistent with experimental results a two parameter (χ_1 χ_2) model for describing the plastic strain can be introduced:

$$\varepsilon_{plastic} = \frac{\chi_1 D}{(\chi_2 - D)}$$

This has been chosen in order to allow continuity with phase 2 of the loading. When D reaches χ_2 the strain become very large and the collapse of the material is represented. The term χ_1D allows the magnitude of the plastic strain before "final" collapse to be controlled.

Then the equation can be rewritten as

$$Trace(\varepsilon_{total} - \frac{\chi_1 D}{(\chi_2 - D)} I) = \frac{Trace(\sigma)}{3K_{eff}}$$

To complete the model the kinetics of the damage variable have to be determined. Because we are interested in a single loading a linear relation has been chosen between damage kinetics $\dot{D}$ and pressure rate $\dot{P}$ (the pressure of loading), through a one parameter model.

$$\dot{D} = 3\alpha_D \dot{P} \quad \text{if} \quad 3P > Y_{threshold} \quad \text{and} \quad \dot{P} > 0$$

$$\dot{D} = 0 \text{ for the other cases}$$

Finally, during the hydrostatic test the volume change can be written in the following form:

$$\frac{\Delta V}{V} = \frac{B_1 - B_2(3\alpha_D P)}{A_1 - A_2(3\alpha_D P)} P + 3\frac{\chi_1(3\alpha_D P)}{\chi_2 - (3\alpha_D P)}$$

Then 3 parameters, α_D, χ_1, and χ_2, have to be determined.

4.3.5 Identification of the model parameters.

An example of parameter identification is provided hereafter for a GSPP (Glass Syntactic polypropylene) material tested at 20°C. The identification is made on the initial model which takes into account damage only induced by hydrostatic pressure (kinetics proportional to the pressure) and plasticity. The visco elasticity and the damage induced by shear loading are not implemented at this time in the model.

From the input data (table 21), parameters A1 to B2 are determined (table 22). Using an optimization process from Matlab®, the 3 parameters of the model are then determined (table 23). A good agreement between experimental data and the model can be observed on Figure 118.

Volume fraction of micro spheres	0.45
Mean diameter of micro spheres	40 µm
Thickness of micro spheres	1.5 µm
Young's modulus of glass	75 GPa
Poisson's ratio of glass	0.2
Young's modulus of PP	1.3 GPa
Poisson's ratio of PP	0.4
$Y_{threshold}$	0 MPa

Table 21: parameter used in the model

A_1	$6.21 * 10^9$
A_2	$5.53 * 10^9$
B_1	2.79
B_2	1.32

Table 22 : input data

α_D	0.005
χ_1	0.072
χ_2	0.781

Table 23 : model parameters

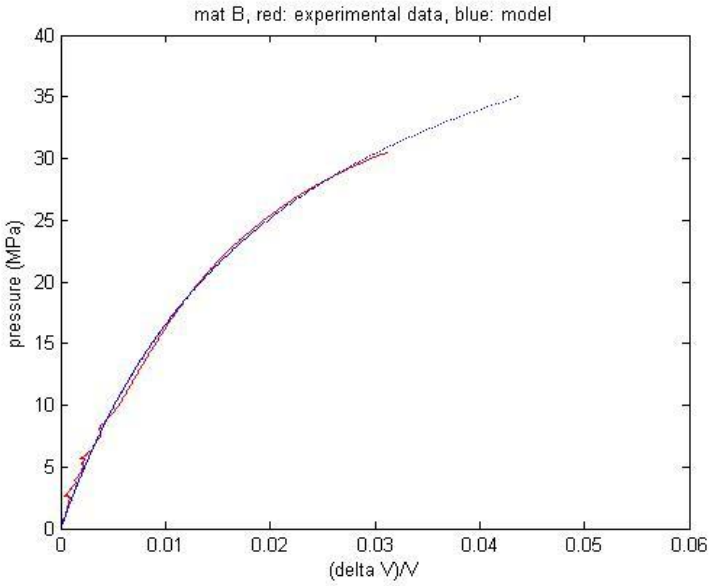

Figure 118 : comparison model – experimental data

The model provides a reasonable representation of the material behaviour in terms of bulk modulus and could be extended to other mechanical properties, shear modulus for example. At this stage the model is limited to quasi static behaviour, temperature effects can be

introduced by acting on the matrix properties. Improving the model is necessary to take into account viscoelastic behaviour, which has been recently identified and which may affect the long term behaviour of the material. Other improvements to the model could also take account of damage due to non-hydrostatic loading, such as shear or compression. For such loading, the kinetics of damage must be completed by taking into account the effect of the stress deviator in addition to the effect of the hydrostatic pressure.

Chapter 5. CONCLUSIONS AND FUTURE WORK

A large campaign of tests aiming to characterize and identify the mechanical behaviour of syntactic foams has been carried out. The objective was not to provide a data sheet of the syntactic foams tested but to identify and eventually to develop test methods adapted to such material. Two materials were used during this study GSEP, glass syntactic epoxy foam and GSPU glass syntactic polyurethane material.

An original and unique method has been used to access the behaviour of the material and the improved knowledge which has been obtained has allowed the basis for a mechanical model to be developed.

Different points are reported hereafter to summarize the contribution of this study:

- The mechanical characterization of syntactic foam must be approached with care. Standard tests generally used for polymer or composite material can provide unreliable data when used for such material. To a first approach GSEP material seems to exhibit a linear elastic response, but even with careful testing it has proved difficult even to verify the relationships of the continuous media mechanics in the elastic domain. The GSPU material exhibits a more complex behaviour with considerable non linearity. The behaviour of this material can be presented as visco elasto plastic damageable behaviour.
- Syntactic foam being an excellent deep-sea material, hydrostatic compression is the main loading condition. Up until now no pertinent test was available to identify the behaviour of the material under such loading. An instrumented hydrostatic compression test has been developed here which can reveal the behaviour of these materials at pressures up to 80 MPa. This method, based on the use of buoyancy measurements, allows the determination of the evolution of the volume of the samples versus pressure. This method can be transferred and will be proposed for standardization. Tests at temperatures up to 150 °C can be carried out, and these are needed to characterize the use of this material as passive insulation for deep sea pipelines.
- Standard uniaxial compression tests of can provide invalid data. Boundary conditions and edge effects can significantly affect the results obtained, which cannot be considered as reliable. A new design of sample is proposed here which results in uniform deformation in the calibrated part of specimen. For materials of low rigidity (e.g GSPU) it is difficult however to avoid buckling initiation limiting access to the behaviour of the material at high load levels.

- It must be noted that there is no direct relation between the stress at break under uniaxial compression and collapse pressure under hydrostatic pressure. Datasheet values for the former cannot be used to qualify deep sea materials.
- Non destructive evaluation using ultrasonic measurement has been used to determine elastic properties of the material. This method is based on an immersion technique classically used to identify mechanical properties of composite materials. For GSEP this method provides relevant data, and may be used to follow the long term evolution of the mechanical properties of samples. The use of this technique for GSPU is limited at this time to compression waves on account of the high attenuation of shear waves in this material. During the development of this technique at Ifremer an original method has been developed to identify temporal shift of ultrasonic signal by coupling Hilbert transforms with cross correlation.
- Following the recent acquisition at Ifremer of a Digital Image Correlation system, this system has been used to verify the validity of the tests performed. This technique can certainly provide an important contribution to the way in which we will perform mechanical tests in the future, in particular on materials with specific behaviour. The strain gradients on samples during test can be clearly identified and this allows a better understanding of the test limitations.
- Shear tests on these materials are particularly delicate. The Iosipescu test must be used coupled with a DIC system: The use of strain gauges to identify the shear deformation is not easy and considering the high axial stress gradients imposed the use of a small length gauge is necessary but these are very difficult to install properly. GSEP is a brittle material which is very sensitive to the edge effects and the Iosipescu test allows a limited shear strain range. For GSPU the shear deformation is limited by the fixture. A modified Arcan test has been developed and allows large shear stress deformations to be reached. However, at this stage it is difficult to clearly estimate the behaviour of the material using this test. Improvement is needed in the analysis of this test to apply this test configuration but it is well-suited for complex loading (shear + tension, shear + compression) and could provide access to the full failure envelope of the material.
- From all these previous considerations it appears difficult today to provide a set of reliable data on the mechanical behaviour of syntactic foams in which could be used to perform accurate FE analysis of structures using these materials. Nevertheless, the hydrostatic compression test can be the basis for providing useful data for this need in the future.
- In order to study damage, based on the previous work performed in the Mateis Insa laboratory, Xray microtomography has been use to identify in situ the hydrostatic compression behaviour of syntactic foam. The experiment conducted is at this stage

unique, and has clearly indicated the damage behaviour of the material. Early glass microsphere collapse occurs when pressure is increased. For GSPU this collapse induces volume reduction of the sample, while for GSEP this collapse induces overloading of the matrix skeleton. These observations have allowed a phenomenological model of the material to be established and confirmed, and provided the basis of a mechanical model. Currently the equipment is able to subject specimens to up to 50 MPa of pure hydrostatic compression loading.

- Quantification of damage has been performed using accurate glass microsphere density measurements after hydrostatic loading. The use of a pcynometer has allowed the evolution of volume of uncollapsed microspheres to be determined versus level of hydrostatic reached for GSPU. Results obtained from this method can be compared with the results obtained from the instrumented hydrostatic compression. This method has to be improved for GSEP material and can be used for other types of syntactic material.
- Acoustic emission has been used to follow the damage occurring during hydrostatic pressure loading. At this stage damage quantification appears to be difficult particularly given the GSPU behaviour. However, this method reveals very early damage to micro balloons.
- A mechanical model has been developed to describe the behaviour established from tests and allows prediction of other experimental situations. This model includes damage from hydrostatic pressure and shear loading using homogenisation. Viscoelasticity is introduced via a triangular relaxation spectrum. Non reversible behaviour is described by using a plastic model material is also introduced to represent reorganisation of the matrix skeleton. In a first step the identification of some parameters of a simplified model has been performed, additional work has to be done to fully implement this model.

In terms of perspectives and future work to be performed, the following points have been identified:

- Full implementation of the model proposed, with identification of the model parameters, is needed. This work has been started by Phan [127] on a GSPP material (Glass Syntactic Polypropylene) showing the possible extension of the model proposed to other types of syntactic foam material.
- At this stage it is difficult to estimate the kinetics of damage of syntactic foam material from the matrix behaviour and the microsphere properties. Micromechanics models can be improved by considering poly-dispersion of microsphere diameters as

well as the poly-dispersion of the wall thicknesses. No validated predictive method is currently available.

- Considering that pure hydrostatic loading can be analysed using the method developed during this study it would be interesting to address more complex loading, and in particular hydrostatic compression + uniaxial compression, which is a representative loading condition for syntactic foam material. With this objective a specific device allowing axial loading of specimens coupled with hydrostatic loading has been developed at Ifremer. This equipment allows the sample to be visualised under loading and then with the use of DIC equipment to analyse the behaviour of the material. Figure 119 shows one example.

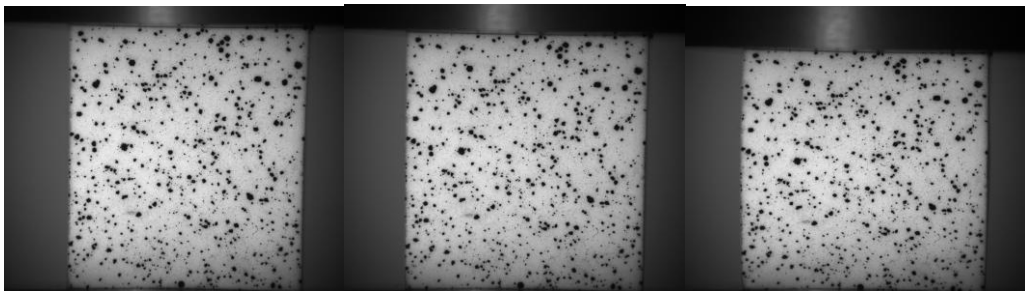

Figure 119 : visualization of specimen loaded at 10 MPa then with increasing axial loading

- The present study has focussed on traditional syntactic foams, with microspheres. However, the behaviour of buoyancy materials using macro elements (figure 120) must also be investigated. These materials are based on syntactic foam in which, in order to decrease the specific gravity, macro elements (generally spheres of composite material from 10 mm up to 150 mm in diameter) have been added. The characterization of the properties of such materials is not easy due to the large size of macro elements. The estimation of the properties of such materials has not been developed, and this could be the subject of a follow-up PhD thesis study as this type of material is currently being used as buoyancy material for deep sea applications.

Figure 120 : buoyancy material with macro elements

- The expected service life for deep sea material is generally around 20 – 25 years. The long term behaviour of syntactic foam material has already being investigated [27, 128] however unexpected degradation has been observed after long term exposure to a deep sea environment. In order to guarantee reliability of equipment improvements in long term prediction methods is needed. Figure 121 shows an example of a section through a buoyancy block from the Ifremer nautile submersible after 25 years in service. There is a degraded outer region causing a loss of buoyancy and such changes must be fully understood if long term performance is to be maintained.

Figure 121: superficial degradation of 25 years exposed syntactic foam material (10cm*10cm block)

Chapter 6. APPENDIX

6.1 Buoyancy requirements for the *Nautile* submersible

The total weight of the equipment has to fit the lifting capacity of the support ship:

Then :

Maximum lifting capabilities >

Weight of buoyancy in air (V* SG) + Weight of submarine equipment

Point 2

The equipment must have zero buoyancy during immersion in order to satisfy its functions. Adjustment of the buoyancy of the equipment is verified and performed before each dive by weighing of the submarine.

Then :

Archimedes force of the buoyancy device - Weight of submarine equipment in water + Δ Buoy= 0

or

$$Lc > (V*SG) + Wsa$$

$$(V* (Wd-SG) – Wsw + \Delta \text{ Buoy} = 0$$

With

Lc = lifting capabilities

Wsa = weight of submarine equipment in air

Wsw= weight of submarine equipment in water

Wd = Sea Water density.

Note: the sea water density was considered as constant and equal to 1.02 kg/dm^3. It should be mentioned however, that the specific gravity of sea water depends on numerous parameters: salinity, temperature, depth, location in the world. For more information refer to [84]

V= volume of buoyancy material

SG = specific gravity of buoyancy material

Δ Buoy = positive buoyancy of the submarine in order to guarantee safety of equipment (3000 N)

The positive buoyancy of the submarine is compensated by extra load (steel powder) which is released at the bottom of the sea during the dive.

In order to achieve these objectives, a requirement on specific gravity of the buoyancy can be calculated.

In the case of the Nautile submarine the requirement for the specific gravity was SG< 580 kg/m^3

Different grades of buoyancy material are available on the market, and depending on the nature of the components an appropriate selection of material can be made (from CRP company)

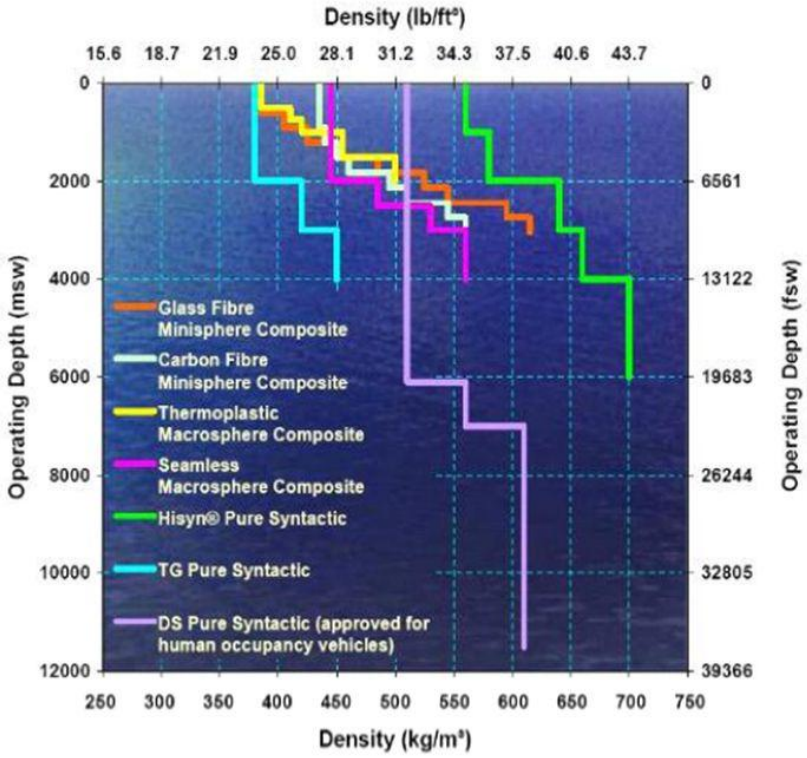

Additional requirements for the material are listed hereafter:

- Collapse pressure Ps *1.5
- Residual collapse pressure after 7 days of aging at 70°C > 1.4Ps
- Buoyancy lost after 7 days of aging at 70°C <1%
- Residual collapse pressure after 1000 hours à 1.2 Ps > 1.3Ps
- Buoyancy lost after 1000 hours à 1.2 Ps <1%
- Residual collapse pressure after 2000 cycles 0-Ps > 1.3Ps
- Buoyancy lost after 2000 cycles 0-Ps <2%

6.2 U value Calculation

The U value, is expressed in [W/(m^2.K)] and describes the capacity for a pipe under steady state conditions to minimize the thermal leakage along the pipe.

For a multilayer pipe, taking into account the thermal conductivity of the different materials and their thicknesses the U value can be calculated from the following formula:

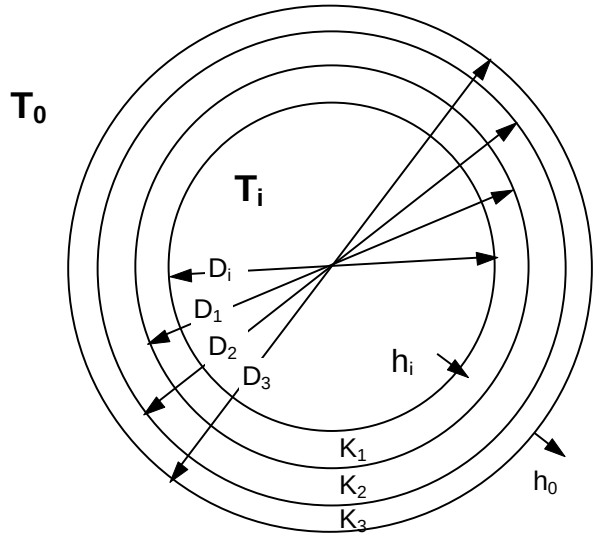

The thermal flux per unit length of the pipe is equal to :

$Q = - U_n A_n (T_0 - T_i)$

The U value is calculated for a given reference surface A_n. .Considering zero thermal resistance between the different layers, the thermal transfer coefficient per unit length ($W/m^2.K$) can be calculated from:

$$\frac{1}{U} = A_n \left[\frac{1}{\pi D_i L h_i} + \sum_1^n \ln \frac{(D_n/D_{n-1})}{2\pi L k_n} + \frac{1}{\pi D_0 L h_0} \right] \quad \text{(éq. 1)}$$

T_i = inner fluid temperature

T_0 = external fluid temperature

D_n = external diameter of layer n

h_i = inner surface transfer coefficient

h_0 = outer surface transfer coefficient

k_n = thermal conductivity of layer n

D_i = internal diameter of the pipe D_0 = external diameter of the pipe

L = length of the pipe A_n = reference surface

6.3 Example of thermal properties requirements

	unit	designed	requirement
Overall insulation thickness	mm	148.2	N/A
Minimum fluid temperature after 13 hours cool down time	°C	22.6	≥ 22.0
Down Time to reach 22°C	hr	13.5	≥ 13.0
U value (based on ID)	$W/m^2.K$	1.85	≤ 3.5

Input data

Initial temperature		42
Final temperature		22
Density of the gas for CDT calculation	Kg/m^3	42
Content Heat capacity	J/kg/K)	2500
Ambient temperature		4°C
OD	mm	273.1
Wt	mm	16.8

(1) Only 50% of the corrosion allowance is considered in the cool down time simulations for carbon

steel lines i.e. 1.5mm removed from wall thickness

In order to reach these requirements a 5LPP system has been retained. The data used for the evaluation of the performance are listed on table.

material		λ	Cp (at 20°C)	ρ
Steel (Superduplex)	16.8	15	500	7.8

Steel (Carbon steel)	16.8	45	460	7.85
1st layer FBE	.25	.3	1500	1.45
2nd layer Adhesive PP	.25	.22	2100	.9
3nd layer Solid PP	2.7	.22	1450	.9
4nd layer GSPP	141	.16	1300	.66
5nd layer Solid PP	4	.22	1450	.9

6.4 Programme “temporal shift”

Function : determine the time shift between two signals with similar forms

```
clear;
close all;

A=xlsread('signaux');
% "signaux" est le document Excel dont chaque colonne représente un signal.
% Le programme calcule le décalage en abscisse de chacun des signaux par
% rapport au premier d'entre eux.

t=size(A,1);
nbCol=size(A,2);

for i=t+1:1:2*t
   for j=1:1:nbCol
      A(i,j)=0;
   end
end

M=zeros(2*t+1,nbCol-1);

% Calcul de la fonction d'intercorrélation
for m=2:1:nbCol
  for i=1:1:t
     temp=correlation_1(A,i,m);
     M(t+1+i,m-1)=temp;
   end
end
```

```
for m=2:1:nbCol
   M(t+1,m-1)=correlation_1(A,0,m);
end

for m=2:1:nbCol
   for i=1:1:t
      temp=correlation_2(A,i,m);
      M(t+1-i,m-1)=temp;
   end
end

% Calcul de l'enveloppe de la fonction d'intercorrélation
H=zeros(2*t+1,nbCol-1);
abscisses_maxima=zeros(nbCol-1,1);

H=hilbert(M);
H=abs(H);


% Recherche du maximum de l'enveloppe
for k=1:1:nbCol-1
   abscisse_mxm=1;
   mxm=H(1,k);
   for j=2:1:2*t+1
      if H(j,k)>mxm
         mxm=H(j,k);
         abscisse_mxm=j;
      end
   end
```

```
    abscisses_maxima(k)=abscisse_mxm-t;
end

% Représentation graphique
figure;
plot(1:1:2*t+1,M,'r');
hold on
plot(1:1:2*t+1,H,'b');

abscisses_maxima
```

```
function v = correlation_1(A,deltaT,p);

t=size(A,1)/2;
integrale=0;

% calcul de l'intégrale
for n=1:1:t
    integrale=integrale+A(n,p)*A(n+deltaT,1);
end

v=integrale;

return
```

```
function v = correlation_2(A,deltaT,p);
```

```
t=size(A,1)/2;
integrale=0;

% calcul de l'intégrale
for n=1:1:t
   integrale=integrale+A(n,1)*A(n+deltaT,p);
end

v=integrale;

return
```

6.5 Programme « mth_ultrasons »

Function : calculate the elastic constants of a material from its density and wave speeds.

```
VL=input('Vitesse ondes longitudinales? ');
VT=input('Vitesse ondes transversales? ');
rho=input('Masse volumique? ');

% Coefficients de Lamé
lambda=0;
mu=0;

% Constantes mécaniques
E=0;
nu=0;
G=0;
K=0;

% calculs
mu=rho*VT^2;
lambda=rho*(VL^2-2*VT^2);

E=mu*(3*lambda+2*mu)/(lambda+mu)
nu=lambda/(2*lambda+2*mu)
G=mu
K=(3*lambda+2*mu)/3
```

6.6 Drawing of tank 1

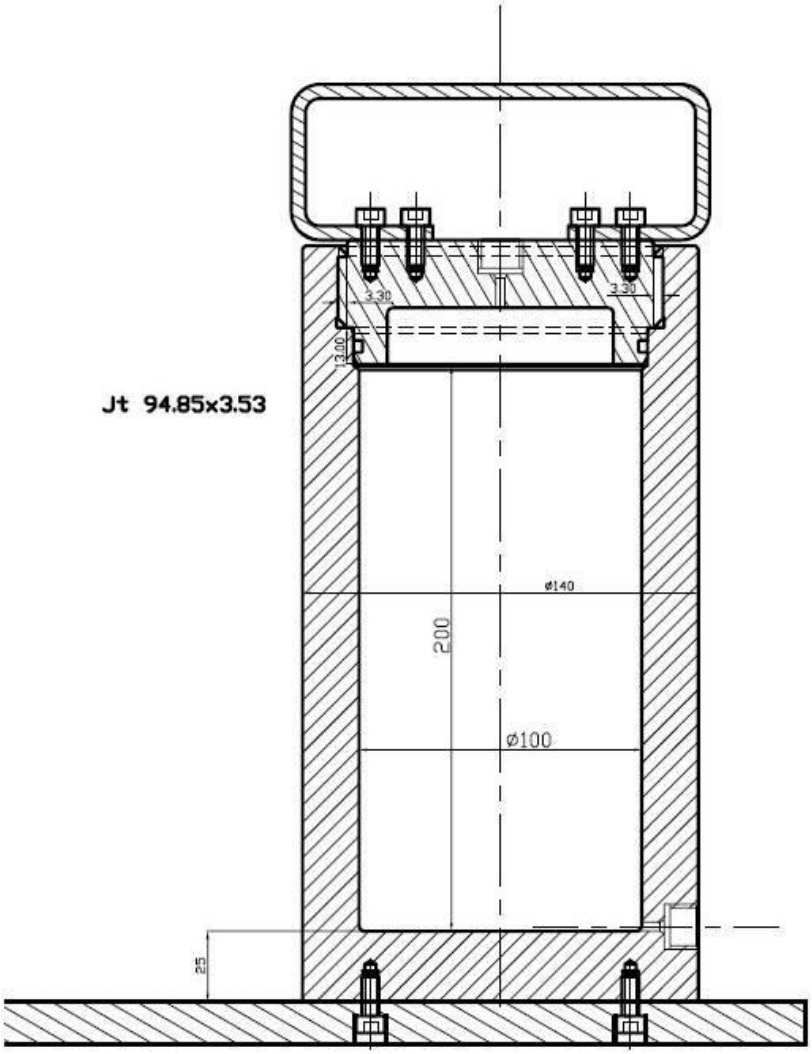

6.7 Drawing of tank 2

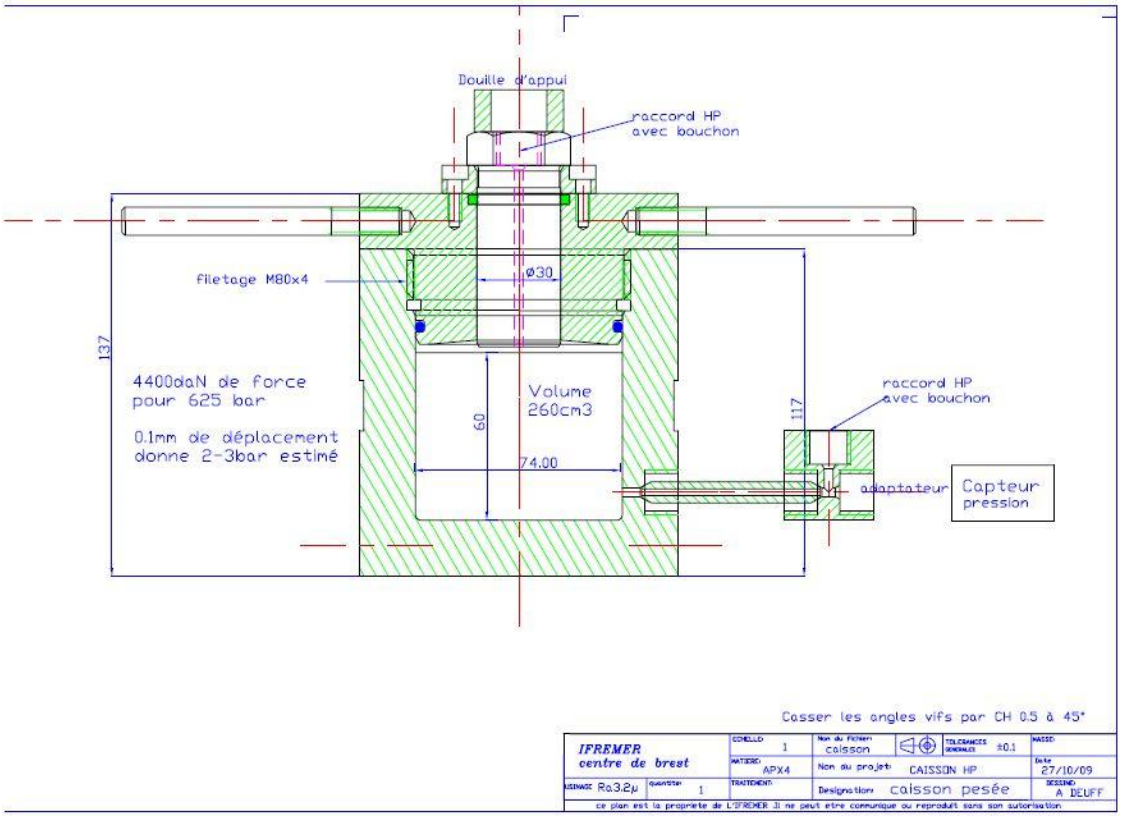

6.8 Drawing of tank 3

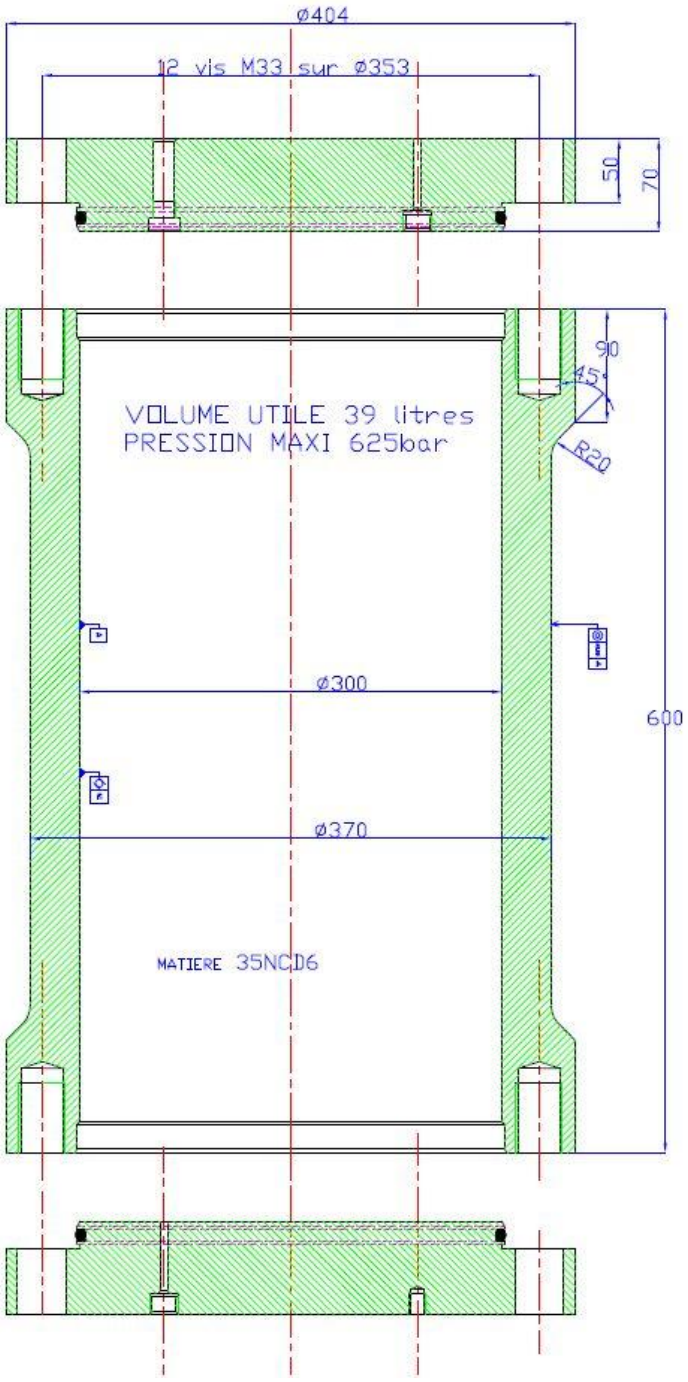

6.9 Hydrostatic compression test procedure

Typical sample volume: 1 dm^3

Use of balance with accuracy better than 0.0001 kg with under plateau hook in order to allow weighing of sample in water

The sample is weighed at room temperature in air

Additional steel weight is added to the specimen to guarantee full immersion of the sample when immerged.

The sample is weighed in water

Additional steel weight is released

The specimen is conditioned at test temperature in an oven for 24 hours. This is done in order to guarantee through thickness temperature homogeneity and to limit the preconditioning time at temperature in water.

The heated specimen is placed in the tank and fixed to the hook of the hydrostatic balance

The tank is filled with tap water at room temperature.

Data acquisition (temperature, pressure, force) is started.

The tank is closed and pressure is increased to the pressure of the network (about 0.5 MPa). This is done in order to avoid vaporisation when pressure increases for tests at temperature >100°C.

Pressure is maintained at the pressure of the local circuit

Tank is conditioned at test temperature (about 1 hour).

Increase of pressure up to 80MPa. Typically for hydrostatic compression test with estimation of the crush pressure a rate of pressure increase of 1MPa per minute is chosen. The rate corresponds to the speed of a pressure increase for material following free fall in water.

Release of pressure to network pressure at a rate of 1MPa/min

Heating device switched off

Pressure release when room temperature is reached

Tank is opened

The specimen is weighed in air at room temperature. This operation is performed in order to verify if water uptake has occurred during the test.

End of test.

It must be mentioned that during the temperature conditioning phase, the data analysis is quite complex. The analysis has to take into account changes of volume of the specimen due to temperature change and also the change of water density. In general during this phase no analyis of results is performed, the main difficulty consisting of the lack of knowledge of the through thickness temperature of the specimen.

6.10 Xray tomography images

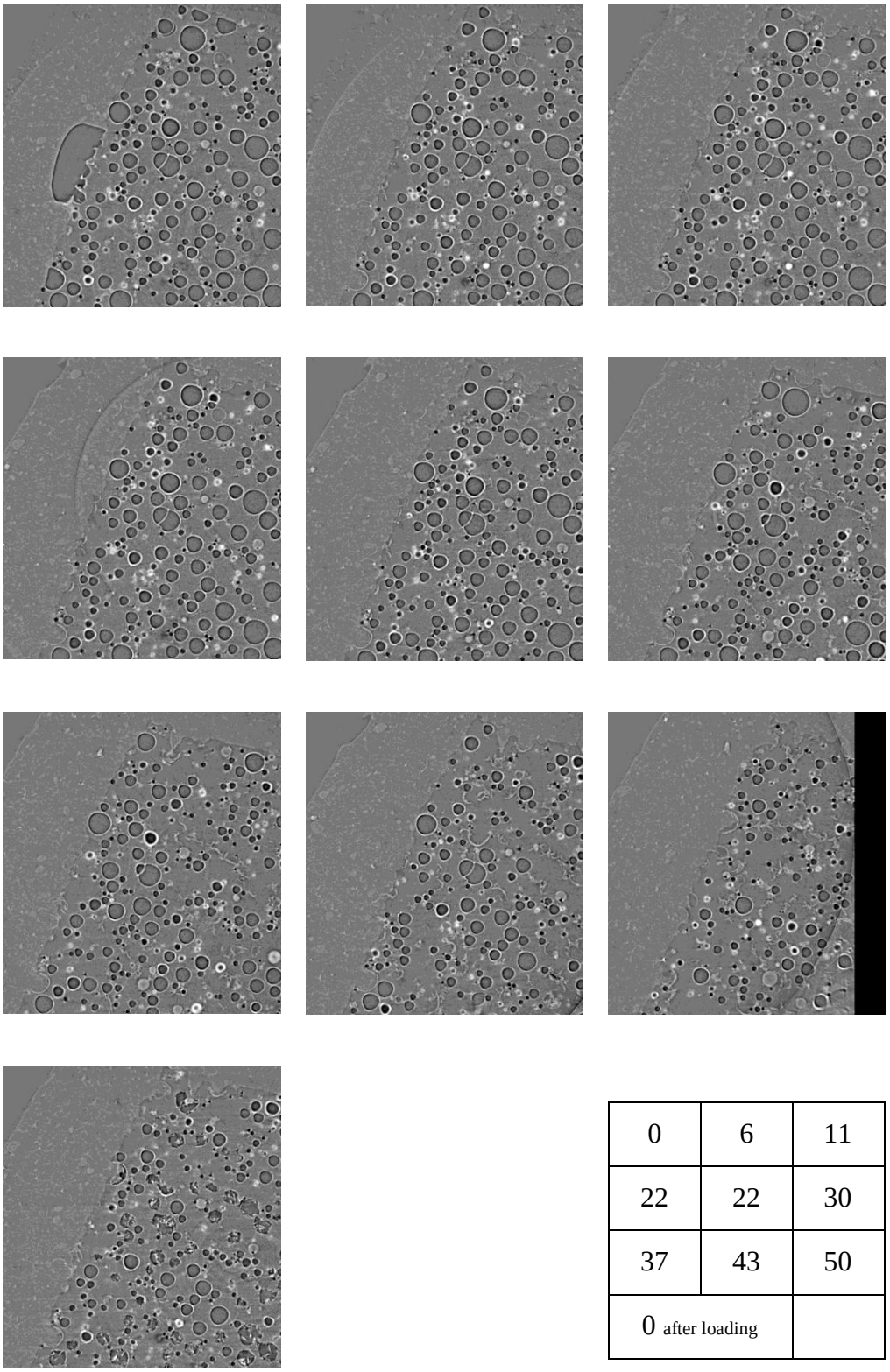

0	6	11
22	22	30
37	43	50
0 after loading		

Test pressure (MPa)

Figure Slice 243 of GSPU sample

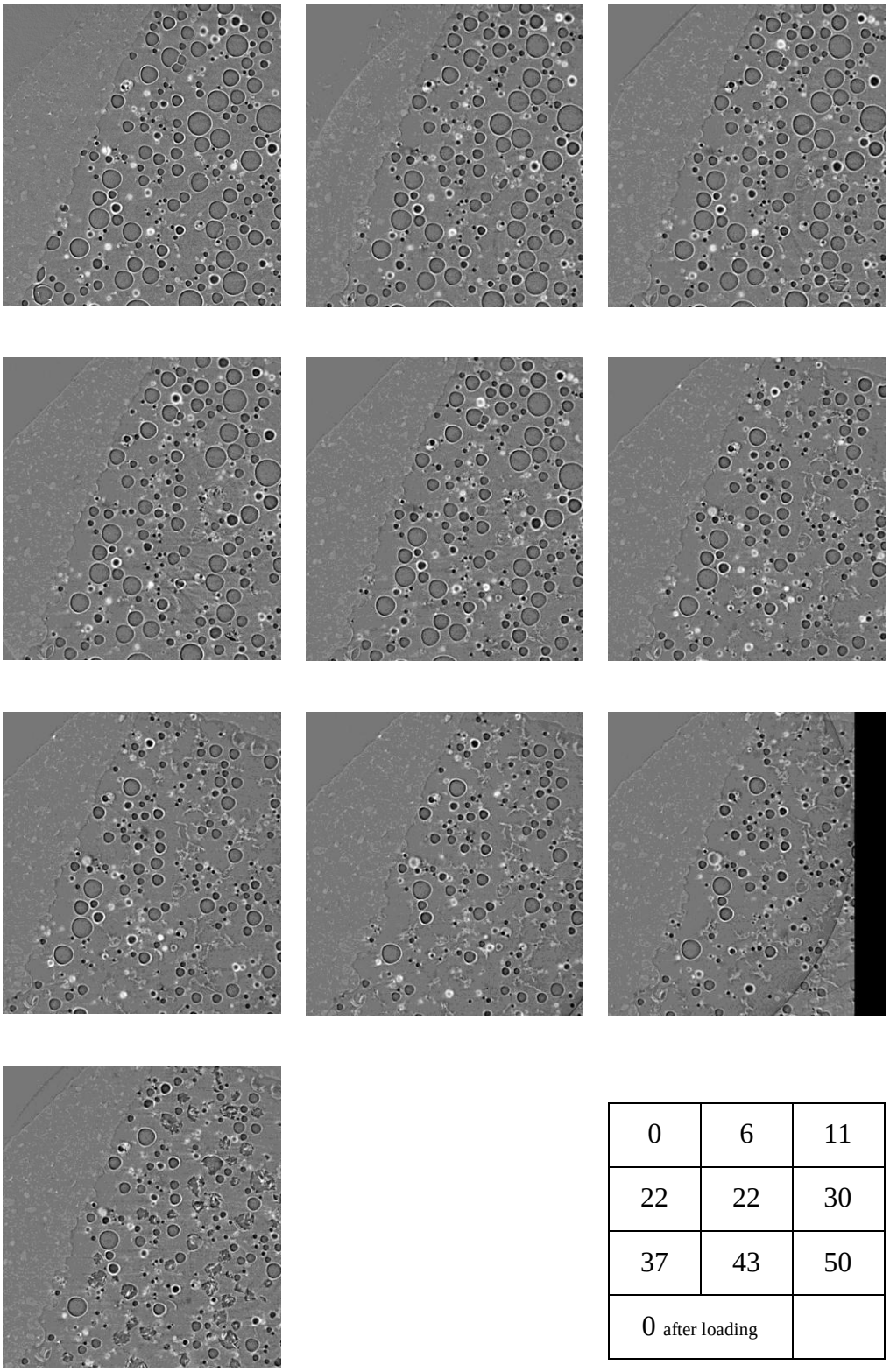

0	6	11
22	22	30
37	43	50
0 after loading		

Test pressure (MPa)

Figure Slice 394 of GSPU sample

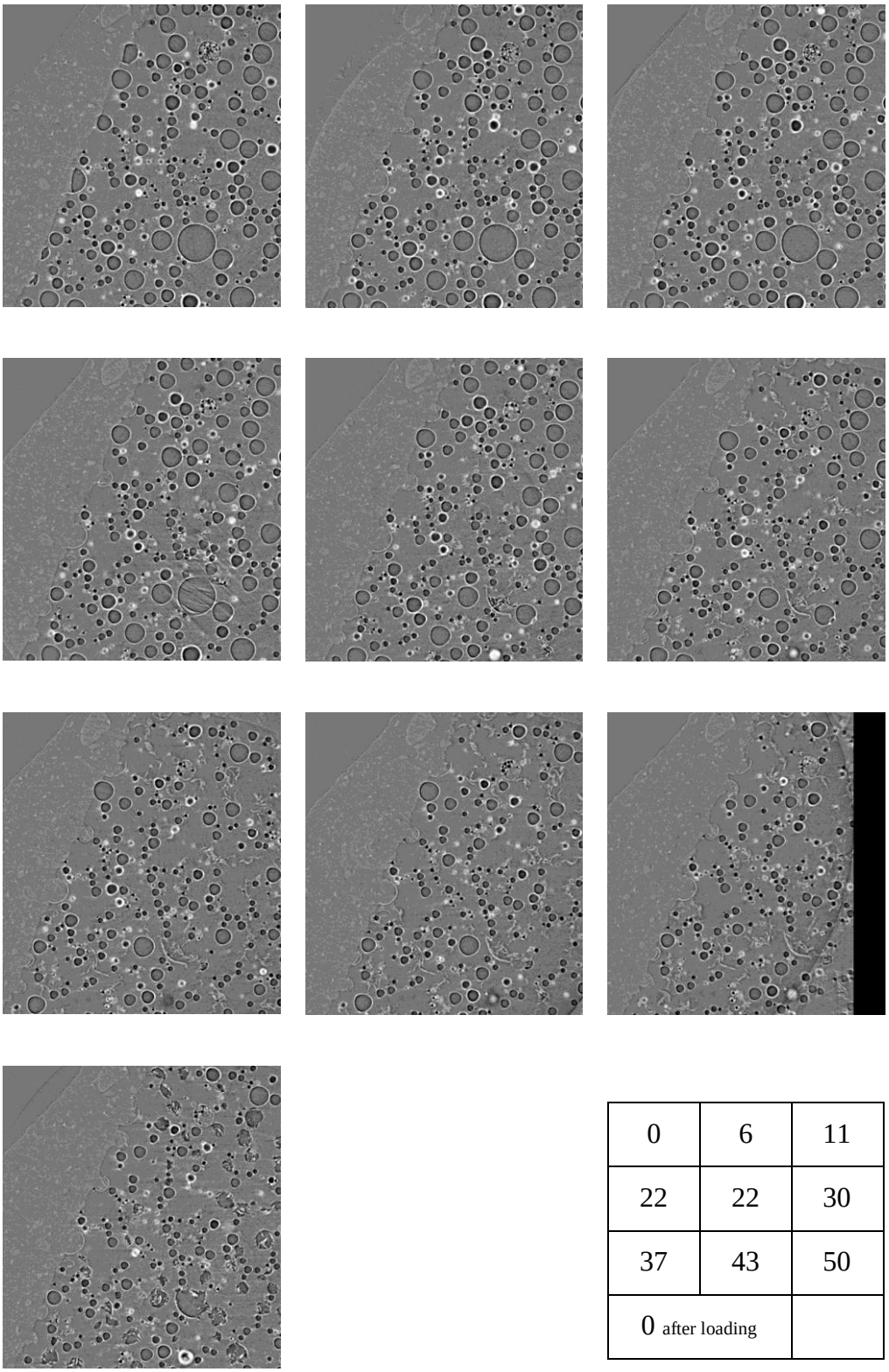

0	6	11
22	22	30
37	43	50
0 after loading		

Test pressure (MPa)

Figure Slice 436 of GSPU sample

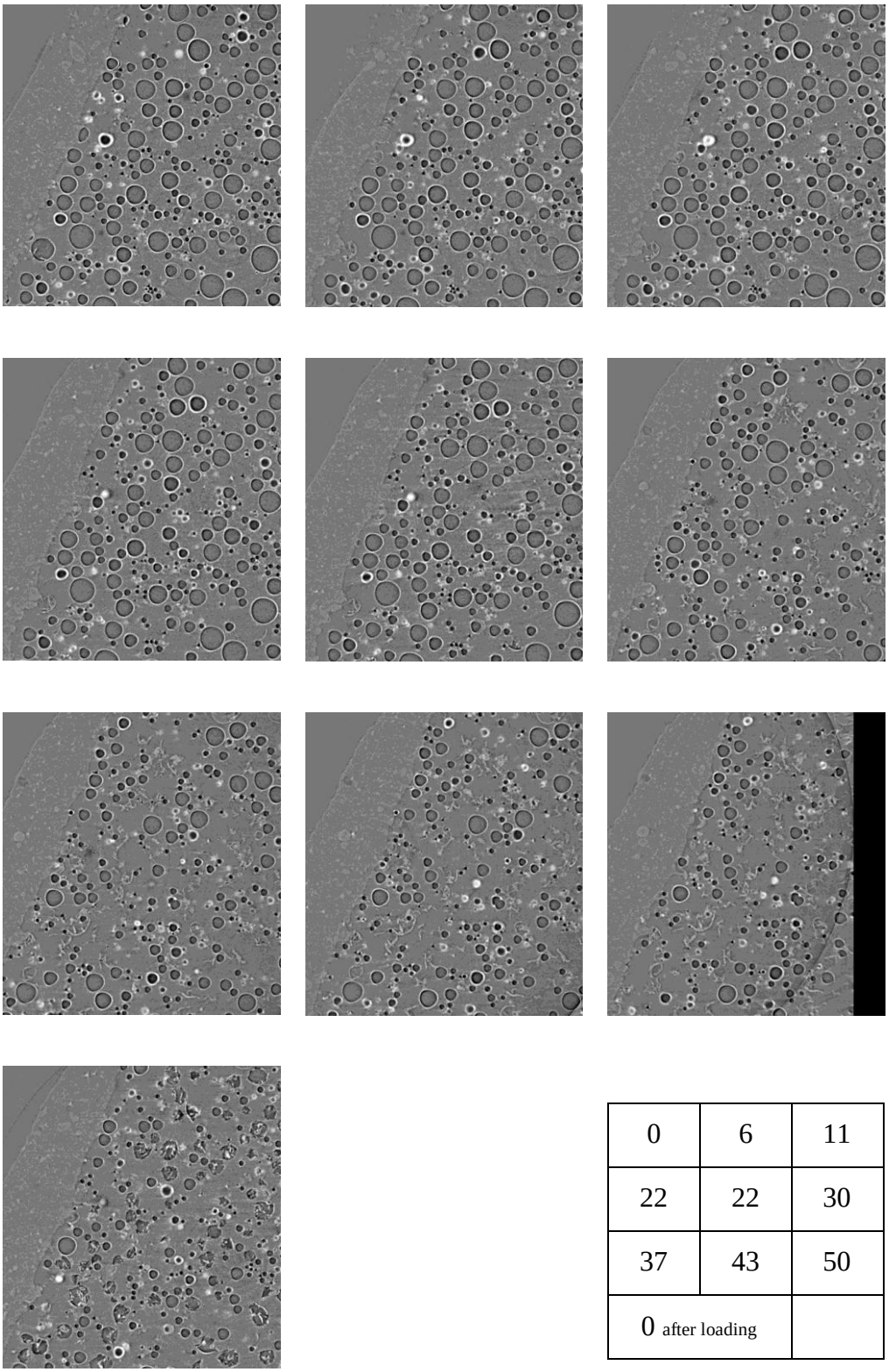

0	6	11
22	22	30
37	43	50
0 after loading		

Test pressure (MPa)

Figure Slice 660 of GSPU sample

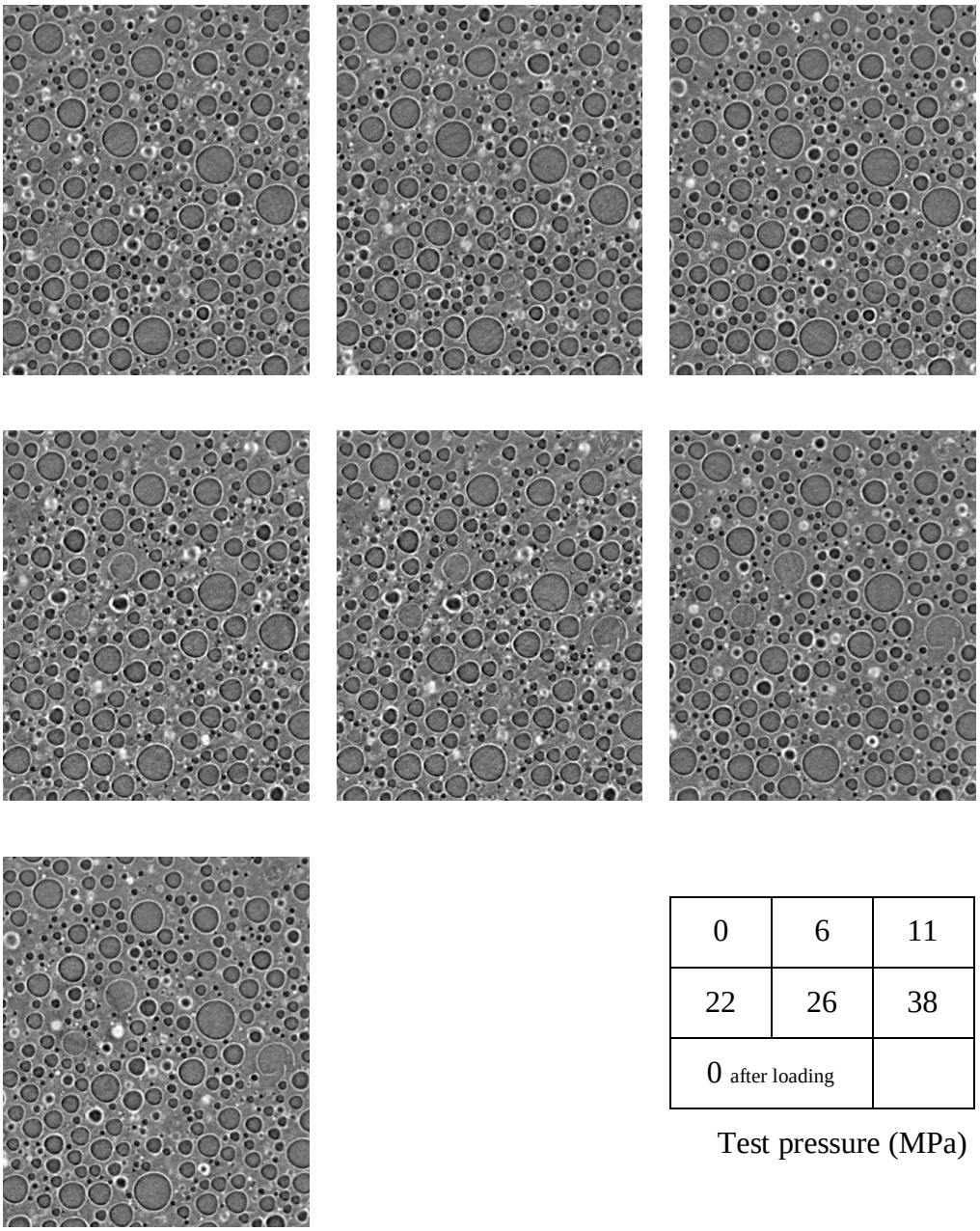

0	6	11
22	26	38
0 after loading		

Test pressure (MPa)

Figure Slice 255 of GSEP sample

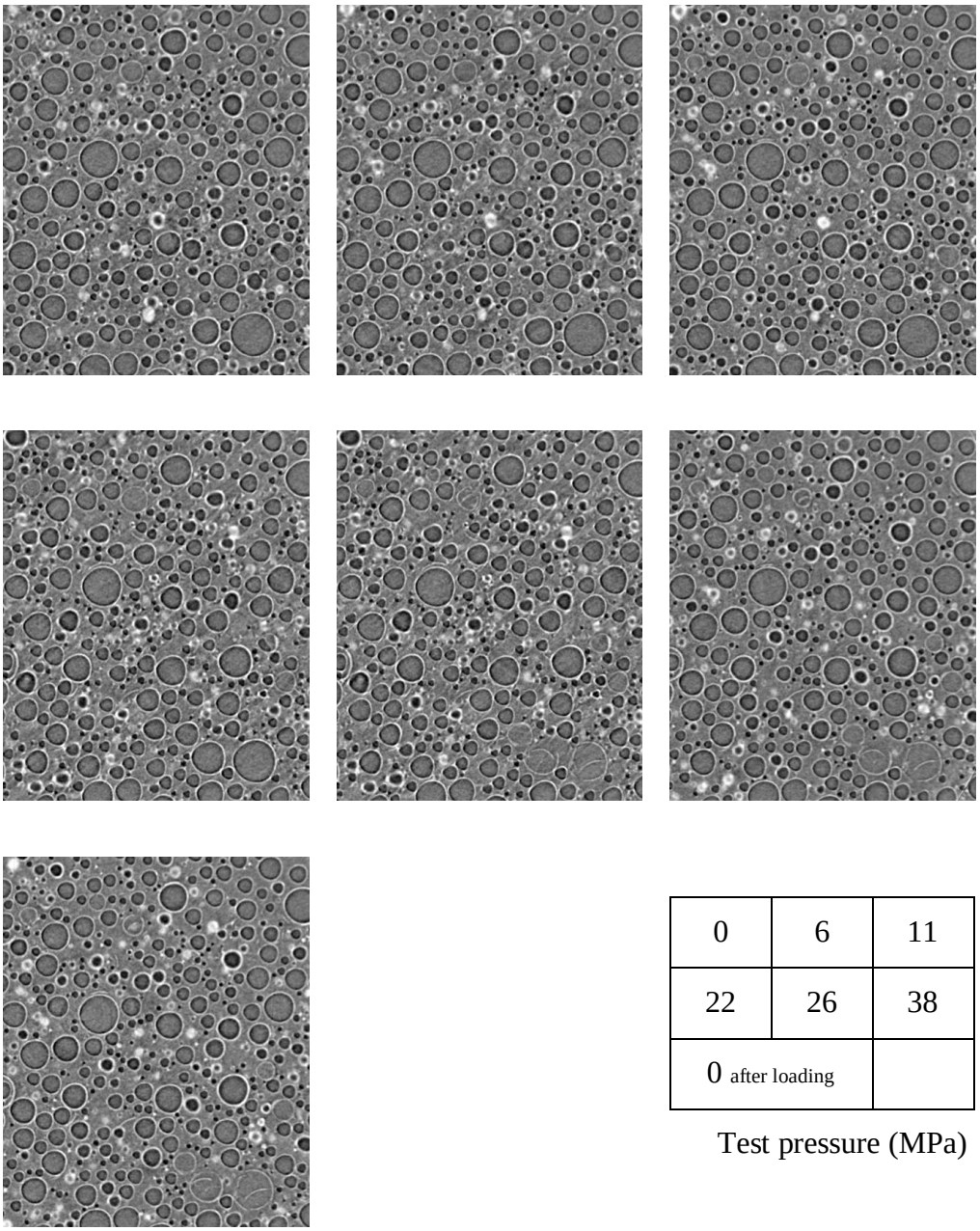

0	6	11
22	26	38
0 after loading		

Test pressure (MPa)

Figure Slice 323 of GSEP sample

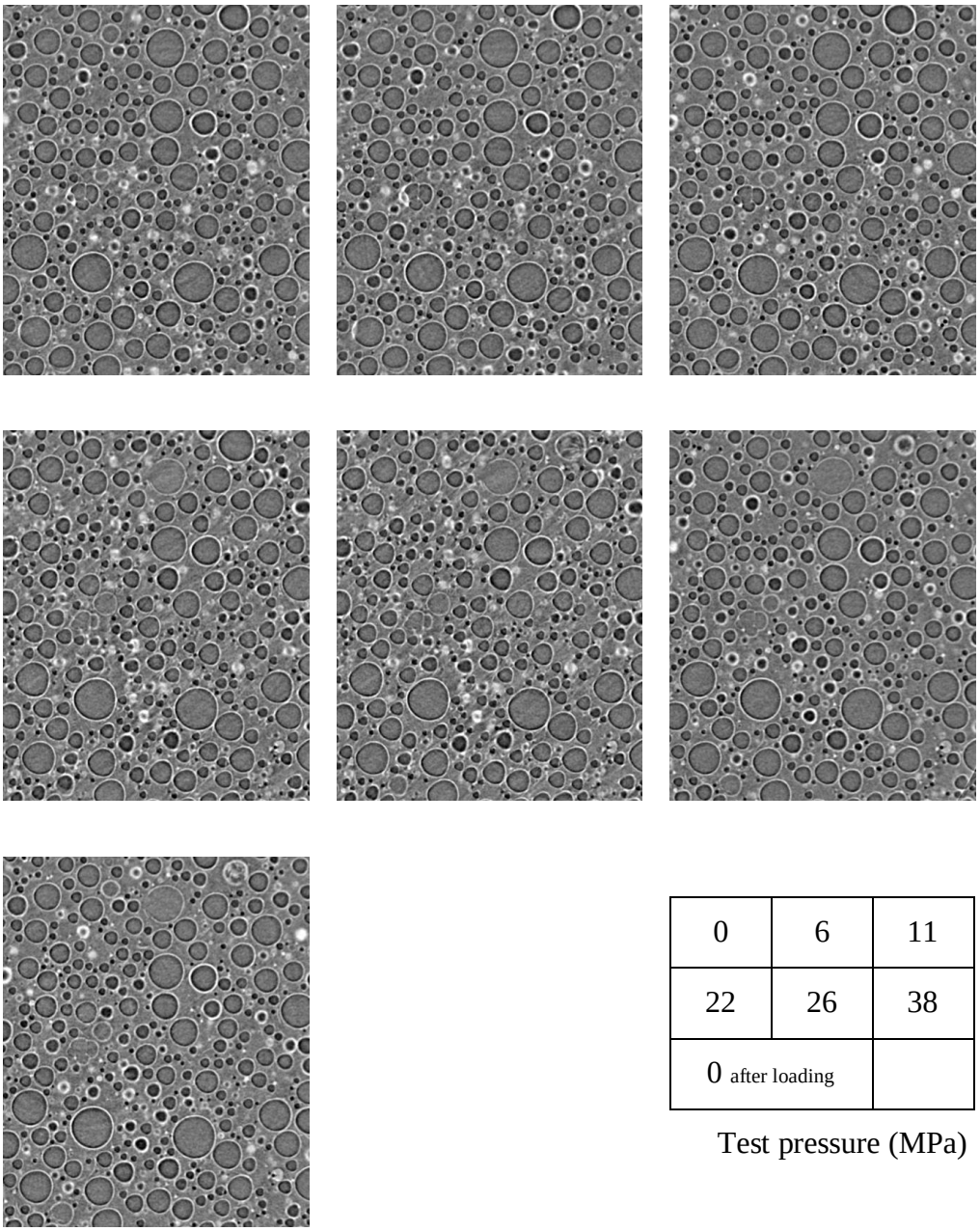

0	6	11
22	26	38
0 after loading		

Test pressure (MPa)

Figure Slice 400 of GSEP sample

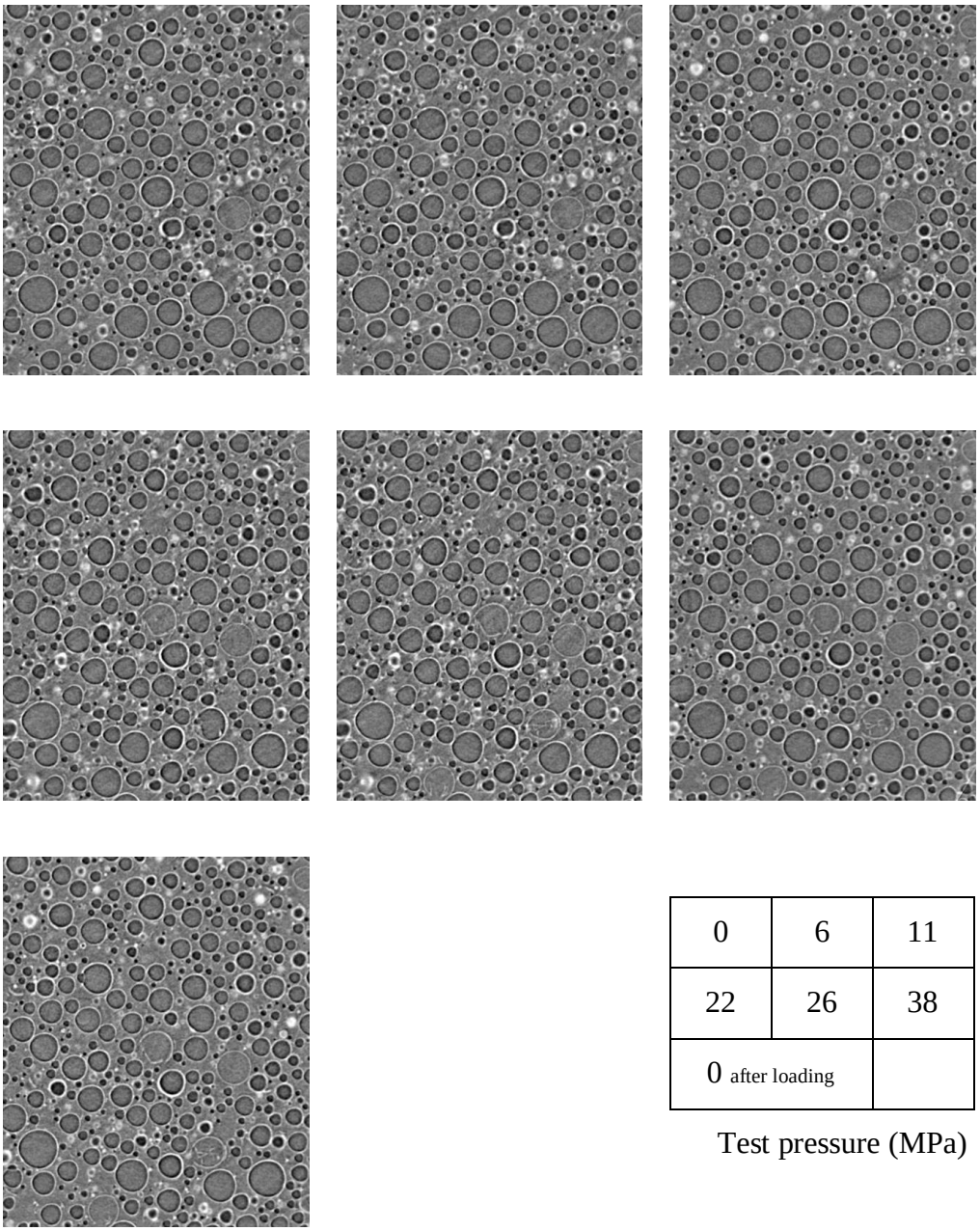

0	6	11
22	26	38
0 after loading		

Test pressure (MPa)

Figure Slice 527 of GSEP sample

6.11 Pycnometer principle

The principle of a double chamber gas pycnometer is as follows:

Phase 1: filling of the capacity 1

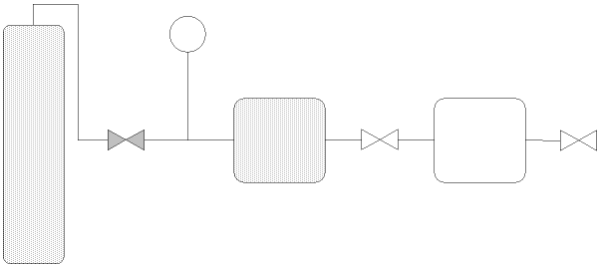

Phase 2: pressure equilibrium on capacity1

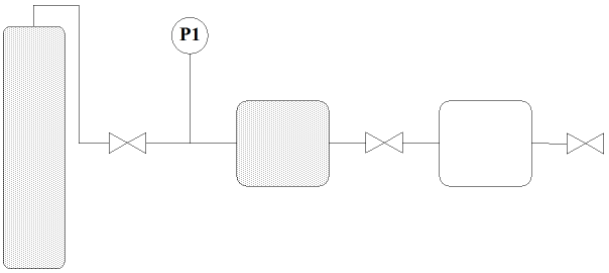

Phase 3: pressure equilibrium in capacity 1 and 2

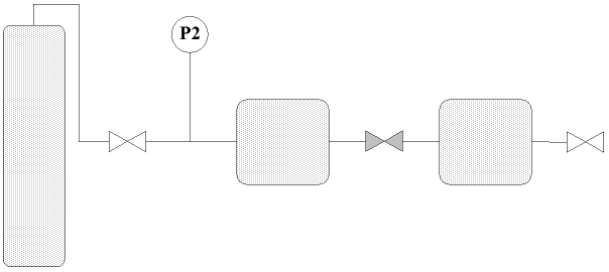

Phase 4: purge

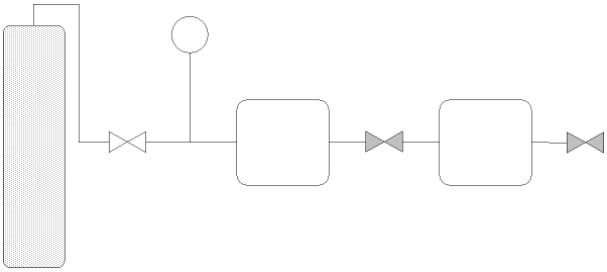

Phase 5: filling of the capacity 1 + calibrated volume

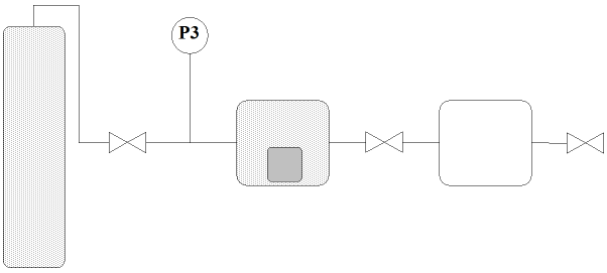

Phase 6: pressure equilibrium in capacity 1 and 2

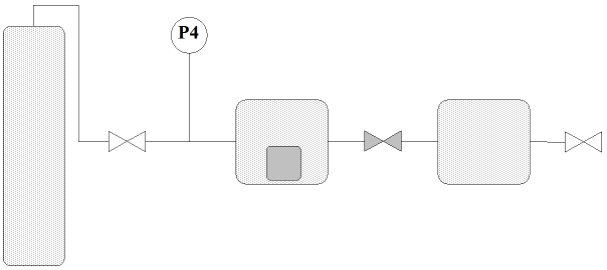

Phase 7: purge, end of calibration phase

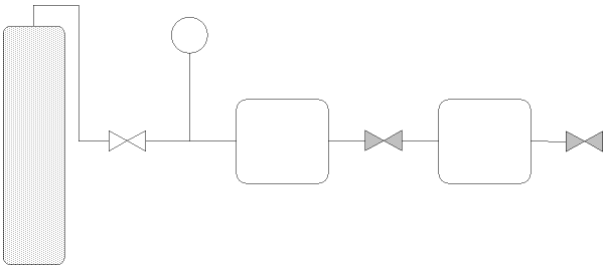

At this stage the volume of the two capacities can be determined as follows :

$$V_{c1} = \frac{V_{ref}(P3 - P4)}{(P3 - P4) - \frac{P4}{P2}(P1 - P2)}$$

And

$$V_{c2} = V_{C1} * \frac{P1 - P2}{P2}$$

With

$V_{C1} = volume\ of\ capacity1$

$V_{C2} = volume\ of\ capacity2$

$V_{ref} = calibrated\ volume$

Phase 8: filling of the capacity 1 + unknown volume

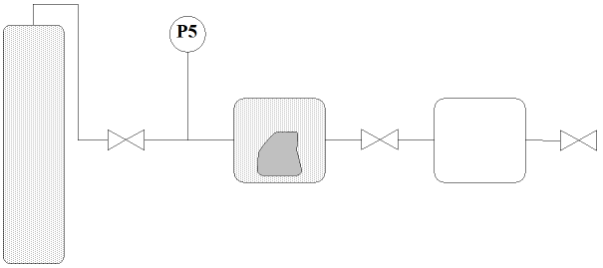

Phase 9: pressure equilibrium in capacity 1 and 2, end of measurement

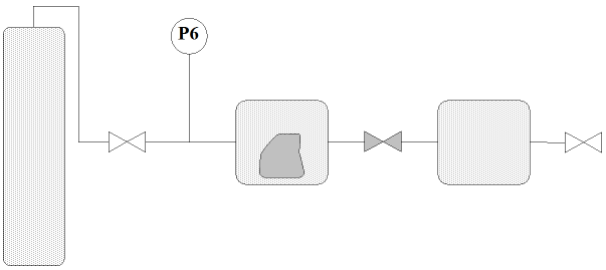

The volume of the specimen is then determined.

$$V_{specimen} = V_{c1} - \frac{V_{c2}}{\frac{P5}{P6} - 1}$$

6.12 *Accupyc* Pcynometer

The AccuPyc II 1340 Pycnometer is an easy-to-use, fully automatic gas displacement pycnometer.

The AccuPyc 1340 determines density and volume by measuring the pressure change of helium within calibrated volumes. It also reports the chamber temperature at the end of the requested cycles.

The AccuPyc II 1340 Pycnometer consists of a control module and an analysis module. When ordering a single unit, the control module is built into the same unit as the analysis module for convenience. The pycnometer is controlled by a user-friendly Windows interface. The operational status of the pycnometer can be continually monitored in a Status window shown on the computer screen.

The pycnometer uses helium (99.995% pure or better) to provide rapid, accurate analyses.

A 10 cm^3 chamber model has been selected. On the figure below the stainless steel chamber and the calibration sample are shown.

The equipment is controlled by software and each value provided is typically the result of 10 successive measurements on the same sample.

The system is automatically purged by venting of the two chamber with helium prior to each measurement phase.

The measurement is performed in five steps:

pressurizing the measurement chamber to 19.540 psi

equilibrium of measuring and expansion chambers to reach stabilized pressure (pressure rate change < 0.005 psi/min)

purge expansion chamber (pressure rate change < 0.005 psi/min)

purge expansion and measurement chamber (pressure rate change < 0.005)

equilibrium of measuring and expansion chamber to reach pressure stabilized (pressure rate change < 0.005 psi/min)

With this measurement sequence volume measurement accuracy better than 0.0001 cm^3 can be obtained.

The volume of the sample to be analyzed must correspond to about 50% of the volume of the chamber. For material volumes inferior to 1 cm^3 in a measuring chamber volume of 10 cm^3 , the accuracy of the measurement is drastically decreased.

The results are reported in the following form

AccuPyc II 1340 V1.05	Unit 1	Serial #: 1402	Page 1
Sample:	PU4_1		
Operator:			
Submitter:			
Bar Code:			
File:	C:\1340\DATA\PU4_1.SMP		
Analysis Gas:	Helium	Analysis Start:	06/04/2012 9:42:16
Reported:	06/04/2012 10:58:43	Analysis End:	06/04/2012 10:21:06
Sample Mass:	1.3118 g	Equilib. Rate:	0.005 psig/min
Temperature:	21.85 °C	Expansion Volume:	9.1411 cm^3
Number of Purges:	10	Cell Volume:	11.7590 cm^3
Summary Report			
Sample Volume			
Average:	3.1044 cm^3		
Standard Deviation:	0.0010 cm^3		
Sample Density			
Average:	0.4226 g/cm^3		
Standard Deviation:	0.0001 g/cm^3		

AccuPyc II 1340 V1.05	Unit 1	Serial #: 1402	Page 1
Sample:	PU4_1		
Operator:			
Submitter:			
Bar Code:			
File:	C:\1340\DATA\PU4_1.SMP		
Analysis Gas:	Helium	Analysis Start:	06/04/2012 9:42:16
Reported:	06/04/2012 10:58:43	Analysis End:	06/04/2012 10:21:06
Sample Mass:	1.3118 g	Equilib. Rate:	0.005 psig/min
Temperature:	21.85 °C	Expansion Volume:	9.1411 cm³
Number of Purges:	10	Cell Volume:	11.7590 cm³

Density and Volume Table

Cycle#	Volume (cm³)	VolumeDeviation(cm³	Density (g/c	DensityDeviation(g/cm³)	Elapsed Time (mm:ss)	Temperature (°C)
1	3.1033	-0.0011	0.4227	0.0001	10:41	21.86
2	3.1053	0.0009	0.4224	-0.0001	13:34	21.86
3	3.1053	0.0009	0.4224	-0.0001	16:37	21.85
4	3.1036	-0.0008	0.4227	0.0001	20:06	21.84
5	3.1043	-0.0001	0.4226	0.0000	23:13	21.86
6	3.1049	0.0005	0.4225	-0.0001	26:00	21.86
7	3.1048	0.0004	0.4225	-0.0001	28:50	21.84
8	3.1048	0.0004	0.4225	-0.0001	31:28	21.85
9	3.1053	0.0009	0.4224	-0.0001	34:37	21.86
10	3.1024	-0.0020	0.4228	0.0003	37:35	21.84

Summary Data	Average	Standard Deviation
Volume:	3.1044 cm³	0.0010 cm³
Density:	0.4226 g/cm³	0.0001 g/cm³

6.13 Accupyc result for GSPU

ref	pressure (bar)	mass (gr)	density (kg/m^3)
1-2	0	1.3126	0.4175
2-2	0	1.3799	0.4338
1-3	0	1.3708	0.4209
1-1	0	1.2518	0.4251
2-1	0	1.3116	0.428
3-1	50	1.4472	0.4207
4-1	100	1.3118	0.4226
4-2	100	1.3525	0.422
5-1	150	1.4205	0.4425
5-2	150	1.4976	0.4396
6-1	200	1.4166	0.4487
6-2	200	1.3044	0.4509
7-1	250	1.5079	0.4557
7-2	250	1.4263	0.4476
8-1	300	1.5284	0.4648
8-2	300	1.3975	0.4614
9-1	350	1.4968	0.5542
9-2	350	1.5223	0.5545
10-1	400	1.7492	0.6732
10-2	400	1.7244	0.6676
11-1	500	1.8642	0.7717
11-2	500	2.0028	0.7744
12-1	600	1.9286	0.8493
12-2	600	1.9666	0.8559
13-1	800	1.9837	0.9834
13-2	800	2.269	0.9935

Chapter 7. BIBLIOGRAPHY

1. Fontblanc, G., *Mousses syntactiques : matériaux composites pour grandes profondeur* 1986, Bordeaux University.
2. Ruckebusch, J.M., *Microspheres Creuses de Verre Pour Mousses Syntactiques*: Ed. Techniques Ingénieur.
4. Shutov, F., *Syntactic polymer foams, Chromatography/Foams/Copolymers*, 1986, Springer Berlin / Heidelberg. p. 63-123.
5. Watkins, L. *Syntactic foam buoyancy for ultradeep marine riser*. in *OTC*. 1982. Houston.
6. Lamy, M., *Développement des matériaux allégés pour utilisations en milieux marins hyperbars*, in *ATMA, Association Technique Maritime et Aéraunautique*1984.
7. Avena, A., *Comportement à long terme de matériaux composites en immersion à grande profondeur*, 1987, Ecole des mines, Paris.
8. Dan, W., *Etude micromécanique de l'endommagement des mousse syntactiques* 1987, Ecole Centrale, Paris.
9. Baptiste, D., *Damage micromechanics modelling of discontinuous reinforced composites.* Continuum Damage Mechanics of Materials and Structures, 2002: p. 115-163.
10. Hashin, Z., *The moduli of an elastic solid, containing spherical particules of another elastic material*, in *IUTAM symposium on non-homogeneity in elastic and plasticity*1958: Warsaw. p. 463-478.
11. Christensen, R.M. and K.H. Lo, *Solutions for Effective Shear Properties in 3 Phase Sphere and Cylinder Models.* Journal of the Mechanics and Physics of Solids, 1979. **27**(4): p. 315-330.
12. Ben Hamida, A., *Etude micromécanique des mousses syntactiques* 1987, Pierre et Marie Curie University, Paris.
13. Krzhechkovskii, P.G., *Determining elastic and strength properties of composites with hollow spherical inclusions.* Strength of Materials, 1979. **11**(3): p. 265-269.
14. Krzhechkovskii, P.G., *Fracture mechanics of syntactic foam composites.* Strength of Materials, 1982. **14**(11): p. 1556-1564.
15. Bardella, L. and F. Genna, *On the elastic behavior of syntactic foams.* International Journal of Solids and Structures, 2001. **38**(40-41): p. 7235-7260.
16. Bardella, L., et al., *A critical evaluation of micromechanical models for syntactic foams.* Mechanics of Materials, 2012. **50**: p. 53-69.
17. Yuan, Y.L. and Z.X. Lu, *Modulus prediction and discussion of reinforced syntactic foams with coated hollow spherical inclusions.* Applied Mathematics and Mechanics-English Edition, 2004. **25**(5): p. 528-535.
18. Rizzi, E., E. Papa, and A. Corigliano, *Mechanical behavior of a syntactic foam: experiments and modeling.* International Journal of Solids and Structures, 2000. **37**(40): p. 5773-5794.

19. Marur, P.R., *Effective elastic moduli of syntactic foams.* Materials Letters, 2005. **59**(14-15): p. 1954-1957.

20. Brini, A., *Modélisation multi-échelles du comportement et du vieillissement des mousses syntactiques immergées* 2004, Pierre et Marie Curie University, Paris.

21. Zouari, R., *Approche itérative d'homogénéisation pour le comportement des composites polydisperses : Application à l'endommagement des mousses syntactiques Immergées* 2006, Pierre et Marie Curie University, Paris.

22. Zouari, R., A. Benhamida, and H. Dumontet, *A micromechanical iterative approach for the behavior of polydispersed composites.* International Journal of Solids and Structures, 2008. **45**(11-12): p. 3139-3152.

23. Antunes, F.V., J.A.M. Ferreira, and C. Capela, *Numerical modelling of the Young's modulus of syntactic foams.* Finite Elements in Analysis and Design, 2011. **47**(2): p. 78-84.

24. Gupta, N. and E. Woldesenbet, *Hygrothermal studies on syntactic foams and compressive strength determination.* Composite Structures, 2003. **61**(4): p. 311-320.

25. Kochetkov, V.A. and R.D. Maksimov, *Water absorption and swelling of glass/epoxy syntactic foams.* Mechanics of Composite Materials, 1996. **32**(1): p. 61-70.

26. Tagliavia, G., M. Porfiri, and N. Gupta, *Influence of moisture absorption on flexural properties of syntactic foams.* Composites Part B-Engineering, 2012. **43**(2): p. 115-123.

27. Gimenez, N., *Vieillissement hydrolytique de mousses syntactiques époxy-amine/verre pour l'isolation thermique sous hautes pressions : mécanismes de dégradation et simulation de la prise en eau* 2006, INSA Lyon.

28. Sauvant-Moynot, V., et al., *Hot wet aging of glass syntactic foam coatings monitored by impedance spectroscopy.* Progress in Organic Coatings, 2007. **59**(3): p. 179-185.

29. Sauvant-Moynot, V., N. Gimenez, and H. Sautereau, *Hydrolytic ageing of syntactic foams for thermal insulation in deep water: degradation mechanisms and water uptake model.* Journal of Materials Science, 2006. **41**(13): p. 4047-4054.

30. Carlisle, K.B., et al., *Characterization of the binder phase in a three-phase carbon microballoon syntactic foam.* Cellular Polymers, 2007. **26**(3): p. 157-165.

31. Carlisle, K.B., et al., *Finite element modeling of the uniaxial compression behavior of carbon microballoons.* Acta Materialia, 2007. **55**(7): p. 2301-2318.

32. Sankaran, S., et al., *Characterization of epoxy syntactic foams by dynamic mechanical analysis.* Journal of Materials Science, 2006. **41**(13): p. 4041-4046.

33. Lin, T.C., N. Gupta, and A. Talalayev, *Thermoanalytical characterization of epoxy matrix-glass microballoon syntactic foams.* Journal of Materials Science, 2009. **44**(6): p. 1520-1527.

34. Chavez, G.M., M.W. Lewis, and L.R. Lenke, *Shear properties of CMB syntactic foam.* Journal of Materials Science, 2006. **41**(13): p. 4015-4022.

35. Kim, H.S. and P. Plubrai, *Manufacturing and failure mechanisms of syntactic foam under compression.* Composites Part a-Applied Science and Manufacturing, 2004. **35**(9): p. 1009-1015.

36. Gupta, N., E. Woldesenbet, and P. Mensah, *Compression properties of syntactic foams: effect of cenosphere radius ratio and specimen aspect ratio.* Composites Part a-Applied Science and Manufacturing, 2004. **35**(1): p. 103-111.

37. Gupta, N., E. Woldesenbet, and Kishore, *Compressive fracture features of syntactic foams-microscopic examination.* Journal of Materials Science, 2002. **37**(15): p. 3199-3209.

38. Karthikeyan, C.S., S. Sankaran, and Kishore, *Elastic behaviour of plain and fibre-reinforced syntactic foams under compression.* Materials Letters, 2004. **58**(6): p. 995-999.

39. Song, B. and W. Chen, *Dynamic compressive response and failure behavior of an epoxy syntactic foam.* Journal of Composite Materials, 2004. **38**(11): p. 915-936.

40. Tagliavia, G., M. Porfiri, and N. Gupta, *Analysis of particle-to-particle elastic interactions in syntactic foams.* Mechanics of Materials, 2011. **43**(12): p. 952-968.

41. Aureli, M., M. Porfiri, and N. Gupta, *Effect of polydispersivity and porosity on the elastic properties of hollow particle filled composites.* Mechanics of Materials, 2010. **42**(7): p. 726-739.

42. Poveda, R., N. Gupta, and M. Porfiri, *Poisson's ratio of hollow particle filled composites.* Materials Letters, 2010. **64**(21): p. 2360-2362.

43. Porfiri, M. and N. Gupta, *Effect of volume fraction and wall thickness on the elastic properties of hollow particle filled composites.* Composites Part B-Engineering, 2009. **40**(2): p. 166-173.

44. Adrien, J., et al., *Experimental study of the compression behaviour of syntactic foams by in situ X-ray tomography.* Acta Materialia, 2007. **55**(5): p. 1667-1679.

45. Lemiere, Y., *The evolution of composite materials in submarine structures*, in *Nautical construction with composites materials*, Ifremer, Editor 1992: Paris. p. 441-449.

46. Bibin John, C.P.R.N., *Update on Syntactic Foams*2010: iSmithers.

47. Bouchonneau, N., et al., *Experimental testing and modelling of an industrial insulated pipeline for deep sea application.* Journal of Petroleum Science and Engineering, 2010. **73**(1-2): p. 1-12.

48. Total *Pazflor, one of the world's largest ever deepwater development*. 2012.

49. Guo, B., *Offshore pipelines*2005, Amsterdam ; Boston: GPP.

50. Pham, Q.T., *The Use of Lumped Capacitance in the Finite-Element Solution of Heat-Conduction Problems with Phase-Change.* International Journal of Heat and Mass Transfer, 1986. **29**(2): p. 285-291.

51. Choqueuse, D., A. Chomard, and C. Bucherie, *Thermal insulation for ultra deep pipelines. A research and evaluation program*, in *DOT, Deep Offshore Technology*2000: Rio, Brasil.

52. Bai, Y. and Q. Bai, *Subsea pipelines and risers*2005, Amsterdam ; London: Elsevier.

53. ISO, *Petroleum and natural gas industries. Wet thermal insulation coatings for pipelines, flow lines, equipment and subsea structures*, 2012.

54. Socotherm *Five layer Syntactic Polypropylene*. 2010.

55. Total *Girassol, a pioneering development in Angola's deep offshore*. 2012.

56. Choqueuse, D., A. Chomard, and P. Chauchot. *How to Provide Relevant Data for the Prediction of Long Term Behavior of Insulation Materials Under Hot/Wet Conditions?* in *Offshore Technology Conference*. 2004. Houston, USA.

57. Choqueuse, D., A. Chomard, and C. Bucherie. *Insulation Materials for Ultra deep Sea Flow Assurance: Evaluation of the Material Properties*. in *Offshore Technology Conference* 2002. Houston, USA.

58. Choqueuse, D., A. Chomard, and C. Bucherie, *Insulation materials for ultra deep sea flow assurance. "How to predict a 20 years life time ?"*, in *DOT, Deep Offshore Conference*2001: New Orleans, USA.

59. Grosjean, F., et al., *Comprehensive analyses of syntactic foam behaviour in deepwater environment.* Journal of Materials Science, 2009. **44**(6): p. 1462-1468.

60. Lefebvre, X., et al., *Durability of Syntactic Foams for Deep Offshore Insulation: Modelling of Water Uptake under Representative Ageing Conditions in Order to Predict the Evolution of Buoyancy and Thermal Conductivity.* Oil & Gas Science and Technology-Revue De L Institut Francais Du Petrole, 2009. **64**(2): p. 165-178.

61. Mylavarapu, P. and E. Woldesenbet, *Characterization of syntactic foams - An ultrasonic approach.* Journal of Cellular Plastics, 2008. **44**(3): p. 203-222.

62. Hosten, B. and B. Castagnede, *Optimization of the Computation of Elastic-Constants from the Measurements of Ultrasonic Velocities.* Comptes Rendus De L Academie Des Sciences Serie Ii, 1983. **296**(5): p. 297-300.

63. Baudouin, S. and B. Hosten, *Comparison between prediction and measurement of viscoelastic moduli in composite materials versus temperature using ultrasonic immersion technique with oil.* Journal of the Acoustical Society of America, 1997. **102**(6): p. 3450-3457.

64. Castagnede, B., J. Roux, and B. Hosten, *Correlation Method for Normal Mode Tracking in Anisotropic Media Using an Ultrasonic Immersion System.* Ultrasonics, 1989. **27**(5): p. 280-287.

65. Hosten, B. and M. Castaings, *Comments on the ultrasonic estimation of the viscoelastic properties of anisotropic materials.* Composites Part a-Applied Science and Manufacturing, 2008. **39**(6): p. 1054-1058.

66. Hosten, B., *Stiffness Matrix Invariants to Validate the Characterization of Composite-Materials with Ultrasonic Methods.* Ultrasonics, 1992. **30**(6): p. 365-371.

67. Leduc, F., *Mesures de vitesses ultrasonores sur des plaques de matériaux composites en immersion*, 1993, IFREMER.

68. Burg, E.v.d. and W. Grill, *Characterization of elastomers with transverse sonic waves.* Polymer Testing, 2010. **29**(2): p. 281-287.

69. ASTM, *ASTM D695 - 10 Standard Test Method for Compressive Properties of Rigid Plastics*, 2010, ASTM.

70. ASTM, *ASTM D1621 - 10 Standard Test Method for Compressive Properties Of Rigid Cellular Plastics*, 2010, ASTM.

71. Lee, J.K., et al., *Macroscopic observation of healing process in stress-whitened polypropylene under hydrostatic pressure.* Polymer Engineering and Science, 2002. **42**(12): p. 2351-2360.

72. Bhateja, S.K. and K.D. Pae, *Effects of Hydrostatic-Pressure on Compressibility, Crystallization, and Melting of Polymers.* Journal of Macromolecular Science-Reviews in Macromolecular Chemistry and Physics, 1975. **C 13**(1): p. 77-133.

73. Silano, A.A., K.D. Pae, and J.A. Sauer, *Effects of Hydrostatic-Pressure on Shear Deformation of Polymers.* Bulletin of the American Physical Society, 1977. **22**(3): p. 430-430.

74. Pae, K.D. and K.S. Carlson, *The combined effects of hydrostatic pressure and strain-rate on the compressive properties of a laminated, multi-directional, graphite/epoxy thick-composite.* Journal of Composite Materials, 1998. **32**(1): p. 49-67.

75. Pae, K.D., *Influence of hydrostatic pressure on the mechanical behavior and properties of unidirectional, laminated, graphite-fiber/epoxy-matrix thick composites.* Composites Part B-Engineering, 1996. **27**(6): p. 599-611.

76. Cartie, D., et al., *The influence of hydrostatic pressure on the interlaminar fracture toughness of carbon/epoxy composites.* Composites Part B-Engineering, 2006. **37**(4-5): p. 292-300.

77. Cognard, J.Y., et al., *Analysis of the Influence of Hydrostatic Stress on the Behaviour of an Adhesive in a Bonded Assembly.* Journal of Adhesion Science and Technology, 2010. **24**(11-12): p. 1977-1994.

78. Kim, Y. and S. Kang, *Development of experimental method to characterize pressure-dependent yield criteria for polymeric foams.* Polymer Testing, 2003. **22**(2): p. 197-202.

79. Viot, P., *Hydrostatic compression on polypropylene foam.* International Journal of Impact Engineering, 2009. **36**(7): p. 975-989.

80. Ozturk, U.E. and G. Anlas, *Hydrostatic compression of anisotropic low density polymeric foams under multiple loadings and unloadings.* Polymer Testing, 2011. **30**(7): p. 737-742.

81. Moreu, Y.M. and N.J. Mills, *Rapid hydrostatic compression of low-density polymeric foams.* Polymer Testing, 2004. **23**(3): p. 313-322.

82. Fine, R. and F. Millero, *Compressibilities of water as a function of temperature and pressure.* Journal of Chemical Physics, 1973. **59**: p. 5529-5536.

83. Saunders, P.M. and N.P. Fofonoff, *Conversion of Pressure to Depth in Ocean.* Deep-Sea Research, 1976. **23**(1): p. 109-111.

84. Copin-Montegut, G., *Propriétés physiques de l'eau de mer*, T. Ingénieur, Editor 2002.

85. AFNOR, *Milieu marin - Instrumentation océanographique - Guide d'essais en environnement.*, 1995.

86. Mussi, A., et al., *Determination of mechanical properties of parallelepiped materials embedded in solid medium and deformed under confining pressure.* Materials Science and Engineering a-Structural Materials Properties Microstructure and Processing, 2008. **478**(1-2): p. 140-146.

87. Choqueuse, D., et al., *Mechanical Behavior of Syntactic Foams for Deep Sea Thermally Insulated Pipeline.* Applied Mechanics and Materials, 2010. **24**: p. 97-102.

88. Gupta, N. and E. Woldesenbet, *Characterization of flexural properties of syntactic foam core sandwich composites and effect of density variation.* Journal of Composite Materials, 2005. **39**(24): p. 2197-2212.

89. Melin, L.N. and J.M. Neumeister, *Measuring constitutive shear behavior of orthotropic composites and evaluation of the modified Iosipescu test.* Composite Structures, 2006. **76**(1-2): p. 106-115.

90. Pierron, F. and A. Vautrin, *Accurate Comparative Determination of the Inplane Shear Modulus of T300/914 by the Iosipescu and 45-Degrees Off-Axis Tests.* Composites Science and Technology, 1994. **52**(1): p. 61-72.

91. Pierron, F., *Saint-Venant effects in the Iosipescu specimen.* Journal of Composite Materials, 1998. **32**(22): p. 1986-2015.

92. Adams, D.F., *The Iosipescu Shear Test Method as Used for Testing Polymers and Composite-Materials.* Polymer Composites, 1990. **11**(5): p. 286-290.

93. Adams, D.F. and D.E. Walrath, *Current Status of the Iosipescu Shear Test Method.* Journal of Composite Materials, 1987. **21**(6): p. 494-507.

94. Iosipescu, N., *New Accurate Procedure for Single Shear Testing of Metals.* Journal of Materials Chemistry, 1967. **2**(3): p. 537-566.

95. Arcan, M., *The Iosipescu Shear Test as Applied to Composite-Materials - Discussion.* Experimental Mechanics, 1984. **24**(1): p. 66-67.

96. Doleski, R., et al., *The rate sensitivity oh high strength syntactic foam,* in *International Conference on the Mechanical Behavior of Materials, ICM9*2003: Geneva, Switzerland.

97. Pierron, F. and A. Vautrin, *Experimental strain analysis of the Iosipescu shear test specimen* Experimental Mechanics, 1997. **37**(1): p. 12-12.

98. Melin, L.N. and J.M. Neumeister, *Sensitivity to specimen imperfections of Iosipescu shear for composite laminates,* in *ICCM-16*2007: Kyoto, Japan.

99. Neumeister, J.M. and L.N. Melin, *Specimen clamping and performance of the Iosipescu shear tests applied for composite materials,* in *ICCM-16* 2007: Kyoto, Japan.

100. Cognard, J.Y., et al., *Analysis of the nonlinear behavior of adhesives in bonded assemblies - Comparison of TAST and Arcan tests.* International Journal of Adhesion and Adhesives, 2008. **28**(8): p. 393-404.

101. Cognard, J.Y., L. Sohier, and P. Davies, *A modified Arcan test to analyze the behavior of composites and their assemblies under out-of-plane loadings.* Composites Part a-Applied Science and Manufacturing, 2011. **42**(1): p. 111-121.

102. Arcan, M., Z. Hashin, and A. Voloshin, *A method to produce uniform plane-stress states with applications to fiber-reinforced materials - A specially designed specimen yields material properties under pure shear or uniform plane-stress conditions.* Experimental Mechanics, 1978. **18**(4): p. 141-146.

103. Taher, S.T., et al., *Determination of mechanical properties of PVC foam using a modified Arcan fixture.* Composites Part A: Applied Science and Manufacturing, 2012. **43**(10): p. 1698-1708.

104. Cognard, J.Y., et al., *Influence of adhesive thickness on the behaviour of bonded assemblies under shear loadings using a modified TAST fixture.* International Journal of Adhesion and Adhesives, 2010. **30**(5): p. 257-266.

105. Davies, P., D. Choqueuse, and G. Bourbouze, *Micro-Tomography to Study High-performance Sandwich Structures.* Journal of Sandwich Structures & Materials, 2011. **13**(1): p. 7-21.

106. Salvo, L., et al., *X-ray micro-tomography an attractive characterisation technique in materials science.* Nuclear Instruments & Methods in Physics Research Section B-Beam Interactions with Materials and Atoms, 2003. **200**: p. 273-286.

107. Maire, E., et al., *X-ray tomography applied to the characterization of cellular materials. Related finite element modeling problems.* Composites Science and Technology, 2003. **63**(16): p. 2431-2443.

108. Maire, E., et al., *X Ray Tomography Study of Cellular Materials: Experiments and Modelling.* Iutam Symposium on Mechanical Properties of Cellular Materials, 2009. **12**: p. 35-42.

109. Maire, E., et al., *X-ray tomography and three-dimensional image analysis of epoxy-glass syntactic foams.* Philosophical Transactions of the Royal Society a-Mathematical Physical and Engineering Sciences, 2006. **364**(1838): p. 69-88.

110. Buffiere, J.Y., et al., *Three dimensional imaging of damage in structural materials using high resolution micro-tomography.* Nuclear Instruments & Methods in Physics Research Section B-Beam Interactions with Materials and Atoms, 2005. **238**(1-4): p. 75-82.

111. Maire, E., et al., *In situ X-ray tomography measurements of deformation in cellular solids.* Mrs Bulletin, 2003. **28**(4): p. 284-289.

112. Roux, H. and B. Petremont, *Pression isostatique et mousses syntactiques*, 2009, INSA lyon.

113. Dal Maso, F., *Canalisations en composites : Étude du perlage*, 1999, Techniques de l'ingénieur.

114. Maire, E., et al., *Damage quantification in aluminium alloys using in situ tensile tests in X-ray tomography.* Engineering Fracture Mechanics, 2011. **78**(15): p. 2679-2690.

115. Huguet, S., et al., *Use of acoustic emission to identify damage modes in glass fibre reinforced polyester.* Composites Science and Technology, 2002. **62**(10-11): p. 1433-1444.

116. Godin, N., et al., *Clustering of acoustic emission signals collected during tensile tests on unidirectional glass/polyester composite using supervised and unsupervised classifiers.* Ndt & E International, 2004. **37**(4): p. 253-264.

117. Barre, S. and M.L. Benzeggagh, *On the Use of Acoustic-Emission to Investigate Damage Mechanisms in Glass-Fiber-Reinforced Polypropylene.* Composites Science and Technology, 1994. **52**(3): p. 369-376.

118. Dan, W., *Etudes micromécaniques de l'endommagement des mousses syntactiques*, 1987, Ecole Centrale de Paris, France.

119. Weller, T., *Etude des comportements thermique et élastique des mousses syntactiques*, 2001, LM2S, Paris 6 University.

120. Timoshenko, S. and J. Gere, *Mechanics of Materials* 1997.

121. Bompard, P., et al., *Mechanical and fracture behaviour of porous materials.* Engineering Fracture Mechanics, 1987. **28**(5-6): p. 627-642.

122. Lee, K.J. and R.A. Westmann, *Elastic properties of hollow-sphere reinforced composites.* Journal of Composite Materials, 1970. **4**: p. 242-252.

123. Genna, F. and L. Bardella, *On the elastic behavior of syntactic foams.* International Journal of Solids and Structures, 2001. **38**(40-41): p. 7235-7260.

124. Marur, P.R., *Numerical estimation of effective elastic moduli of syntactic foams.* Finite Elements in Analysis and Design, 2010. **46**(11): p. 1001-1007.

125. Treasurer, P., et al. *Caractérisation et analyse de tubes composites carbone / époxyde*. in *JNC 16*. 2009. Toulouse, France.

126. Thevenin, P. and D. Perreux, *The use of homogenization methods for estimating anisotropic viscosities of composite melts.* Composites Science and Technology, 1996. **56**(5): p. 595-603.

127. Phan, V.T., et al., *Experimental analysis and modelling of the long term thermo-mechanical behaviour of glass/polypropylene syntactic used on thermally insulated offshore pipeline.* Progress in organic coating, 2012 submitted.

128. Grosjean, F. and V. Sauvant-Moynot, *Acoustic emission analyses of the hygrothermal ageing of glass syntactic foams.* Science and Engineering of Composite Materials, 2011. **18**(4): p. 217-223.